

**Epitaxial Growth and Characterization of Rare
Earth doped Ga₂O₃ Films**



March 2017

**Department of Science and Advance Technology
Graduate School of Science and Engineering**

Saga University

Zhengwei CHEN

Epitaxial Growth and Characterization of Rare Earth doped Ga₂O₃ Films

Abstract

Wide-bandgap semiconductors, such as Ga_xAl_{1-x}N, Zn_xMg_{1-x}O and Ga₂O₃, have attracted great attention due to their potential for use in solid-state lighting, high power devices, ultraviolet region optoelectronic devices and efficiency host materials for rare earth (RE) ions. In the past decade, RE ions doped wide bandgap semiconductors were promising materials for integrated optoelectronic applications due to their narrow emission line from the intra-4*f*-shell transitions in RE ions. It has been reported that the luminescence efficiency of dopant emissions could be highly improved with a wide bandgap host. Among all the materials, monoclinic Ga₂O₃ (β -Ga₂O₃) is considered as an emerging candidate for its larger bandgap (~ 4.8 eV) and chemical-physical stabilities. It is expected that RE ions doped Ga₂O₃ films have more efficient and stability light emission than other materials. However, up to now, there is few report available related to RE doped Ga₂O₃ luminescence thin films although this research is of vital importance for the future application. In this study, the purpose of this dissertation mainly includes: (1) Investigation of the growth parameter influence of the structure and optoelectronic properties of Eu and Er doped Ga₂O₃ deposited by using pulsed laser deposition (PLD) method. (2) Analysis of temperature dependence luminescence behavior of Eu and Er doped Ga₂O₃ to understand the energy transfer mechanism. (3) Fabrication of the green light-emitting

devices (LEDs) based on Ga₂O₃:Er/Si heterojunctions.

In Chapter 1, we present the background of this study, including the properties of RE ions and the introductions of wide bandgap semiconductors. The purpose of this study was also presented.

In Chapter 2, we introduce the film epitaxy growth and characterization methods.

In Chapter 3, we investigate the Eu contents and substrate temperature influence on the structure and properties of Ga₂O₃ films deposited on sapphire substrate by PLD. Herein, (1) Eu doped Ga₂O₃ films are obtained at substrate temperature as low as 500 °C. Moreover, the single crystal film can be obtained at 400 °C. (2) Eu doping amount in the films can be controlled by adjusting Eu contents in the target. (3) Intense red emissions at 613 nm are clearly observed for the Eu doped films and we demonstrate that intensity quenching is related to polycrystalline growth of Ga₂O₃. (4) Temperature dependence of luminescence spectra in Eu doped Ga₂O₃ films are investigated by using different light source. We also demonstrate that the variation of the emission intensity may be attributed to the thermal activated distribution of electrons among ⁷F_j and thermal quenching effect.

In Chapter 4, we have investigated the Er contents influence on the structure and properties of Ga₂O₃ films deposited on sapphire substrate by PLD. In this Chapter, (1) we fabricate Er doped Ga₂O₃ films on sapphire substrates for the first time. (2) Intense pure green emissions at 550 nm were clearly observed for the Er doped films. (3) Temperature dependence of luminescence spectra in Er doped Ga₂O₃ films are investigated by using 488 nm light source. No peak shift at 550 nm is found with

temperatures ranging from 77 to 450 K. (4) The intensity of the Er doped Ga_2O_3 films has a smaller variation with temperature compared to GaN.

In Chapter 5, we fabricate the $\text{Ga}_2\text{O}_3\text{:Er/Si}$ LEDs. In this Chapter, (1) Bright green emission (548 nm) can be observed by naked eye from $\text{Ga}_2\text{O}_3\text{:Er/Si}$ LEDs. (2) The driven voltage of this LEDs is 6.2V which is lower than that of ZnO:Er/Si or GaN:Er/Si devices. (3) The mechanism is demonstrated that Ga_2O_3 contain more defect-related level which will enhance the effects of recombination, resulting in the improvement of the energy transfer to Er ions.

In Chapter 6, the summary of this study is described.

Contents

1 Introduction	1
1.1 Background	1
1.2 Review of studies on rare earth ions doped semiconductors	1
1.2.1 RE ions.....	1
1.2.2 Wide bandgap semiconductors	5
1.3 Review of studies on RE ions doped Ga ₂ O ₃ films.....	8
1.3.1 Europium doped Ga ₂ O ₃	8
1.3.2 Erbium doped Ga ₂ O ₃	10
1.4 Purpose and Outline	10
References.....	12
2 Epitaxial growth and characterization methods	16
2.1 Epitaxial growth techniques	16
2.2 Characterization methods	20
References.....	27
3 Growth and characterization of Eu doped Ga₂O₃ films	28
3.1 Eu content influence.....	28

3.1.1 Introduction.....	28
3.1.2 Experiment.....	30
3.1.3 Results and discussion	32
3.2 Substrate temperature influence	43
3.2.1 Introduction.....	43
3.2.2 Experiment.....	43
3.2.3 Results and discussion	45
3.3 Conclusions.....	57
References.....	58
4 Growth and characterization of Er doped Ga₂O₃ films	62
4.1 Introduction	62
4.2 Experiment	64
4.3 Results and discussion	65
4.4 Conclusions	77
References.....	78
5 Light-emitting devices based on Ga₂O₃:Er/Si	80
5.1 Introduction.....	80
5.2 Experiment.....	82
5.3 Results and discussion	85

5.4 Conclusions	99
References.....	100
6 Summary.....	103
Acknowledgments	105
List of publications.....	106

Chapter 1

Introduction

1.1 Background

Trivalent rare earth (RE) doped semiconductors are promising materials for integrated optoelectronic applications due to their narrow emission line from the intra-4*f*-shell transitions in RE ions. It has been reported that the luminescence efficiency of dopant emissions could be highly improved with a wide bandgap host. Moreover, the wide bandgap semiconductors exhibit highly thermal and chemical stability, which make them ideal hosts for RE ions. In the literatures, TiO₂ (~ 3.2 eV), ZnO (~ 3.3 eV), and GaN (~ 3.4 eV) have been used as the host materials for RE ions. Recently, with a wider bandgap (~ 4.8 eV) than that of GaN or ZnO, Ga₂O₃ has been investigated for use as an efficient host for RE ions. The research of RE ions doped Ga₂O₃ paves the way for the development of optoelectronic devices.

1.2 Review of studies on RE ions doped semiconductors

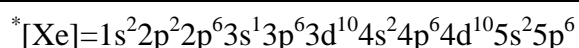
1.2.1 RE ions

RE element, as defined by international union of pure and applied chemistry, is one of a set of seventeen chemical elements in the periodic table, specifically the fifteen lanthanides, as well as scandium and yttrium as shown in Table 1.1. They are found in the earth's crust that are vital to many modern technologies, including consumer electronics, computers and networks, communications, clean energy,

advanced transportation, health care, environmental mitigation, national defense, and many others¹⁻³.

Table 1.1 Periodic table of RE elements.

⁵⁷ Lanthanum	⁵⁸ Cerium	⁵⁹ Praseodymium	⁶⁰ Neodymium	⁶¹ Promethium	⁶² Samarium
*[Xe]5d ¹ 6s ²	[Xe]4f ¹ 5d ¹ 6s ²	[Xe]4f ³ 6s ²	[Xe]4f ⁴ 6s ²	[Xe]4f ⁵ 6s ²	[Xe]4f ⁶ 6s ²
⁶³ Europium	⁶⁴ Gadolinium	⁶⁵ Terbium	⁶⁶ Dysprosium	⁶⁷ Holmium	⁶⁸ Erbium
[Xe]4f ⁷ 6s ²	[Xe]4f ⁷ 5d ¹ 6s ²	[Xe]4f ⁹ 6s ²	[Xe]4f ¹⁰ 6s ²	[Xe]4f ¹¹ 6s ²	[Xe]4f ¹² 6s ²
⁶⁹ Thulium	⁷⁰ Ytterbium	⁷¹ Lutetium		²¹ Scandium	³⁹ Yttrium
[Xe]4f ¹³ 6s ²	[Xe]4f ¹⁴ 6s ²	[Xe]4f ¹⁴ 5d ¹ 6s ²		3d ¹ 4s ²	4d ¹ 5s ²



From Table 1.1, in the case of RE³⁺ ions, electron configurations assume the form [Xe] 4fⁿ (n = 0-14), in which the xenon core displays 5s² and 5p⁶ filled orbitals that are radially more external than 4f orbitals. This, in turn, results in a low interaction of 4f electrons with the chemical environment, which culminates in a low degree of covalence in their chemical bonds and in a high similarity in chemical properties. On the other hand, the RE elements help make many technologies more efficiency, performance, miniaturization, speed, durability, and thermal stability due to their unique magnetic, luminescent, and electrochemical properties. In the past decade, the devices based on the RE elements have been widely used in laser gain media, cathode ray tube phosphors, thin film electroluminescence devices and color display and so on⁴⁻⁸.

Table 1.2 Ground levels and numbers of states arising from $4f^n$ configurations.

$4f^n$	Example	Ground level	$4f^n$	Example	Ground level	Number of levels	Number of microstates
$4f^0$	La ³⁺	¹ S ₀	$4f^{14}$	Lu ³⁺	¹ S ₀	1	1
$4f^1$	Ce ³⁺	² F _{5/2}	$4f^{13}$	Yb ³⁺	² F _{7/2}	2	14
$4f^2$	Pr ³⁺	³ H ₄	$4f^{12}$	Tm ³⁺	³ H ₆	13	91
$4f^3$	Nd ³⁺	⁴ I _{9/2}	$4f^{11}$	Er ³⁺	⁴ I _{15/2}	41	364
$4f^4$	Pm ³⁺	⁵ I ₄	$4f^{10}$	Ho ³⁺	⁵ I ₈	107	1001
$4f^5$	Sm ³⁺	⁶ H _{5/2}	$4f^9$	Dy ³⁺	⁶ H _{15/2}	198	2002
$4f^6$	Eu ³⁺	⁷ F ₀	$4f^8$	Tb ³⁺	⁷ F ₆	295	3003
$4f^7$	Gd ³⁺	⁸ S _{7/2}	--	--	--	327	3432

Due to a large increase in the effective positive charge over $5s^2$ and $5p^6$ electrons with increasing atomic numbers, as an effect of the low shielding power of $4f$ electrons. The lanthanoid contraction accounts for the decrease of basicity of RE³⁺ ions along the series and results in very subtle differences in solubility and crystal structures of their compounds. Spectroscopic properties of RE³⁺ ions are governed by the shielding effect of $5s^2$ and $5p^6$ electrons over $4f$ electron, which gives rise to well-defined energy levels^{4, 9,10}. Meanwhile, spectrochemical descriptions of RE³⁺ ions mostly comprise the evaluation of energy levels arising from $4f^n$ configurations, where the number of states can be very high. As show in Table 1.2, we can see the ground levels and numbers of states arising from $4f^n$ configurations. On the other hand, it should be noted that the RE ions alone are weakly luminescence due to the parity forbidden intra- $4f$ -shell transitions necessitates the use of semiconductor host materials to excite the RE ions efficiently in full spectral range¹¹. Since the electrons in the outer $5s$ and $5p$ orbitals substantially screen electrons in the incomplete $4f$ orbital from the local electric field of the host materials. This screen reduces the

effects of the host materials on the emissive and absorptive properties of the RE dopant, resulting in spectrally narrow emission and absorption bands from the radiative transitions within the free ions like $4f$ states.

In the literature, P.N. Favennec *et al*¹². have reported the luminescence of Er-doped IV, III-V, and II-VI semiconductors, and they have demonstrated that luminescence efficiency of dopant emissions could be highly improved with a wide bandgap host. Therefore, it is necessary for using wide bandgap materials as the host for RE ions. How to define wide bandgap semiconductors will be discussed in the next Chapter.

1.2.2 Wide bandgap semiconductors

Typically, wide bandgap materials have bandgaps larger than 2.3 eV. They are the key component used to make light emitting diodes (LEDs) and laser diodes (LDs) from the visible and short spectra range (blue-green, and ultraviolet), and are also used in devices supported by high breakdown field, certain radio frequency applications, notably military radars. Their inherent qualities make them suitable for a wide range of roles, and they are one of the leading contenders for next-generation devices for general semiconductor use¹³⁻¹⁸.

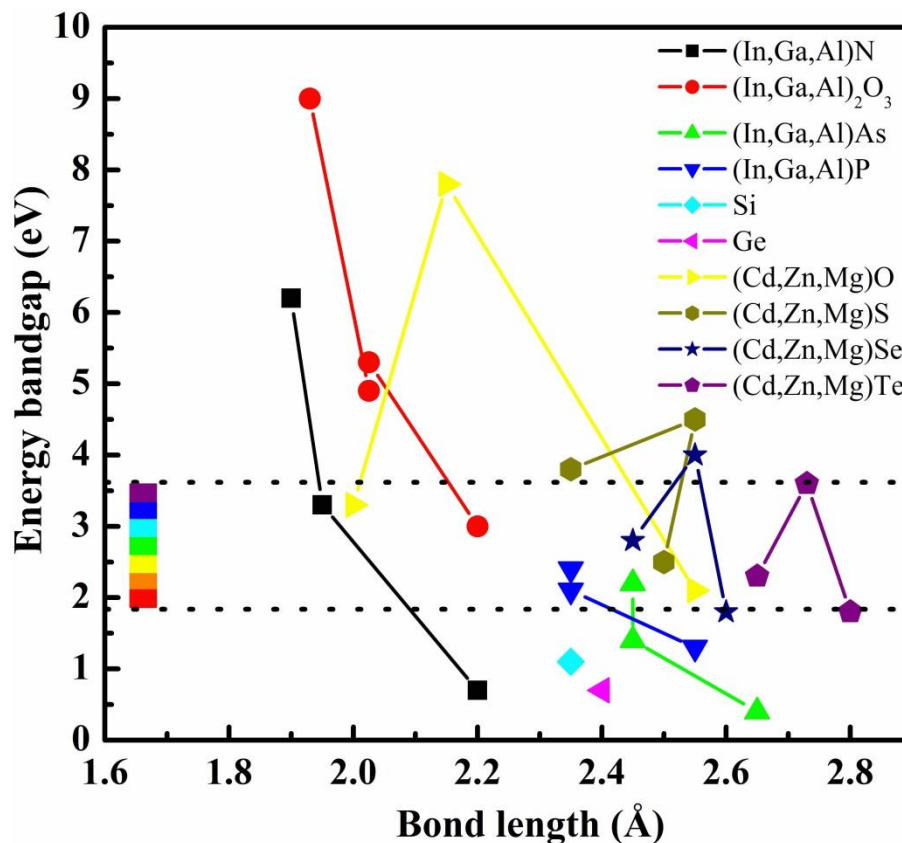


Figure 1.1 Relationship between energy bandgap and bond length for various compound semiconductors promising for practical applications.

Table 1.3 Basic introductions of various wide bandgap semiconductors¹⁹⁻²⁴.

Semiconductors	Brief history	Applications	<ul style="list-style-type: none"> ● Advantages ◆ Disadvantages
(Zn,Mg,Cd)(Se,S) --Se:(1.8-4.0 eV) --S: (2.5-3.8 eV)	From the late 1980s	Enabling the formation of LEDs and LDs that cover the blue-green to blue range etc.	<ul style="list-style-type: none"> ● Lattice-matched to the substrate (GaAs etc.) ● Low-cost ● Easy to grow ◆ Short lifetime
(In,Ga,Al)N (0.7-6.2 eV) GaN: 3.39 eV	From the late 1990s	High brightness green white LEDs, blue/UV LDs; covers the visible to deep-UV range (GaN alloyed with AlN or InN) Host materials for RE LEDs	<ul style="list-style-type: none"> ● High quality (Ga, In, Al)N epilayers on sapphire are grow easily. ● High density optical disks ● Applied to power devices ◆ Short lifetime ◆ Develop green-to-yellow optical devices is still underway.
(Zn,Mg,Cd)O (2.1-7.8 eV) ZnO: 3.4 eV	From about 1995	Deep UV detector Transparent conductive oxide UV LEDs Host materials for RE LEDs	<ul style="list-style-type: none"> ● High exciton binding energy ● Easy to grow ◆ Difficulty in forming reliable <i>pn</i> junctions
(In,Ga, Al) ₂ O ₃ (3.0-9.0 eV) <i>β</i> -Ga ₂ O ₃ : 4.9 eV	From about 2009	Deep UV detector Transparent Power devices Host materials for RE LEDs	<ul style="list-style-type: none"> ● Wide bandgap ● High efficiency deep UV devices ◆ High quality (Ga, In, Al)₂O₃ are grown difficultly.

Figure 1.2 shows the relationship between the energy bandgap and wavelength of various compound semiconductors promising for practical applications. Table 1.3

summarized the basic introductions of various wide bandgap semiconductors. We found that these semiconductor materials have different applications due to their different bandgap. Compared with the narrow bandgap semiconductors, the wide bandgap semiconductor materials have a high breakdown electric field, so that the output power of the device can be large-scale upgrade¹⁷. In addition, the wide bandgap materials have a high thermal conductivity, anti-radiation ability, high Baliga's figure of merit and high chemical stability. Therefore, the devices can work in harsh environments and anti-radiation high-power microwave devices. Herein, it should be noted an important application that the wide bandgap semiconductors as host materials for RE elements can highly improve the luminescence efficiency of RE-LEDs^{12,25}. The wide bandgap semiconductors are expected to be applied to solid-state lighting and power devices, supporting a future energy-saving society.

With a direct wide bandgap and chemical and physical stabilities, Ga₂O₃ based devices, such as Ga₂O₃/GaN, Ga₂O₃/SiC and Ga₂O₃/Si heterojunctions, have been investigated for use as ultraviolet photodetectors and efficient host for RE LEDs²⁶⁻³⁰. In Chapter 1.2.1, we know that the trivalent RE ions doped wide bandgap semiconductors are promising materials for integrated optoelectronic applications and compact color displays due to their narrow emission line from the intra-4*f*-shell transitions in RE ions. Historically, GaN and ZnO have been used as host for RE elements. Recently, Ga₂O₃ with wider bandgap than that of GaN or ZnO has attracted tremendous attention as a host material for phosphors in display applications. We will discuss the research of Ga₂O₃ and RE doped Ga₂O₃ films in the next Chapter.

1.3 Review of studies on RE ions doped Ga₂O₃

1.3.1 Europium doped Ga₂O₃

It is known that properties of Ga₂O₃ depend highly on its structures. In the past decade, five polymorphs (α , β , γ , δ , and ε phase) for Ga₂O₃ have been reported by other researchers³¹. They have demonstrated that the monoclinic Ga₂O₃ (β -Ga₂O₃), with a melting point of 1740 °C, was the most stable crystalline structures³². The researchers have reported that the RE doped wide bandgap semiconductors are promising materials for integrated optoelectronic applications, compact color displays and full color or white LEDs. It is expected that full color or white LEDs could be fabricated based on RE ions doped or co-doped Ga₂O₃ films. Furthermore, three primary (red blue and green) RBG colors are the basis for white luminescence and all panchromatic luminescence. Therefore, it is necessary to investigate the RE doped RBG emission. As shown in Table 1.4, we chose europium (Eu) and erbium (Er) as the red and green RE ions in this work.

Table 1.4 Detail of full color display of RE ions

Full color display (Light emission)	Blue	Tm (~ 477 nm)
	Green	Er (~ 537, ~ 550 nm) ; Tb (~ 565 nm)
	Red	Eu (~ 610 nm); Pr (~ 650 nm) Sm (~ 600 nm, ~ 650 nm)

Eu element is a hard metal used to create visible light in compact fluorescent bulbs and in color displays. Eu phosphors help to bring bright red to color displays

and to drive the popularity of early generations of color television sets. We know that Eu ions alone are weakly luminescence due to a fact that the parity forbidden intra-4*f*-shell transitions necessitates the use of semiconductor host materials to excite the Eu ion efficiently in full spectral range. On the other hand, it has been demonstrated that the luminescence efficiency of dopant emissions could be highly improved with a wide bandgap host. Moreover, the wide bandgap semiconductors exhibit highly thermal and chemical stability, which make them ideal hosts for Eu ions^{9,10}. Therefore, Eu doped wide bandgap semiconductors, which exhibit strong, sharp, and red emission around 610 nm due to intra-4*f*-shell transitions in Eu ion cores, have been intensively studied for their potential use in efficient light emitting diodes^{33,34}. It is expected that Eu doped Ga₂O₃ films have more efficient and stability red light emission.

In the literatures, various growth techniques have been tried to fabricate europium (Eu) doped Ga₂O₃ films. Hao *et al.*³⁵ have grown Eu doped β-Ga₂O₃ films by using spray pyrolysis and annealing at 600-900 °C. Tokida *et al.*³⁶ fabricated Eu doped Ga₂O₃ films at 800-900°C by metal organic deposition method. It is well known that pulsed laser deposition (PLD) is a promising growth method to prepare thin films for the completely compositional consistency between a target and a deposited film, and is especially suitable for low temperature growth of thin films³⁷⁻³⁹. However, no low temperature growth of Eu doped Ga₂O₃ films have been reported up to now although there are some previous works on the growth of Eu doped Ga₂O₃ films by PLD at substrate temperature of 850°C^{40,41}.

1.3.2 Erbium doped Ga₂O₃

Er can be found in neutron-absorbing control rods. It is a key component of high-performance fiber optic communications systems, and can also help create lasers, including some used for medical purposes. On the other hand, efficient pure green light emission (~550 nm) is difficult to obtain because of the lack of semiconductors with direct bandgap in the range of 2.2-2.4 eV⁴². Similar with Eu ions, Er doped Ga₂O₃, which exhibit strong, sharp, and green emission due to intra-4*f*-shell transitions in Er ion cores, have potential applications in color display and luminescence devices. However, up to now, there is no report available related to Er doped Ga₂O₃ pure green luminescence thin films although this research is of vital importance for the future application.

1.4 Purpose and Outline

As has discussed above, we know that the luminescence efficiency of dopant emissions could be highly improved with a wide bandgap host. Moreover, the β -Ga₂O₃ exhibits highly thermal and chemical stability, which make it ideal hosts for RE ions. However, up to now, there are few reports available related to RE doped Ga₂O₃ luminescence thin films although the RE ions doped Ga₂O₃ films are expected to fabricate the efficient and stability LEDs. The purpose of this dissertation mainly includes: (1) Investigation of the growth parameter influence of the structure and optoelectronic properties of Eu and Er doped Ga₂O₃ deposited on sapphire and Si substrates by PLD. (2) Analysis of temperature dependence luminescence behavior of Eu and Er doped Ga₂O₃ to understand the energy transfer mechanism. (3) Fabrication

of the green light-emitting devices based on Ga₂O₃:Er/Si.

In Chapter 1, the background and the purpose of this study were presented.

In Chapter 2, the film growth and characterization methods were introduced.

In Chapter 3 and 4, the Eu and Er contents influence on the structure and properties of Ga₂O₃ films deposited on (0001) α -Al₂O₃ by PLD have been investigated⁴³⁻⁴⁵. The thickness of all samples was determined by a surface step profile analyzer. The structural properties of these films have been investigated by X-ray diffraction (XRD), Raman spectroscopy, and reflection high energy electron diffraction (RHEED). The optical properties of these films have been investigated by photoluminescence (PL). The surface morphology and roughness of the films were studied by atomic force microscope (AFM) on 2×2 μ m areas under ambient conditions. The element compositions in the prepared films were measured by energy dispersive spectroscopy (EDS) and X-ray photoelectron spectroscopy (XPS).

In Chapter 5, the light-emitting devices based on Ga₂O₃:Er/Si heterojunction have been fabricated. Bright green (~548 nm) emission can be observed by naked eye from Ga₂O₃:Er/Si LEDs. The current-voltage characteristics, electroluminescence (EL) spectra were measured by Advantest DC voltage current source, while the EL spectra in the visible recorded by using high sensitivity spectra multi-channel photo detector

⁴⁶.

In Chapter 6, the summary of this study was described.

References

- 1 J.-C.G Bünzli, G.R. Choppin, Lanthanide Probes in Life, Chemical and Earth Sciences; Elsevier: Amsterdam, 1989.
- 2 S.V. Eliseeva, J.-C.G. Bünzli, *New J. Chem.* 35 (2011) 1165.
- 3 V. R. Sastri, J.-C.G. Bünzli, V.R. Rao, G.V.S. Rayudu, J.R. Perumareddi, *Modern Aspects of Rare Earth and Their Complexes*; Elsevier: Amsterdam, 2003.
- 4 C. Paulo, F.L. Juliana, A.S. Osvaldo *J. Braz. Chem. Soc.* 26 (2015) 2471.
- 5 N. Poudyal, J.P. Liu, *J. Phys. D: Appl. Phys.* 46 (2013) 043001.
- 6 D. Chen, Y. Wang, M. Hong, *Nano Energy* 1 (2012) 73.
- 7 X. Huang, S. Han, W. Huang, X. Liu, *Chem. Soc. Rev.* 42 (2013) 173
- 8 T. Tanaka, M. Kuzuhara, M. Watada, M. Oshitani, *J. Alloys Compd.* 323 (2006) 408-412.
- 9 P. Wellenius, A. Suresh, J.F. Muth, *Appl. Phys. Lett.* 92 (2008) 021111.
- 10 P. Wellenius, E.R. Smith, S.M. LeBoeuf, H.O. Everitt, J.F. Muth, *J. Appl. Phys.* 107 (2010) 103111.
- 11 N. Woodward, J. Poplawsky, B. Mitchell, A. Nishikawa, Y. Fujiwara, V. Dierolf, *Appl. Phys. Lett.* 98 (2011) 011102.
- 12 P.N. Favennec, H. L'Haridon, M. Salvi, D. Moutonnet, Y. L. Guillou, *Electron. Lett.* 25 (1989) 718.
- 13 Ü. Özgür, Y.I. Alivov, C. Liu, A. Teke, M.A. Reshchikov, S. Doğan, V. Avrutin, S.-J. Cho, and H. Morkoç *J. Appl. Phys.* 98 (2005) 041301.

- 14 J.D. Albrecht, P.P. Ruden, S. Limpijumnong, W.R.L. Lambrecht, and K.F. Brennan, *J. Appl. Phys.* 86 (1999) 6864.
- 15 M. Orita, H. Ohta, M. Hirano, and H. Hosono, *Appl. Phys. Lett.* 77 (2000) 4166.
- 16 M. Higashiwaki, K. Sasaki, A. Kuramata, T. Masui, and S. Yamakoshi, *Appl. Phys. Lett.* 100 (2012) 013504.
- 17 H. Morkoç, S. Strite, G.B. Gao, M.E. Lin, B. Sverdlov, and M. Burns, *J. Appl. Phys.* 76 (1994)1363.
- 18 S. Fujita, *Jpn. J. Appl. Phys.* 54 (2015) 030101.
- 19 J. Heikenfeld, M. Garter, D.S. Lee, R. Birkhahn, A.J. Steckl, *Appl. Phys. Lett.* 75 (1999) 1189.
- 20 S. Shirakata, R. Sasaki, T. Kataoka, *Appl. Phys. Lett.* 85 (2004) 2247.
- 21 A. Nishikawa, N. Furukawa, T. Kawasaki, Y. Terai, Y. Fujiwara, *Appl. Phys. Lett.* 97 (2010) 051113.
- 22 S. Harako, S. Yokoyama, K. Ide, X. Zhao, S. Komoro, *Phys. Stat. Sol. (a)* 205 (2008) 19.
- 23 Y. Yang, Y. Li, L.L. Xiang, X.Y. Ma, D.R. Yang, *Appl. Phys. Lett.* 102 (2013) 181111.
- 24 H.L. Li, Y.B. Lv, J.Z. Li, K. Yu, *J. Alloys Compd.* 617 (2014) 102-107.
- 25 J.M. Zavada, S.X. Lin, N. Nepal, J.Y. Lin, H.X. Jiang, P. Chow, B. Hertog, *Appl. Phys. Lett.* 84 (2004) 1061.
- 26 S.D. Wolter, B.P. Luther, D.L. Waltemyer, C. Onneby, S.E. Mohny, R.J. Molnar, *Appl. Phys. Lett.* 70 (1997) 2156.

- 27 W. Wei, Z.X. Qin, S.F. Fan, Z.W. Li, K. Shi, Q.S. Zhu, G.Y. Zhang, *Nanoscale Res. Lett.* 7 (2012) 562.
- 28 S. Nakagomi, T. Momo, S. Takahashi, Y. Kokubun, *Appl. Phys. Lett.* 103 (2013) 072105.
- 29 Y. Jia, K. Zeng, J. Wallace, J. Gardella, U. Singiseti, *Appl. Phys. Lett.* 106 (2015) 102107
- 30 X.C. Guo, N.H. Hao, D.Y. Guo, Z.P. Wu, Y.H. An, X.L. Chu, L.H. Li, P.G. Li, M. Lei, W.H. Tang, *J. Alloys Compd.* 660 (2016) 136.
- 31 F.B. Zhang, K. Saito, T. Tanaka, M. Nishio, Q.X. Guo, *J. Cryst. Growth*, 387 (2014) 96.
- 32 S. Yoshioka, H. Hayashi, A. Kuwabara, F. Oba, K. Matsunaga, I. Tanaka, *J. Phys.: Condensed Matter*, 19 (2007) 346211.
- 33 M. Nakayama, S. Nakamura, H. Takeuchi, A. Koizumi, *Appl. Phys. Lett.* 106 (2015) 012102.
- 34 Y. Kashiwagi, A. Koizumi, Y. Takemura, S. Furuta, M. Yamamoto, M. Saitoh, M. Takahashi, T. Ohno, Y. Fujiwara, K. Murahashi, K. Ohtsuka, M. Nakamoto, *Appl. Phys. Lett.* 105 (2014) 223509.
- 35 J.H. Hao, M. Cocivera, *J. Phys. D: Appl. Phys.* 35 (2002) 433-439.
- 36 Y. Tokida, S. Adachi, *Jpn. J. Appl. Phys.* 52 (2013) 101102.
- 37 F.B. Zhang, K. Saito, T. Tanaka, M. Nishio, Q.X. Guo, *Appl. Phys. Lett.* 105 (2014) 162107.

- 38 F.B. Zhang, K. Saito, T. Tanaka, M. Nishio, Q.X. Guo, *Solid State Commun.* 186 (2014) 28.
- 39 X.H. Wang, F.B. Zhang, K. Saito, T. Tanaka, M. Nishio, Q.X. Guo, *J. Phys. Chem. Solids*, 75 (2014) 1201.
- 40 H.M. Zhu, R.F. Li, W.Q. Luo, X.Y. Chen, *Phys. Chem. Chem. Phys.* 13 (2011) 4411.
- 41 Y. Tokida, S. Adachi, *J. Appl. Phys.* 112 (2012) 063522.
- 42 M. Garter, J. Scofield, R. Birkhahn, A.J. Steckl, *Appl. Phys. Lett.* 74 (1999) 182-184.
- 43 Z.W. Chen, K. Saito, T. Tanaka, M. Nishio, Q.X. Guo, *J. Cryst. Growth*, 430 (2015) 28.
- 44 Z.W. Chen, X. Wang, S. Noda, K. Saito, T. Tanaka, M. Nishio, M. Arita, Q.X. Guo, *Superlattices Microstruct.* 90 (2016) 207.
- 45 Z.W. Chen, X. Wang, F.B. Zhang, S. Noda, K. Saito, T. Tanaka, M. Nishio, Q.X. Guo, *J. Lumin.* 177 (2016) 48.
- 46 Z.W. Chen, X. Wang, F.B. Zhang, S. Noda, K. Saito, T. Tanaka, M. Nishio, M. Arita, Q.X. Guo, *Appl. Phys. Lett.* 109 (2016) 022107.

Chapter 2

Epitaxial growth and characterization methods

2.1 Epitaxial growth techniques

2.1.1 Pulsed laser deposition

As one of the physical vapor deposition processes, PLD is a very convenient to fabricate the advanced oxide material films under a vacuum system. The mechanism of the PLD system can be described as follows. A pulsed laser is excited from a laser source. Then, the pulsed laser is focused onto a target of the material to be deposited in a high vacuum chamber. The target will be vaporized or ablated by each of the laser pulse if it has sufficiently high laser energy density, and thus create a plasma plume. Furthermore, the ablated materials will transfer forward until it reaches the surface of the substrate and provides materials flux for the deposition of film. In the literatures, it is known that Ga₂O₃ films have been prepared by various methods such as sputtering^{1,2}, chemical vapor deposition^{3,4}, spray pyrolysis⁵, sol-gel method⁶, molecular beam epitaxy (MBE)^{7,8}, and PLD^{9,10}. Among them, PLD method has many advantages due to completely compositional consistency between a target and a deposited film, and is especially suitable for low temperature growth of thin films for the relative high kinetic energies that the ablated species have¹¹. Moreover, PLD has another advantage for growing oxide films such as Ga₂O₃ because of the carriers generated by oxygen vacancies can be controlled by oxygen pressure in PLD¹².

Table 2.1 and Figure 2.1 show the parameters and photos of the PLD equipment in our research, respectively. In this work, the excimer laser (KrF, 248 nm) of the equipment uses combination of a noble krypton and a reactive fluorine gas. Herein, the laser frequency and energy are the important parameters during the growth of the films. From Figure 2.1, the main structure of the growth system includes a main chamber and a load chamber. We can exchange the substrate and remove the grown sample by using the load chamber. The main chamber is used for fabricating the sample. The base pressure of main chamber is in the range of $\sim 10^{-6}$ Pa. High purity oxygen gas or nitride gas (99.9999%) were introduced through mass flow controllers after the pressure of chamber was evacuated to about 10^{-6} Pa using a turbo molecular pump. The growth pressure can set from 1×10^{-5} to 10 Pa while growth temperature can range from room temperature to 650 °C. Figure 2.2 shows the films growth procedures by PLD.

Table 2.1 The parameters of PLD technique.

Parameters of PLD technique	
Laser wavelength (nm)	248
Laser frequency range (Hz)	From 1 to 10
Laser energy range (mJ)	From 80 to 225
Main chamber base pressure (Pa)	8×10^{-6}
Growth atmosphere	vacuum, High pure O ₂ , High pure N ₂ ,
Growth pressure range (Pa)	From 1×10^{-5} to 30
Growth temperature range (°C)	From room temperature to 650

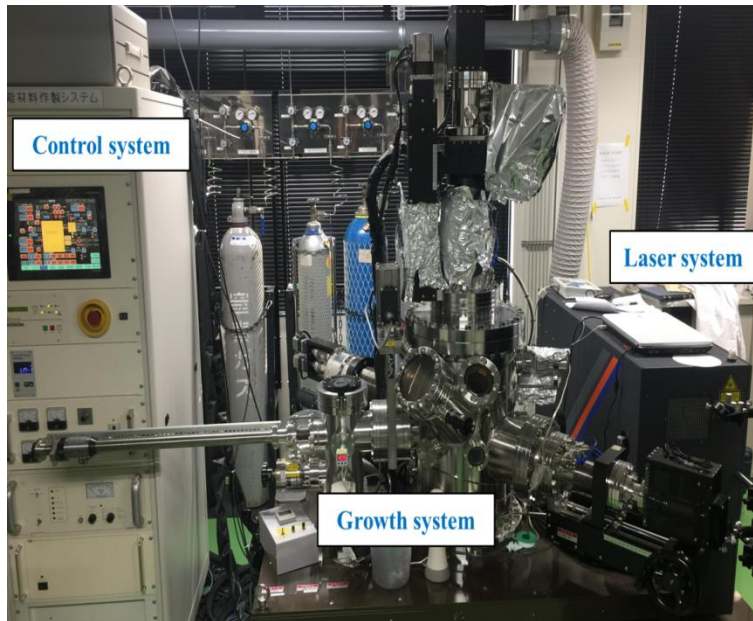


Figure 2.1 The appearance of the PLD equipment.

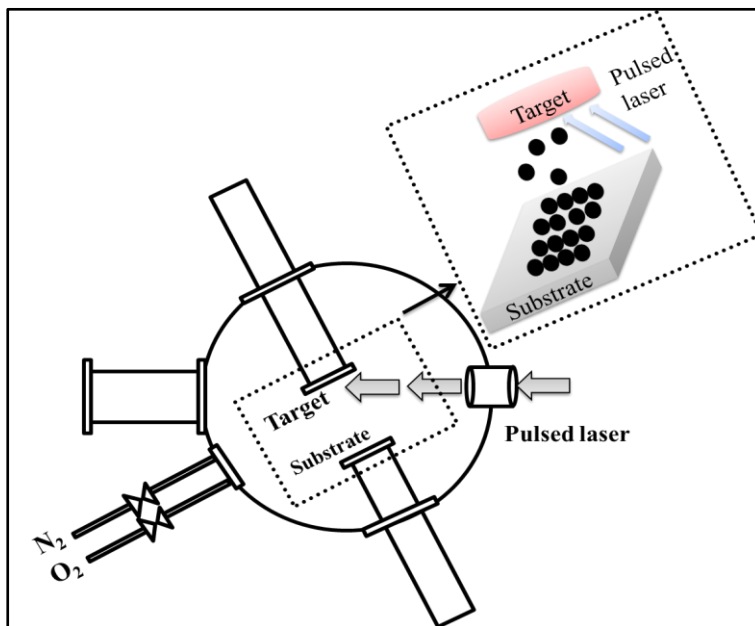


Figure 2.2 Schematic diagrams of the films growth procedures by using PLD equipment.

2.1.2 Micro-fabrication equipment

Microfabrication is the process of fabricating miniature structures of micrometer scales and smaller. Historically, the earliest microfabrication processes were used for integrated circuit fabrication, also known as semiconductor device fabrication. In this study, as shown in Figure 2.3, we use electron beam evaporated technique and direct current sputtering to fabricate the electrodes of LEDs based on $\text{Ga}_2\text{O}_3:\text{Er}/\text{Si}$ heterojunctions.

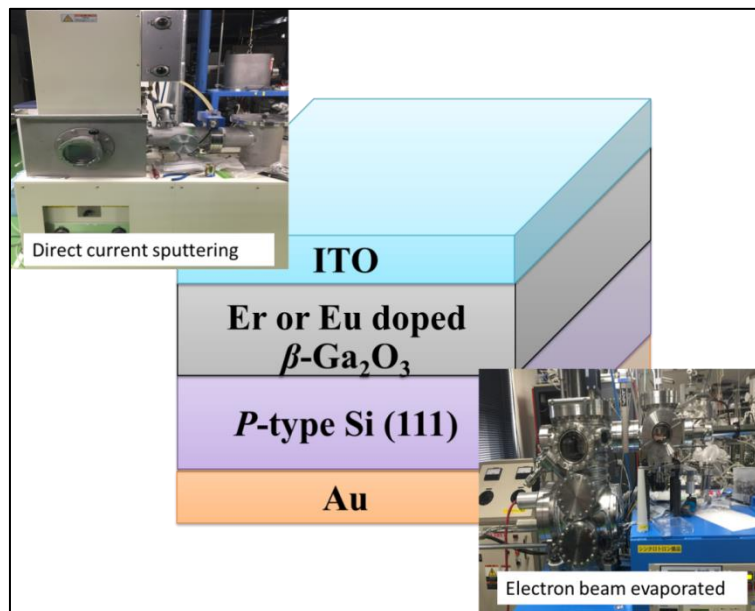


Figure 2.3 Photos of micro-fabrication equipment.

In this work, to form electrical contacts, ~200 nm thick indium tin oxide (ITO) layer onto the Er or Eu doped Ga_2O_3 films were deposited by using direct current sputtering. ~250 nm Au film on the backside of Si substrate by using electron beam evaporated technique.

2.2 Characterization methods

Herein, we present the materials characterization methods used to analyze the thickness, surface morphology, chemical composition, crystallization, optoelectronic properties of the films. Each technique is described in the individual subheading below.

2.2.1 Surface step profile analyzer

Figure 2.4 shows the outlook of the surface step profile analyzer equipment. The thickness of the films was determined by measuring the thickness difference between the substrate surface and the film surface. Generally, we take the average after several measurements, which will give more accurate characterization of the thickness of the film.

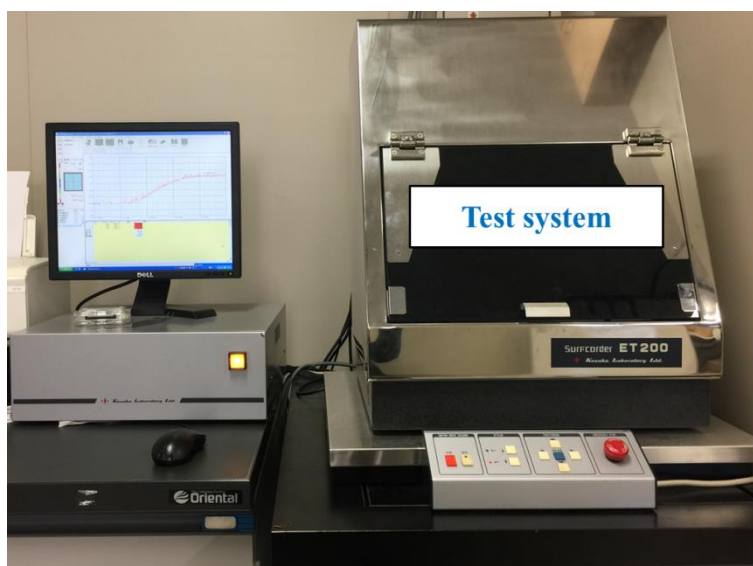


Figure 2.4 Outlook of the surface step profile analyzer equipment.

2.2.2 X-ray diffraction (XRD)

X-ray diffraction (XRD) is a rapid non-destructive analytical technique which primarily used for phase identification of a crystalline material; it can also provide information on unit cell dimensions. By observing the scattered intensity of an X-ray beam hitting a sample as a function of incident angle, one can obtain the information about the crystallization, chemical composition and physical properties.

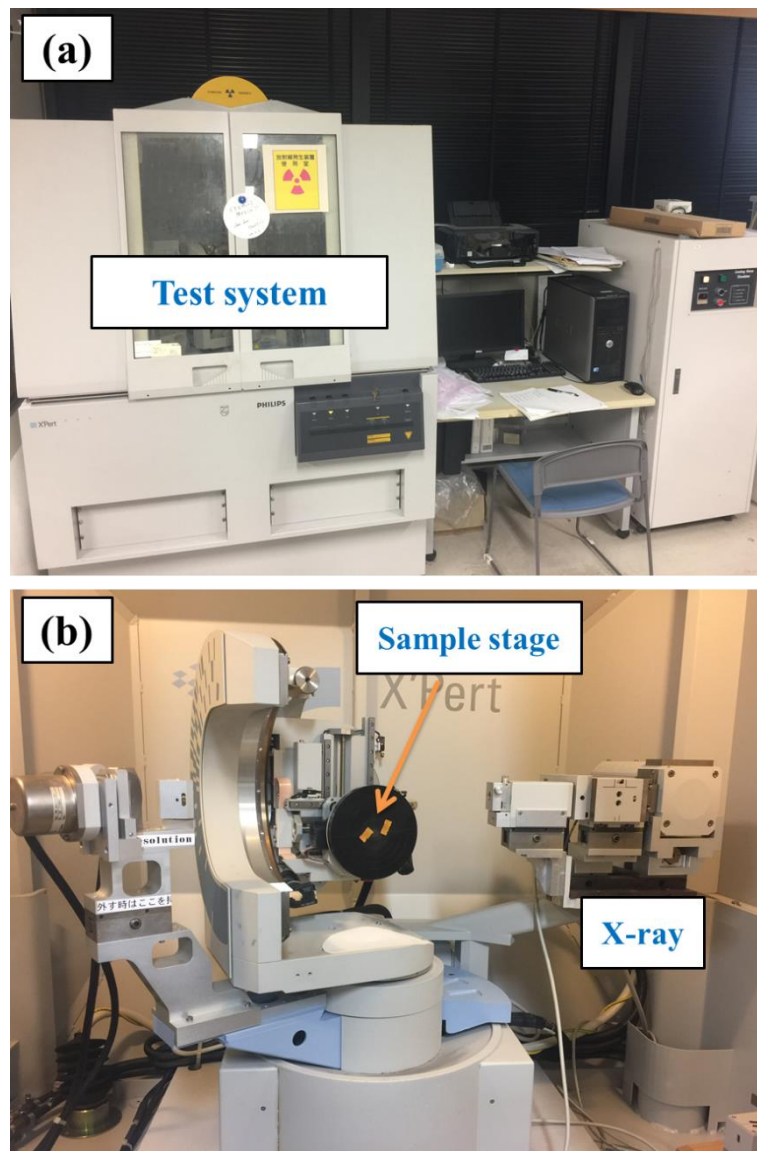


Figure 2.5 Photos (a) and inside (b) of the XRD equipment.

2.2.3 Atomic Force Microscopy (AFM)

In this research, the non-contact AFM was used to characterize the surface morphologies. The outlook of the AFM equipment is shown in Figure 2.6. In the measure process of the AFM, a probe (sharp tip) was used to scan the surface of the sample by measuring forces between the probe and the surface at a very short distance. The topographic image of the surface is produced by recording the variations of the probe height above the surface while the probe is scanned repeatedly across the surface.

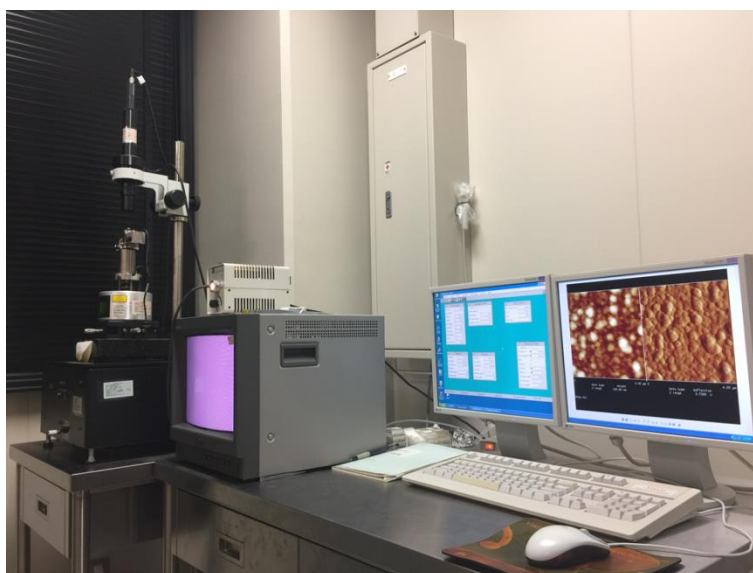


Figure 2.6 Outlook of the AFM equipment.

2.2.4 Photoluminescence (PL)

PL is light emission from any form of matter after the absorption of photons. It is one of many forms of light emission and is initiated by photoexcitation. Typically, a semiconductor is excited with a light-source that provides photons with energy larger than the bandgap energy. Once the photons are absorbed, electrons and holes are formed with finite momenta k in the conduction and valence bands, respectively. The

excitations then undergo energy and momentum relaxation towards the band gap minimum. Finally, the electrons recombine with holes under emission of photons. In this work, the PL measurements were performed on a Horiba Jobin Yvon LabRAM HR 800 system equipped with an Andor DU420 classic charge-coupled device detector. The PL experiments were carried out using a Kimmon Koha He–Cd laser (325 nm) and argon ion laser (488 nm) as the excitation source. We study temperature dependence of PL (TDPL) spectra to search for new luminescence devices at high temperature and phosphors with high quantum efficiency. A Microstat^{HE} hot/cold stage (Oxford instruments) with quartz window was used to heat the films from 77 to 550 K under flowing nitrogen. The temperature was controlled by a *K*-type thermocouple which has an accuracy of better than ± 1 K. For each measurement point, the temperature was kept for 10 min to avoid temperature fluctuations before acquiring a spectrum for 15 min. The outlook of the PL equipment and TDPL system are shown in Figure 2.7.

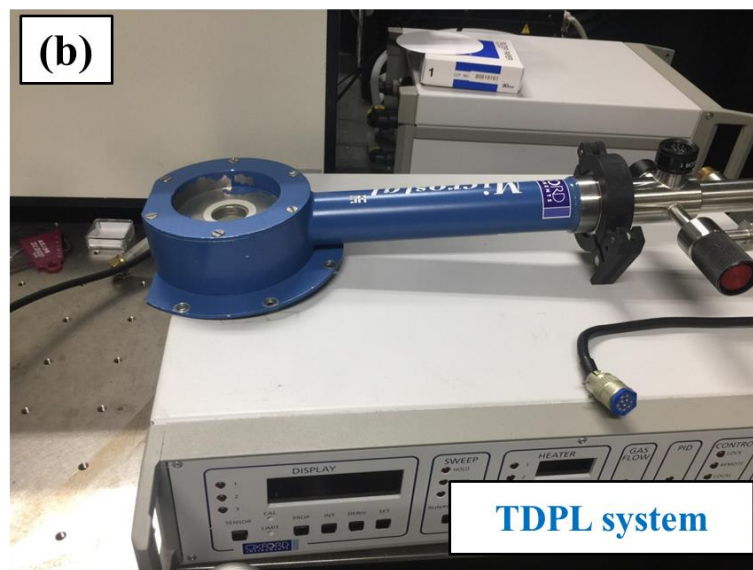
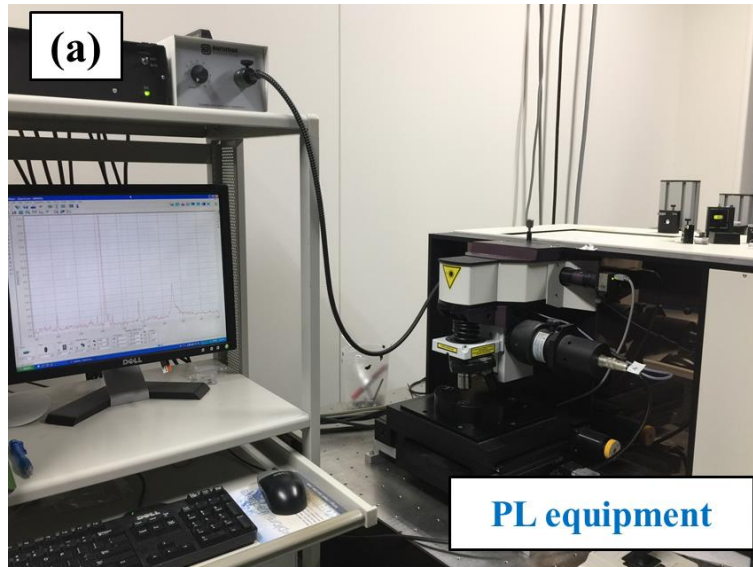


Figure 2.7 Photos of PL equipment (a) and TDPL system (b).

2.2.5 Current-voltage (I - V) characteristics and electroluminescence (EL)

Figure 2.8 shows the outlook of current-voltage (I - V) equipment (a) and electroluminescence (EL) system (b). The current-voltage (I - V) characteristics, electroluminescence (EL) spectrum are measured by Advantest DC voltage current source (R6364), while the EL spectra in the visible recorded by using high sensitivity spectra multi-channel photo detector (MCPD-7000).

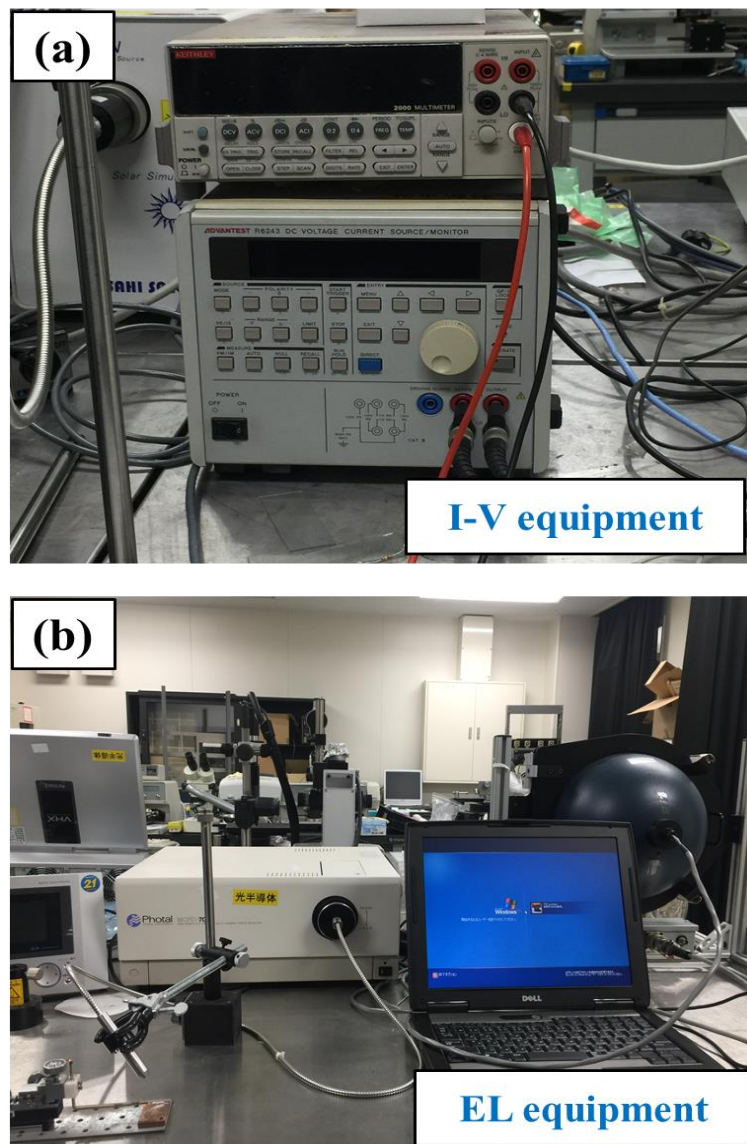


Figure 2.8 The outlook of current-voltage (I - V) equipment (a) and electroluminescence (EL) system (b).

2.2.6 Other characterization methods

The deposited film was characterized using X-ray photoelectron spectroscopy (XPS) to illustrate the chemical compositions and chemical state. XPS spectra are obtained by irradiating a material with a beam of X-rays while simultaneously measuring the kinetic energy and number of electrons that escape from the top 0 to 10 nm of the material being analyzed. In this work, the XPS experiments were done in Kyusyu University, Japan. The XPS measurements were performed using Al K α and Mg K α X-ray source. The surface of the sample was Ar ion (3 keV) etched for 2 min before XPS analysis. The resolution of the peak position of XPS spectra was estimated to be 0.1 eV. The binding energy of C 1s peak (287.2 eV) was used as a standard reference.

The elements composition in the prepared films was measured by energy dispersive spectroscopy (EDS). Scanning electron microscopy (SEM) with built-in EDS analysis capability was used for morphological characterization and to measure the elements composition. The system used in Philips XL30 FEG SEM, a field emission high resolution SEM which can be operated both at low accelerating voltage (200 V) and high accelerating voltage (30 kV).

Optical transmission measurements were carried out to confirm the transmittance and the bandgap of the films. Herein, we measured the room temperature optical transmission spectra by using Jasco V-570 spectrophotometer.

References

- 1 M. Fleischer, W. Hanrieder, H. Meixner *Thin Solid Films*, 190 (1990) 93.
- 2 L. Jianjun, Y. Jinliang, S. Liang, L. Ting, *J. Semicond.*, 31 (2010) 103001.
- 3 C.-Y. Huang, R.-H. Horng, D.-S. Wu, L.-W. Tu, H.-S. Kao, *Appl. Phys. Lett.* 102 (2013) 011119.
- 4 D. Shinohara, S. Fujita, *Jpn. J. Appl. Phys.* 47 (2008) 7311.
- 5 A. Ortiz, J.C. Alonso, E. Andrade, C. Urbiola, *Jpn. J. Appl. Phys.* 148 (2001) F26.
- 6 Y. Kokubun, K. Miura, F. Endo, S. Nakagomi, *Appl. Phys. Lett.* 90 (2007) 031912.
- 7 T. Oshima, T. Okuno, N. Arai, N. Suzuki, S. Ohira, S. Fujita, *Appl. Phys. Express* 1 (2008) 011202.
- 8 T. Oshima, T. Okuno, S. Fujita, *Jpn. J. Appl. Phys.* 46 (2007) 7217.
- 9 H. Hayashi, R. Huang, F. Oba, T. Hirayama, I. Tanaka, *J. Mater. Res.* 26 (2011) 578.
- 10 K. Matsuzaki, H. Hiramatsu, K. Nomura, H. Yanagi, T. Kamiya, M. Hirano, H. Hosono, *Thin Solid Films* 496 (2006) 37.
- 11 M.J. Aziz, *Appl. Phys. A* 93 (2008) 579.
- 12 M. Orita, H. Ohta, M. Hirano, H. Hosono, *Appl. Phys. Lett.* 77 (2000) 4166.

Chapter 3

Growth and characterization of Eu doped Ga₂O₃ films

3.1 Eu content influence

3.1.1 Introduction

Eu doped semiconductors, which exhibit strong and sharp, red emission around 610 nm due to intra-4*f*-shell transitions in Eu ion cores, have been intensively studied for their potential use in efficient light emitting diodes¹⁻⁴. Historically, GaN has been used as a host for RE elements because its large bandgap (3.4 eV) and sufficient carrier mean path⁵⁻⁹. It has been reported that the luminescence efficiency of dopant emissions could be highly improved with a wide bandgap host^{10,11}. Moreover, the wide bandgap semiconductors exhibit highly thermal and chemical stability, which make them ideal hosts for Eu ions^{12,13}. Recently, β -Ga₂O₃ with wider bandgap (4.9 eV) than that of GaN has attracted tremendous attention as a host material for phosphors in display applications¹⁴⁻²².

Various growth techniques have been tried to fabricate Eu doped Ga₂O₃ films. Hao *et al.*¹⁷ have grown Eu doped β -Ga₂O₃ films by using spray pyrolysis and annealing at 600-900 °C. Tokida *et al.*¹⁸ fabricated Eu doped Ga₂O₃ films at 800-900°C by metal organic deposition method. It is well known that PLD is a promising growth method to prepare thin films for the completely compositional consistency between a target and a deposited film, and is especially suitable for low temperature growth of thin films²³⁻²⁶. However, no low temperature growth of Eu

doped Ga₂O₃ films have been reported up to now although there are some previous works on the growth of Eu doped Ga₂O₃ films by PLD at substrate temperature of 850°C^{19,20}.

In this Chapter, we present on the low temperature growth of Eu doped Ga₂O₃ films by PLD at substrate temperature as low as 500 °C. Intense red emissions at 613 nm are clearly observed for the Eu doped Ga₂O₃ films.

3.1.2 Experiment

It is known that the Eu doped semiconductor materials and devices are typically fabricated with dopant concentrations on the order of a few atomic percent ¹⁶. A phenomenon called concentration quenching means that increasing dopant concentration results in increased optical intensity from the films or devices but beyond a critical concentration the luminescence intensity and radiative lifetimes abruptly decrease. Therefore, the Eu content mainly plays too important roles in the PLD process. On the other hand, we have fabricated the high quality (-201) oriented pure Ga₂O₃ films at 500 °C by using PLD ²⁵. In this work, as shown in Table 3.1, Eu doped Ga₂O₃ thin films were grown on (0001) sapphire substrates by PLD method using a KrF excimer laser source with a frequency of 2 Hz and an energy of 225 mJ. The (0001) sapphire substrates were cleaned ultrasonically in organic solvents, chemically etched in a hot H₂SO₄ : H₃PO₄ (3:1) solution, and then rinsed in deionized water before they were introduced into the growth chamber. Facing the substrate, bulks (diameter of 20 mm) with different Eu contents in the target were used as targets. The distance between target and substrate is about 40 mm. High purity oxygen gas (99.9999%) were introduced through mass flow controllers after the pressure of chamber was evacuated to below 10⁻⁶ Pa using a turbo molecular pump. The target was rotated during the growth to avoid crater formation. The oxygen pressure was set at 1 × 10⁻¹ Pa while substrate temperatures at 500 °C. The deposition time was 180 minutes for all samples.

Table 3.1 Growth conditions for Eu content influence

Growth conditions	
Targets	0.2, 0.5, 1.0, 3.0 wt. % Eu doped Ga ₂ O ₃
Substrate	α -Al ₂ O ₃ (0001)
Oxygen pressure (Pa)	1×10^{-1}
Growth temperature (°C)	500
Laser frequency (Hz)	2
Distance from target to substrate (mm)	40

After deposition, the thickness of all samples was determined by a surface step profile analyzer. The elements composition in the prepared films was measured by EDS. The structural properties of the films were examined by conventional θ - 2θ scan XRD using $K\alpha$ emission line of copper. The optical transmission spectra were measured with a spectrophotometer. The surface morphology and roughness of the films were studied by AFM on $2 \times 2 \mu\text{m}$ areas under ambient conditions. Raman and PL measurements were performed on a Horiba Jobin Yvon LabRAM HR 800 system equipped with an Andor DU420 classic charge-coupled device detector. Both of experiments were carried out using an Ar laser operating at a wavelength of 488 nm as the excitation source.

3.1.3 Results and discussion

Figure 3.1 shows the influence of Eu content in the targets on the growth rate of Ga_2O_3 films. The growth rate is obtained by the thickness of the films considering the deposition time. The growth rate decreases with increasing of Eu contents. It can be attributed to the significant difference of vapor pressure between Eu and Ga species. The results suggest that the Ga species have a higher vapor pressure and can be desorbed more easily than that of Eu species at same growth temperature.

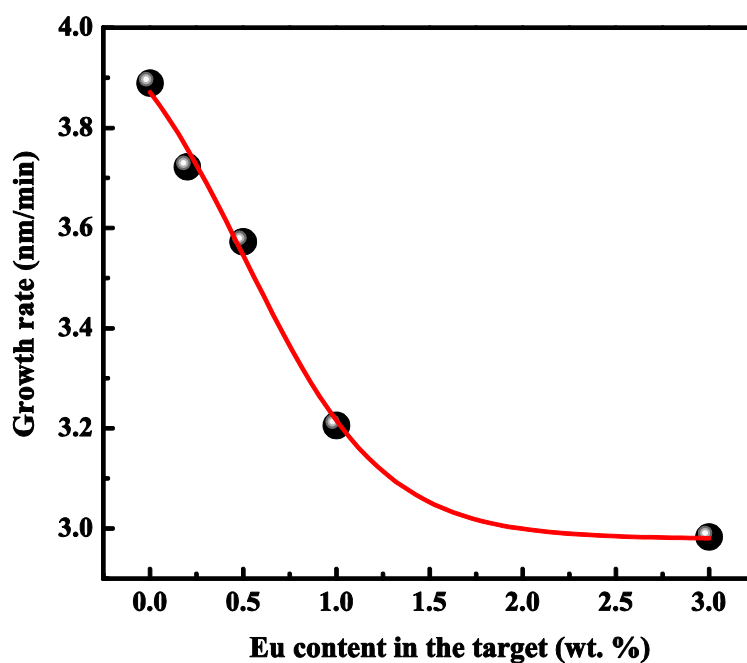


Figure 3.1 Influences of Eu content on growth rate of Ga_2O_3 films

Figure 3.2 (a) presents the EDS of Ga₂O₃ films with various Eu contents ($x_{tar.}$) of the targets. From the spectra, elements of oxygen, gallium and europium are observed. It is clear that the Eu peak intensity increases with the increase of Eu content of the targets. The Eu content in Ga₂O₃ films obtained from the EDS spectra by using a cobalt standard specimen is shown in Fig. 3.2 (b) as a function of Eu content of the targets. From Fig.3.2 (b) we find that the Eu contents in the films increases almost linearly with the increase of Eu contents of the targets. This fact suggests that the Eu doping amount in Ga₂O₃ films can be controlled by adjusting the Eu contents in the targets.

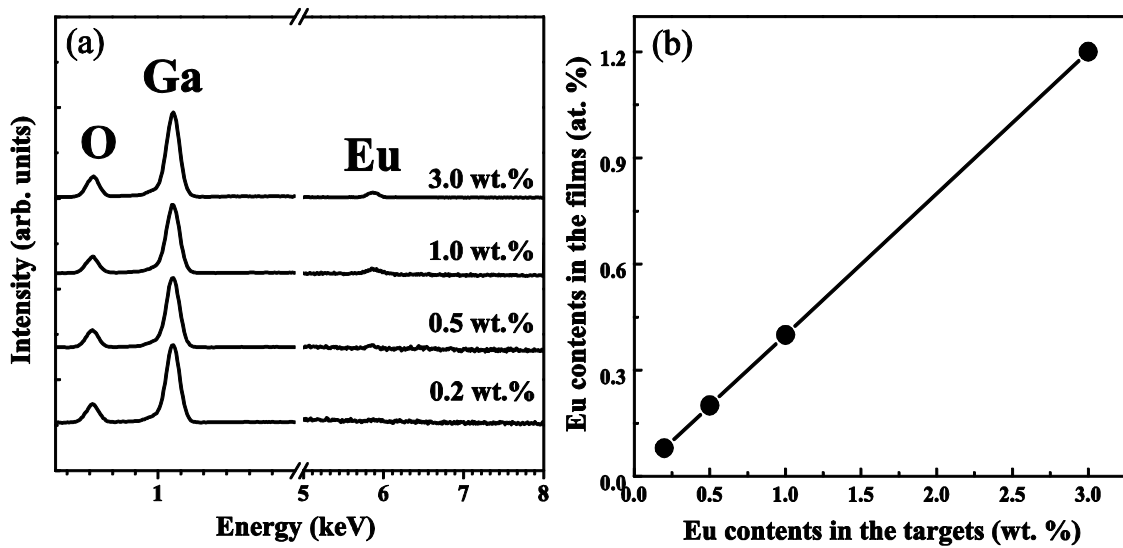


Figure 3.2 (a) EDS of Ga₂O₃ thin films deposited with different Eu contents of the targets (0.0, 0.2, 0.5, 1.0 and 3.0 wt. %). (b) Eu contents in the films as a function of the Eu contents of the targets.

Figure 3.3 (a) shows the XRD patterns of Ga₂O₃ films with different Eu contents. Three peaks are clearly observed 18.89 °, 38.05 °, 58.93 ° which can be assigned as the (-201), (-402), and (-603) planes of monoclinic Ga₂O₃, respectively by comparing measured diffraction data with known diffraction peaks listed in the International Center for Diffraction Data catalog. These results identify an epitaxial relationship with (-201) of β-Ga₂O₃ || (0001) sapphire substrate. Similar results were reported in the literatures^{14,23,27}. As shown in Fig 3.3 (b), the (-402) diffraction peak shifts to a lower diffraction angle with increasing Eu contents. Since the ion radius of Eu³⁺ of 0.95 Å is larger than that of Ga³⁺ of 0.62 Å (octahedral mode coordination) and 0.47 Å (tetrahedral mode coordination), the most probable site for the Eu³⁺ ions substitution is believed to be on the octahedral sites of β-Ga₂O₃²⁸. The incorporation of Eu into β-Ga₂O₃ in a form of Eu³⁺ substituting for Ga³⁺ will increase lattice constants of β-Ga₂O₃ which results in the (-402) diffraction peak shifts to the lower angle. It should be noted that the (004) peak of β-Ga₂O₃ appears for the Eu doped β-Ga₂O₃ samples. This is ascribed to the significant difference in ionic radii between Eu and Ga. The incorporation of Eu into Ga₂O₃ film leads to degradation of crystal quality¹⁶.

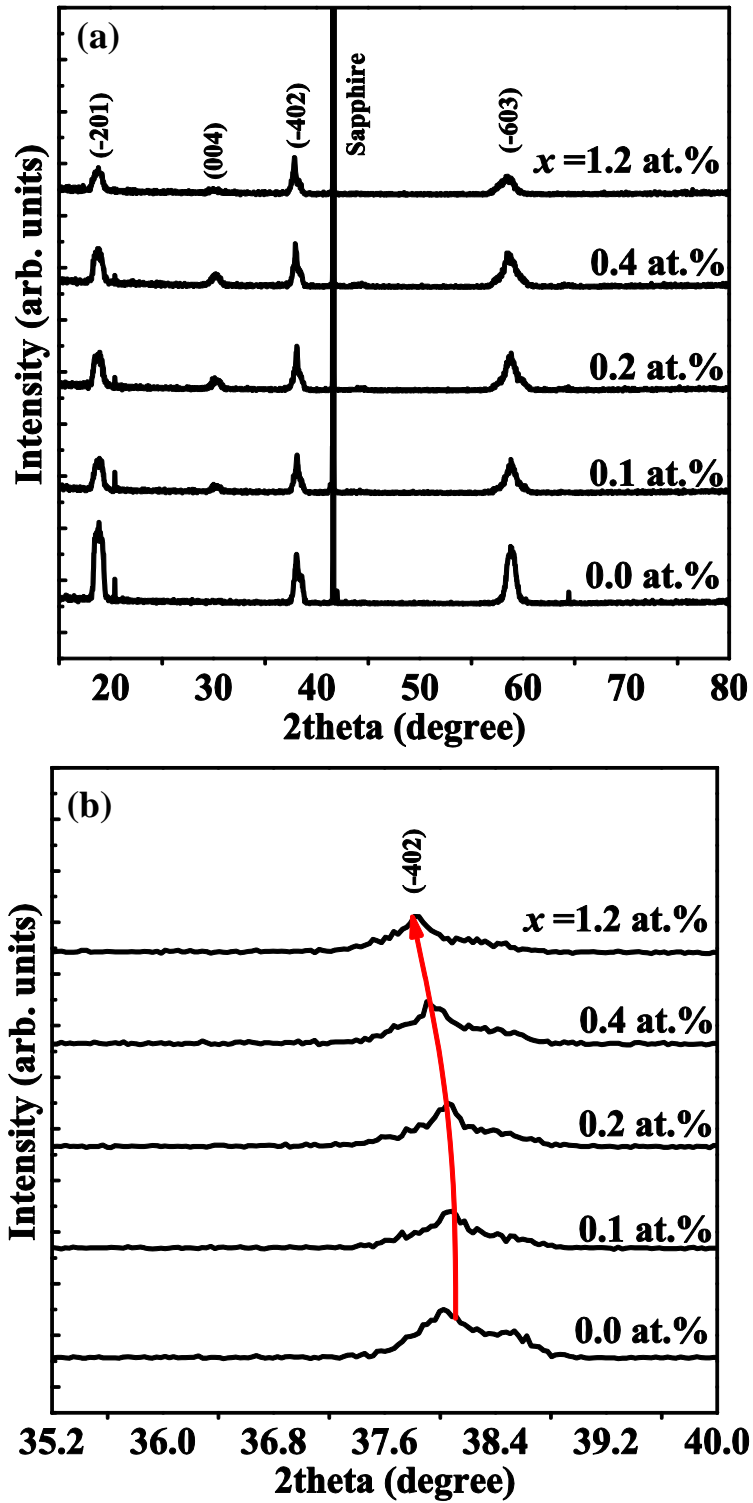


Figure 3.3 (a) XRD patterns of Ga₂O₃ thin films with different Eu doping contents. (b) The corresponding XRD profiles of the near (-402) peaks.

Figure 3.4 displays the Raman spectra obtained at room temperature for Ga₂O₃ films with different Eu contents. Five phonon modes located at 144, 168, 199, 346 and 658 cm⁻¹ are observed for all films. No obvious peak shift is found for the films with different Eu contents. The Raman mode frequencies obtained in this work are summarized in Table 3.2 together with those for bulk β -Ga₂O₃ sample reported by Dohy *et al.*²⁹. The Raman frequencies for β -Ga₂O₃ are classified in three groups of vibrations related with librations and translations (low frequency mode up to ~200 cm⁻¹) of tetrahedral-octahedral chains, vibrations of deformed Ga₂O₆ octahedral (mid frequency modes within 310-480 cm⁻¹) and stretching/bending of GaO₄ tetrahedral (high frequency modes: 550-770cm⁻¹). From Table 3.2, it is clear that the Raman frequencies for Ga₂O₃ films have good agreement with the values of bulk β -Ga₂O₃, verifying that the Ga₂O₃ films with different Eu contents obtained in this work are of monoclinic β -Ga₂O₃ structure which is consistent with the XRD results.

Table 3.2 Comparison of Raman mode frequencies with those measured in β -Ga₂O₃ bulk²².

Mode symmetry	This work (cm ⁻¹)	Bulk β -Ga ₂ O ₃ (cm ⁻¹)
B_g	144	147
A_g	168	169
A_g	199	199
A_g	346	346
A_g	658	657

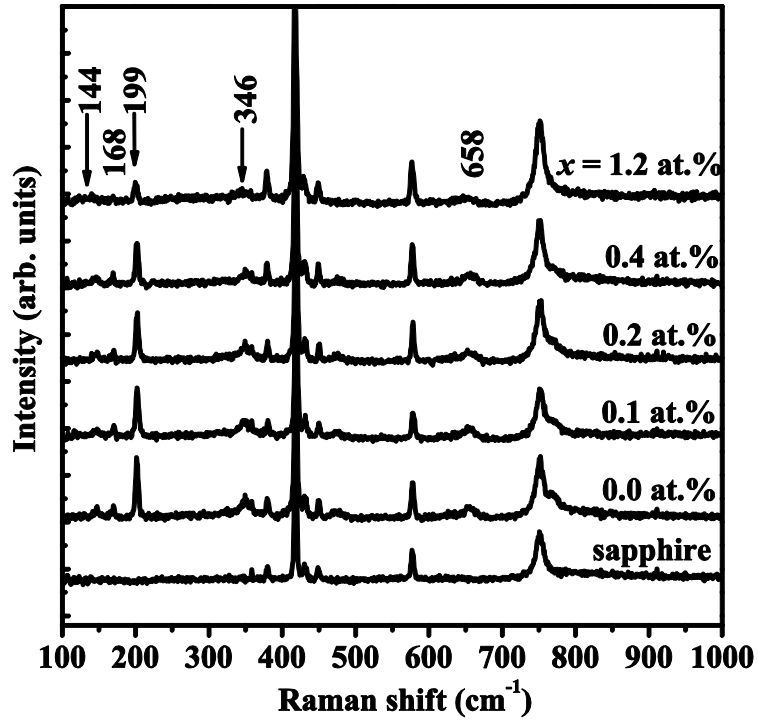


Figure 3.4 Raman spectra of Ga₂O₃ thin films with different Eu doping contents.

Optical transmission measurements were carried out to confirm the bandgap of the films. Fig. 3.5 (a) shows the room temperature optical transmission spectra of Ga₂O₃ films with different Eu contents. All the films have a high transmittance more than 90% in the visible region and 80% in the UV region (280-400 nm). The high transmittance indicates that the high quality Eu doped Ga₂O₃ films can be realized by PLD at substrate temperature as low as 500°C. The spectra of the pure Ga₂O₃ exhibit a sharp intrinsic absorption edge at wavelength of 250 nm, whilst those of Eu doped films shift towards longer wavelength with the increasing Eu contents. The bandgap obtained by extrapolating the linear region of the plot $(ahv)^2$ versus $h\nu$, as shown in the inset of Fig. 3.5 (b) decreases from 4.99 eV for pure β -Ga₂O₃ to 4.85 eV for doped Ga₂O₃ film with 1.2 at.% Eu content. The decrease of the bandgap is ascribed to new

unoccupied electron states in the gap below the conduction band edge due to the incorporation of Eu ions on the substitutional sites of Ga_2O_3 ²².

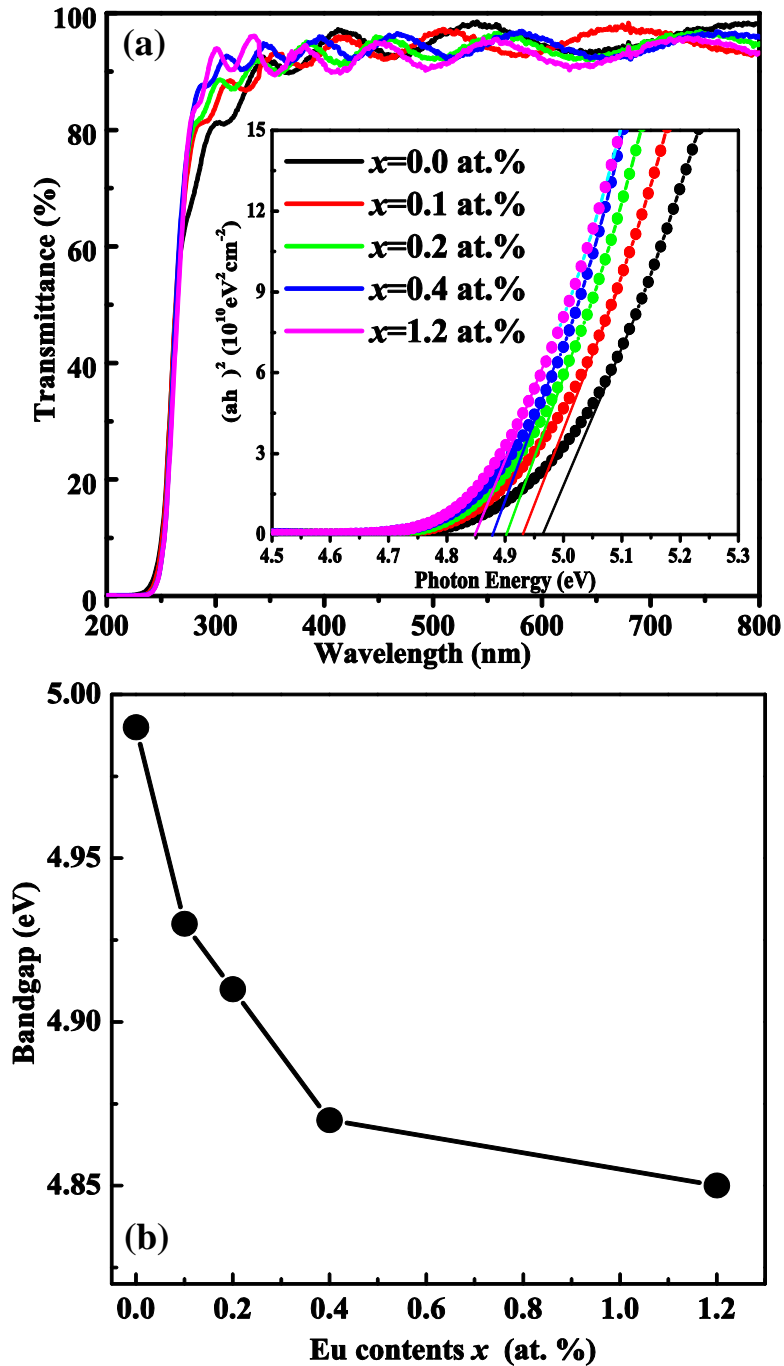


Figure 3.5 Transmittance spectra of Ga_2O_3 thin films with different Eu doping contents, and the plot of $(\alpha h\nu)^2$ versus $h\nu$ in the inset. (b) Bandgap dependence on Eu doping contents.

Figure 3.6 shows the $2 \times 2 \mu\text{m}$ AFM images for $\beta\text{-Ga}_2\text{O}_3$ thin films with different Eu doping contents. It is clear that the morphology changes with different Eu doping contents. As the Eu contents increases, the resulting morphology transform from slim needle like structure into islands structure. The surface root-mean-square (RMS) roughness becomes higher with the increase of Eu doping contents. The maximum roughness of the films is below 9 nm, indicating the films have smooth surface.

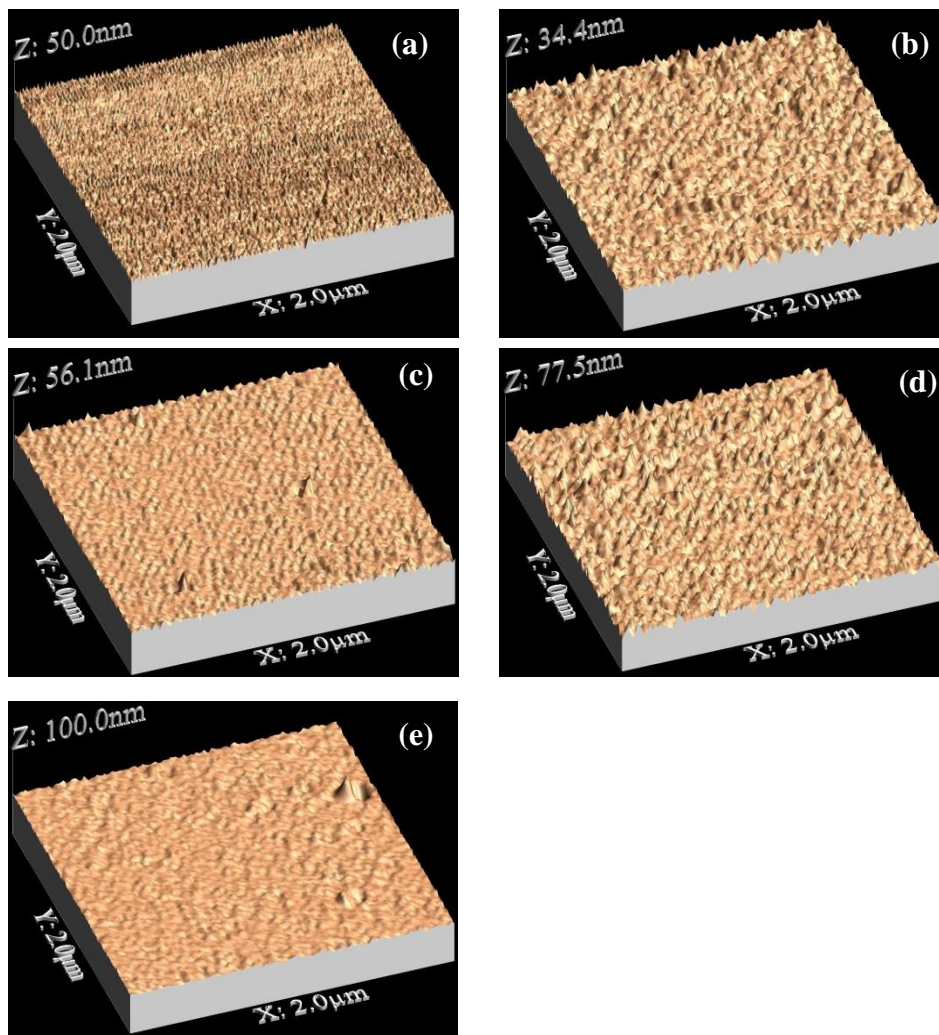


Figure 3.6 AFM images of Ga_2O_3 films with different Eu doping contents, (a) 0.0, (b) 0.1, (c) 0.2, (d) 0.4 and (e) 1.2 at. %, respectively.

Figure 3.7 (a) shows the PL spectra of Ga₂O₃ thin films with different Eu contents measured by using an Ar laser (488 nm) as the excitation source. PL spectra for the Eu doped Ga₂O₃ films demonstrate characteristic europium ion emission with the strongest peak at 613 nm which is caused by the ⁵D₀ to ⁷F₂ transition¹⁶. It is clear that the intensity for the peak observed at 613 nm increases remarkably with increasing Eu doping content in the Ga₂O₃ films as shown in Fig. 3.7 (a). The asymmetric shape of the emission peak with a shoulder at longer wavelength is ascribed to Stark splitting because the ⁵D₀ to ⁷F₂ transition is highly sensitive to local fields due to the large change in the angular orbital quantum number¹⁶. Other weak PL peaks observed at 543, 580, 599, 663, and 710 nm can be assigned to the transitions from ⁵D₁→⁷F₁, ⁵D₀→⁷F₀, ⁵D₀→⁷F₁, ⁵D₀→⁷F₃, and ⁵D₀→⁷F₀, respectively⁵. The energy transfer process between Ga₂O₃ host and Eu ion as shown in Fig. 3.7 (b) can be explained as follows. Since the excitation energy of incident light (2.54 eV) used for measurement in this work is lower than the bandgap of Ga₂O₃ (4.9 eV), the electrons are excited from the valence band to the donor band (oxygen vacancy) by the laser light source. The related energy due to the recombination of electrons in the defect state with the photogenerated holes can transfer to the excited states of Eu ions, which results in the emissions observed in Fig. 3.7 (a)^{5,22}. Here, it is worth to note that the intensity of the XRD peaks of β-Ga₂O₃ in Fig. 3.3 (a) decreases with increasing Eu contents, which should lead to the decrease of the emission intensity. However, the emission intensity of the Eu doped films increases with the increase of Eu content as shown in Fig. 3.7 (a). The results indicate that the emission intensity of

the films is mainly determined by the amount of formation of Eu_2O_3 in this work.

Similar phenomenon has been observed in Eu doped GaN thin films²³.

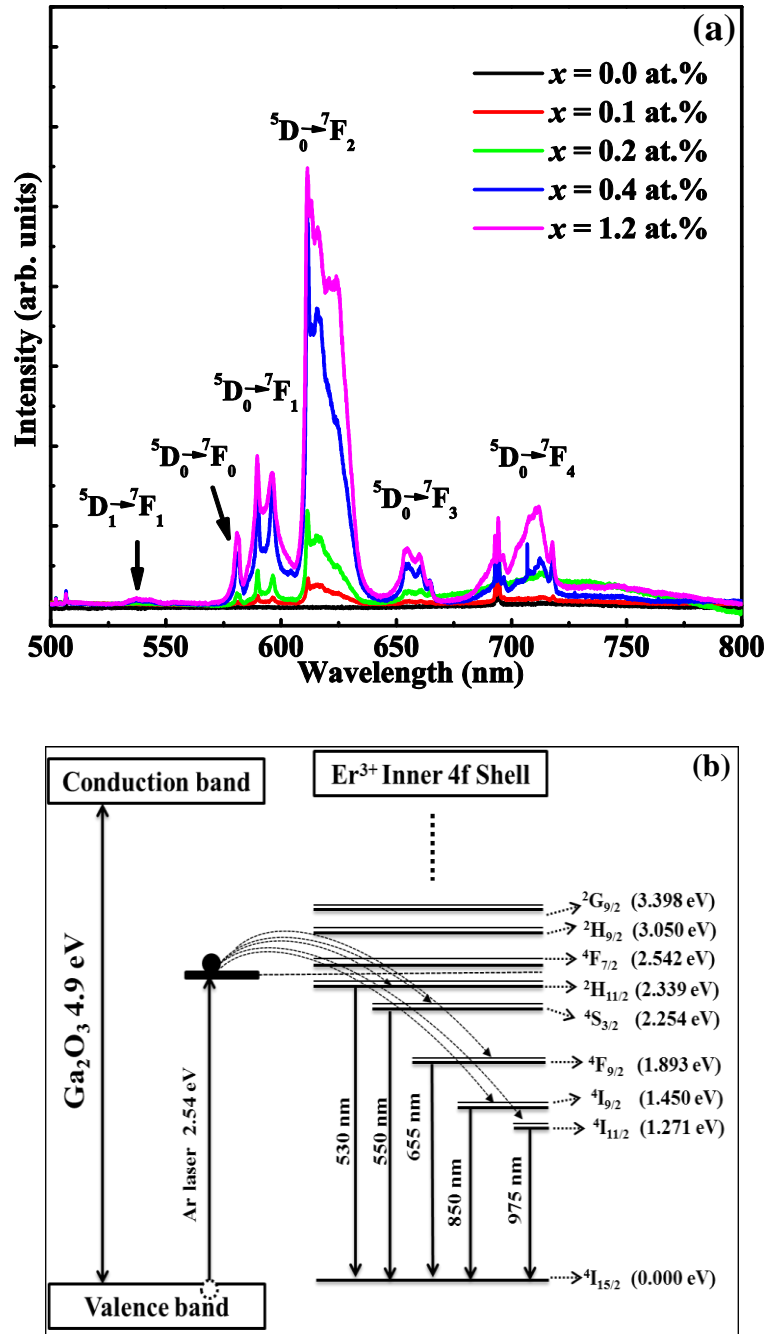


Figure 3.7 (a) PL spectra of Ga₂O₃ thin films with different Eu doping contents. (b) Energy diagram of Ga₂O₃ and Eu and the proposed mechanisms for laser excitation less than 488 nm.

We have grown Ga_2O_3 films on sapphire substrates by PLD with varying Eu contents at substrate temperature as low as 500°C . XRD and Raman spectra analysis indicated that all films have the monoclinic structure with a preferable (-201) orientation. However, it should be noted that the (004) peak of $\beta\text{-Ga}_2\text{O}_3$ appears for the Eu doped $\beta\text{-Ga}_2\text{O}_3$ samples. As we know, the (-201) oriented films in which the b axis is parallel to the substrate is demonstrated to enhanced the conductivity of the $\beta\text{-Ga}_2\text{O}_3$ film. Therefore, it is necessary to fabricate a high quality single (-201) oriented $\beta\text{-Ga}_2\text{O}_3$ films. The substrate temperature plays an important role in PLD deposition process. The films grown at different substrate temperatures will be discussed in the next Chapter.

3.2 Substrate temperature influence

3.2.1 Introduction

Overcoming intensity quenching and increasing the effective number of optically active Eu ion in the host will be necessary to make the devices useful³⁰. However, temperature dependence luminescence behavior of Eu doped Ga₂O₃ has not been reported up to now, which is significant for understanding of the non-radiative and radiative transition process. The process is helpful to search for new luminescence devices at high temperature and phosphors with high quantum efficiency^{31,32}. In this section, we study temperature dependence of luminescence spectra in Eu doped Ga₂O₃ film by using 325 and 488 nm as the excitation source. It is demonstrated that the variation of the emission intensity may be attributed to the thermal activated distribution of electrons among ⁷F_{*j*} and thermal quenching effect.

3.2.2 Experiment

Experiment details have been reported in Chapter 3.1.2. Herein, as show in Table 3.3, bulk with 3 wt. % Eu contents is used as target. The films were grown at various substrate temperatures from 200 to 600 °C.

Table 3.3 Growth conditions for substrate temperature

Growth conditions	
Targets	3.0 wt. % Eu doped Ga ₂ O ₃
Substrate	α -Al ₂ O ₃ (0001)
Oxygen pressure (Pa)	1 × 10 ⁻¹
Growth temperature (°C)	200, 300, 400, 500, 600
Laser frequency (Hz)	2
Distance from target to substrate (mm)	40

After deposition, the elements composition in the prepared films was measured by EDS. The structural properties of the films were examined by conventional θ - 2θ scan XRD using K α emission line of copper and reflection high-energy electron diffraction (RHEED) technique using a 15 KeV electron gun. PL measurements were performed on a Horiba Jobin Yvon LabRAM HR 800 system equipped with an Andor DU420 classic charge-coupled device detector. The PL experiments were carried out using a Kimmon Koha He–Cd laser (325 nm) and argon ion laser (488 nm) as the excitation source. A Microstat^{HE} hot/cold stage (Oxford instruments) with quartz window was used to heat the films from 77 to 550 K under flowing nitrogen. The temperature was controlled by a k -type thermocouple which has an accuracy of better than ± 1 K. For each measurement point, the temperature was kept for 10 min to avoid temperature fluctuations before acquiring a spectrum for 15 min.

3.2.3 Results and discussion

The growth rate of Eu doped Ga_2O_3 films grown at different substrate temperatures are shown in Figure 3.8. The growth rate increases with the substrate temperature from 200 to 400 °C. When the substrate temperature is higher than 400 °C, the growth rate decrease rapidly, which can be attributed to re-evaporation of the adsorbed species on the surface of the substrate³³.

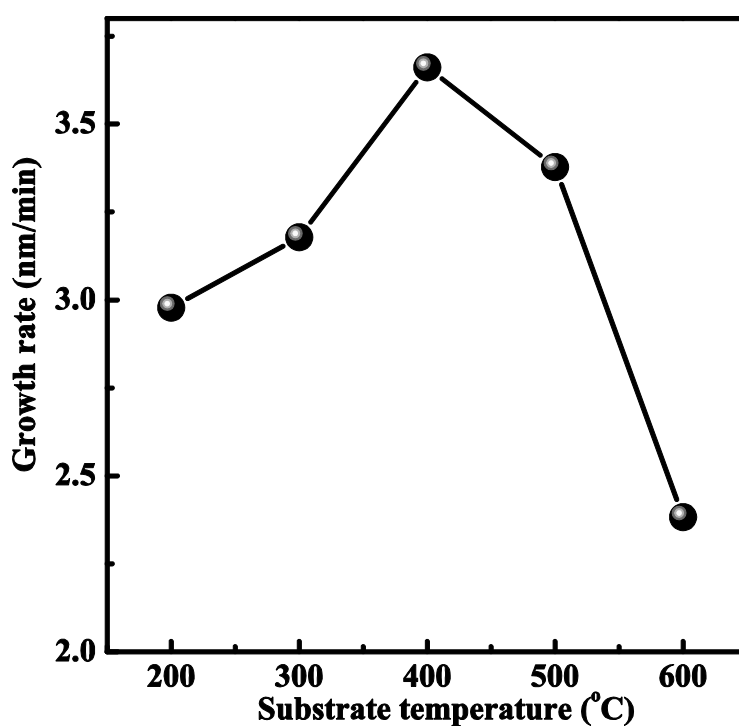


Figure 3.8 Influences of substrate temperature on growth rate of Eu doped Ga_2O_3 films.

XRD measurements were carried out to confirm the crystallization of Eu doped Ga₂O₃ films grown at different substrate temperatures as shown in Fig. 3.9. It is found that the diffraction peak of the films cannot be detected when substrate temperature is lower than 200 °C, indicating the films are of amorphous structure. With increasing the substrate temperature to 400 °C, three peaks are clearly observed 18°, 38° and 58° which can be assigned as the (-201), (-402), and (-603) planes of monoclinic Ga₂O₃ (β -Ga₂O₃), respectively²³. It is indicated that single (-201) oriented β -Ga₂O₃ can be obtained at substrate temperature of 400 °C. As the substrate temperature increases to 600 °C, extra diffraction peak of (004) of Ga₂O₃ phase appear and the intensity of the peaks corresponding to Ga₂O₃ (-201) plane decreases, featuring a polycrystalline nature. The corresponding RHEED images for the films are shown in the insert of Fig. 3.9. Since the RHEED pattern is homogenous without spots, arcs or streaks, the film grown at 200 °C is an amorphous structure. With the substrate temperature increase to 400 °C, the film is single crystal, because sharp diffraction spots are observed in RHEED patterns. At 500 °C, the RHEED pattern consists of short arcs and rings, demonstrating that crystalline quality of the film was deteriorated. Furthermore, the pattern of the films grown at the substrate temperature of 600 °C shows obvious diffused rings, indicating that the film has become polycrystalline^{34,35}. Here, it is worth to note a fact that the ion radius of Eu³⁺ of 0.95 Å is larger than that of Ga³⁺ of 0.62 Å, which should lead to the peak shift due to the difference of Eu contents³⁶. We have demonstrated that the diffraction peaks have no shift for undoped Ga₂O₃ at different substrate temperatures²³. In this section, when the substrate temperatures are

300, 400, 500, and 600 °C, the corresponding lattice constants $d_{(-402)}$ of the films have been calculated to be 2.52, 2.51, 2.51, and 2.51 Å, respectively. Actually, no clear shift was observed for the samples grown at substrate temperature from 400 to 600 °C, which indicates no obvious changes for the Eu contents in these samples.

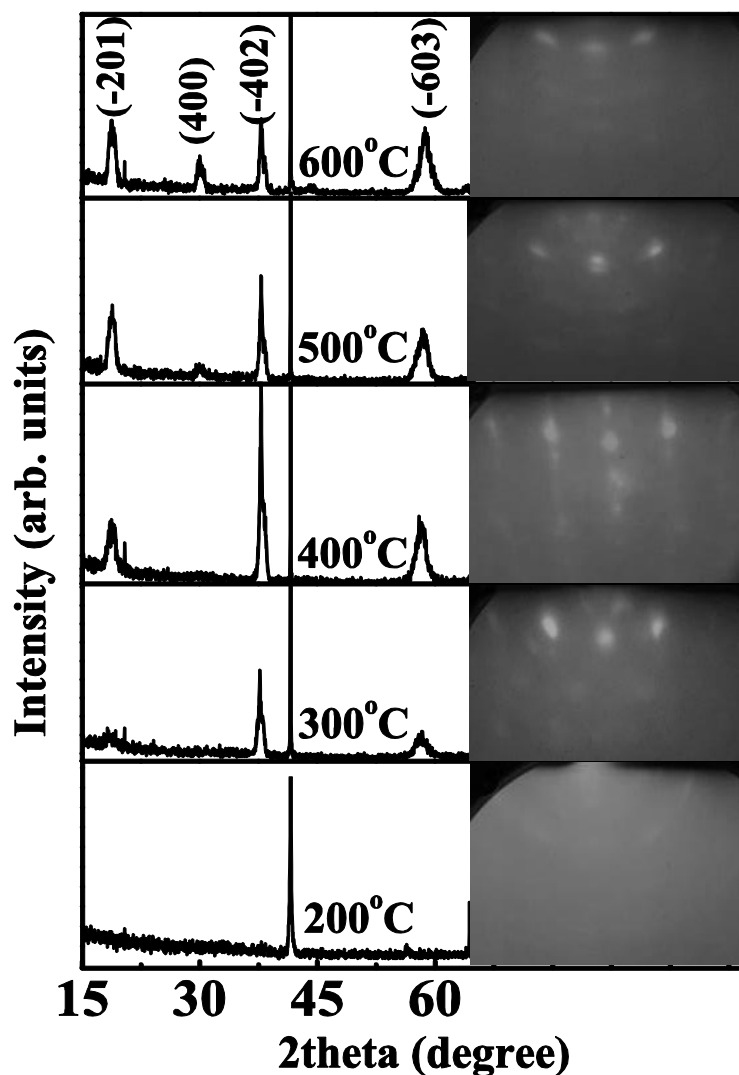


Figure 3.9 XRD patterns of Eu doped Ga₂O₃ films deposited on (0001) sapphire substrates with various substrate temperatures. Insert is the RHEED images for films with different substrate temperatures. The electron beam is parallel to the [11-20] azimuth of the sapphire substrate.

Figure 3.10 presents the EDS of Eu doped Ga₂O₃ films grown at various substrate temperatures. From the spectra, elements of oxygen, gallium and europium are observed²³. We measured the Eu content in three different spots of the films and the overall average value of the error is about 3 %. Thus, when the substrate temperatures are 200, 300, 400, 500 and 600 °C, the corresponding average molar percentage of Eu in films are determined to be 1.4, 1.3, 1.1, 1.1 and 1.1 at.%, respectively. It is indicated that Eu contents decrease slightly with the substrate temperatures increase from 200 to 300 °C, while no obvious change is found with temperatures increase from 400 to 600 °C.

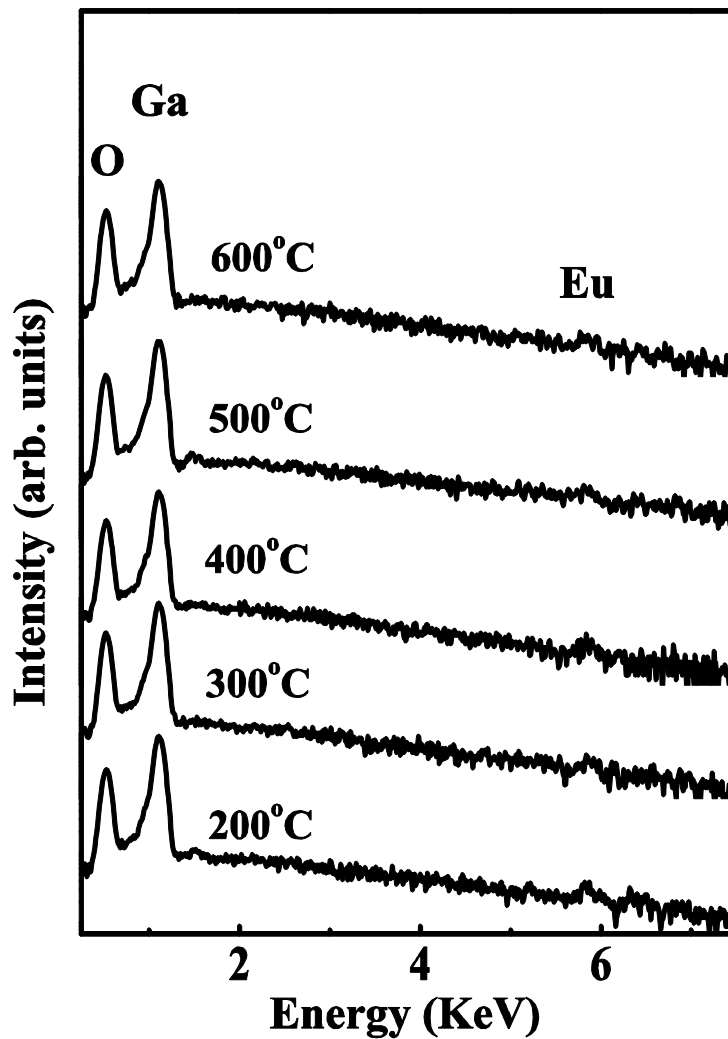


Figure 3.10 EDS of Eu doped Ga₂O₃ thin films deposited with various substrate temperatures.

Figure 3.11 (a) shows room temperature PL spectra of Eu doped Ga₂O₃ films grown at different substrate temperatures. All PL spectra demonstrate characteristic Eu ion emission with the strongest peak at 613 nm which is caused by the ⁵D₀ to ⁷F₂ transition^{16,37,38}. The normalized intensity of the red emission is plotted in Fig. 3.11 (b) as a function of the substrate temperature. It is clear that the intensity of red emission

line observed at 613 nm increases remarkably with increasing substrate temperature up to 400 °C and then decreases from 400 to 600 °C. Other weak PL peaks observed at 581, 590, and 654 nm can be assigned to the transitions from 5D_0 to 7F_0 , 7F_1 , 7F_3 , respectively^{36,39}. All the emission peaks with a shoulder at longer wavelength are ascribed to Stark splitting because the spin-orbit splitting of the energy level. In the literatures, the broad green emission at 500-550 nm have been reported due to the recombination of donor–acceptor pairs (DAPs), in which the oxygen vacancies act as donors and the gallium–oxygen vacancy pairs act as acceptors in Ga_2O_3 ^{40,41}. However, no DAPs band was observed in our Ga_2O_3 films as shown in Fig. 3.11 (a), which may be due to the lower native defects in the Ga_2O_3 films grown by PLD process in this section^{23,42}. The PL spectra indicated that the intensity quenching of Eu related luminescence was observed for the substrate temperature of over 400 °C. Therefore, high quality Ga_2O_3 may be obtained at substrate temperature of 400 °C.

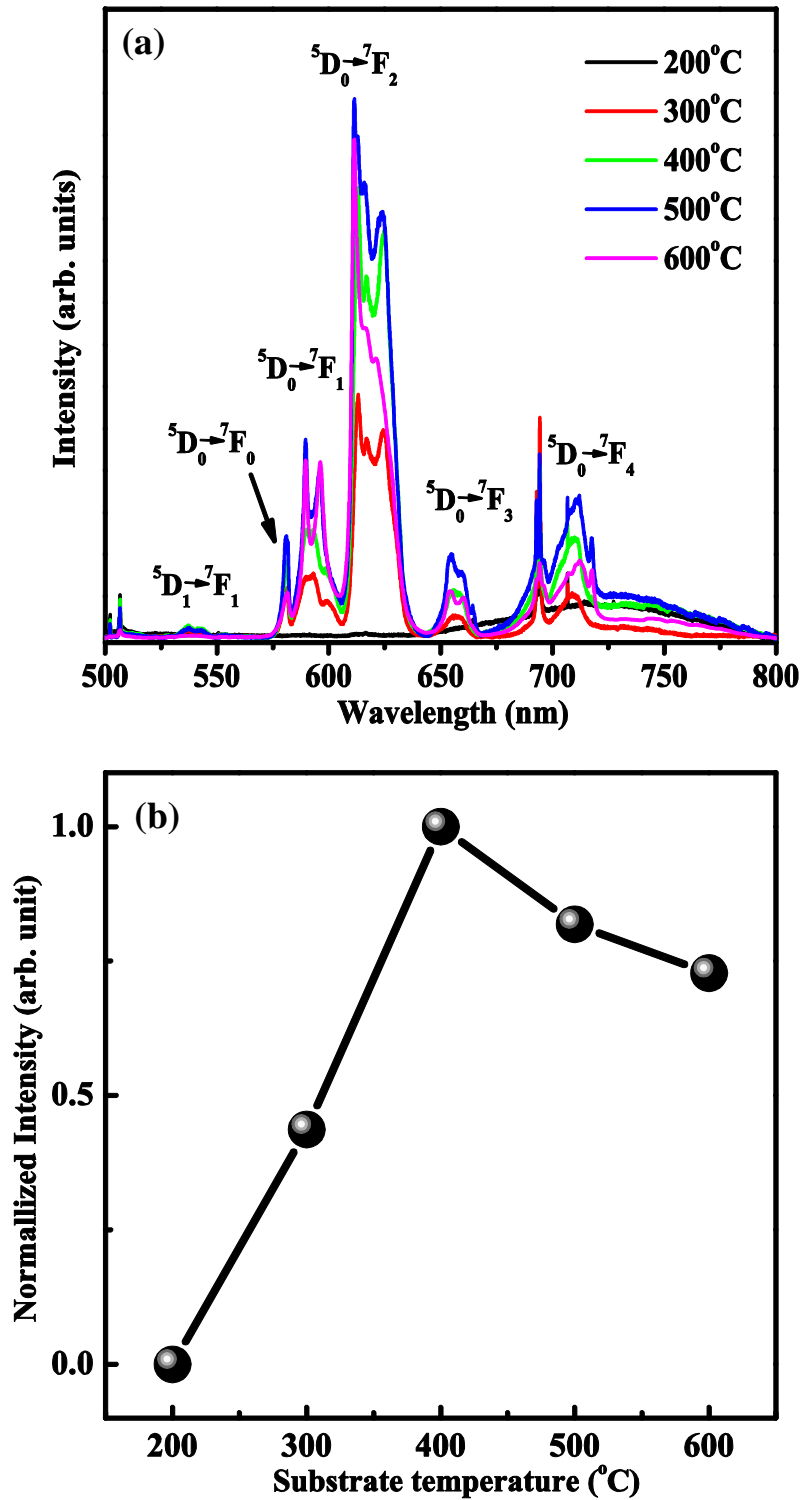


Figure 3.11 (a) Room temperature PL spectra of Ga₂O₃ thin films with different substrate temperatures. (b) Dependence of the normalized intensity of 5D_0 to 7F_2 transition on the substrate temperature.

Figure 3.12 (a) and (b) shows the temperature dependent PL (TDPL) spectra of Ga₂O₃ films grown at 400 °C recorded at the temperature ranging from 77 to 550 K under the excitation of the 325 and 488 nm lights. The sharp emission lines from Eu do not shift significantly with temperature under both the excitation lights. From Fig. 3.12 (a), the intensity of ⁵D₀ to ⁷F₁, ⁷F₂, ⁷F₃, which are dominant for the emission of Eu, remarkably decrease as the temperature increase by using 325 nm light. Fig. 3.12 (b) shows the emission intensity of the peaks is too weak to be detected from 77 to 200 K under 488 nm light. Above 200 K, the emission intensity becomes detectable and increases as the temperature increases. It approaches a maximum at a certain temperature (~500 K), and then decreases as the temperature increases continuously.

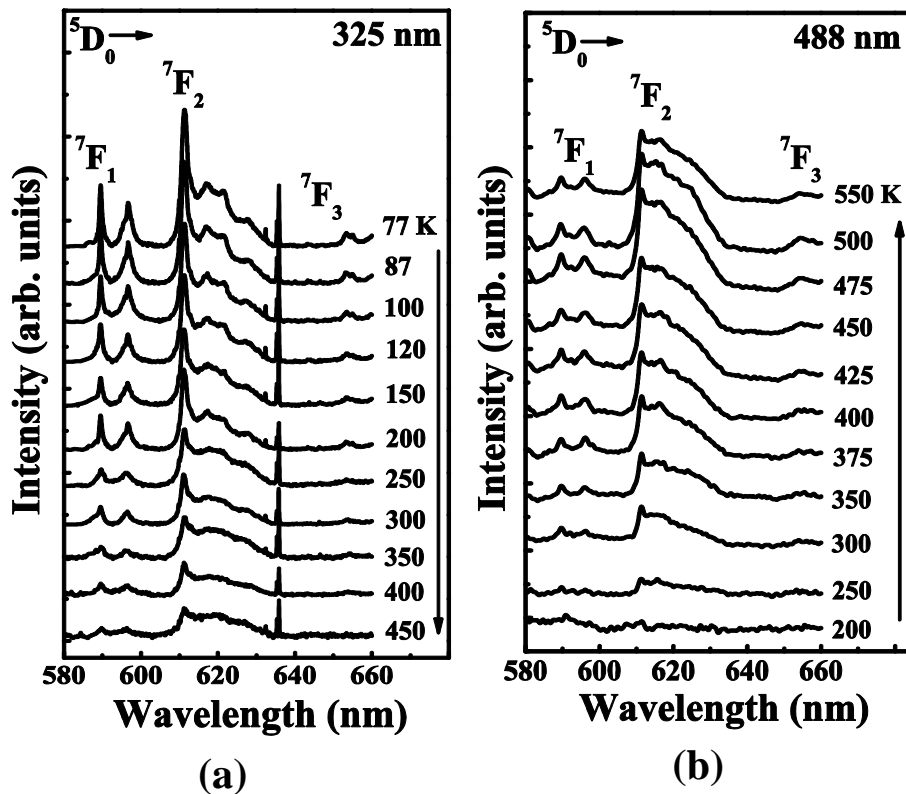


Figure 3.12 Temperature dependence PL spectra from 77 to 550 K of Eu doped Ga₂O₃ films at 400 °C under excitation of different lights (a) 325 nm, (b) 488 nm.

Figure 3.13 (a) and (b) show the temperature dependence of the normalized intensity of 5D_0 to 7F_2 emission under both the excitation lights. According to steady-state luminescence dynamic equations between thermal activated distribution of electrons among 7F_j and thermal quenching effect, the intensity of 5D_0 to 7F_2 can be written approximately as ⁴³

$$I(T) \propto \frac{I'\sigma_j(T)N_j(T)}{I+W_T/W_R} \quad j = 0, 1, 2 \quad (1)$$

where $N_0(T)$ is the population of 7F_0 , σ_j is the absorption cross section from 7F_j to 5D_0 , I' is the excitation intensity of the source light, W_T is the thermal quenching rate, W_R is the radiative transition rate of $\Sigma^5D_0 \rightarrow {}^7F_j$. The normalized electrons populations of 7F_j as a function of temperature calculated by ⁴³

$$N_j(T) = \frac{\exp(-\Delta E_{0j})}{\sum_j G_j \exp(\frac{-\Delta E_{0j}}{kT})} \quad j = 0, 1, 2 \quad (2)$$

k is the Boltzmann's constant. $G_j=2j+1$ is the energy level degeneracy of 7F_j . The thermal quenching rate is determined experimentally by ⁴⁴

$$W_T = W_0 \exp\left(\frac{T}{T_c}\right) \quad (3)$$

where W_0 is the thermal quenching rates at 0 K, T_c is a constant. Therefore, the intensity of 5D_0 to 7F_2 can be written approximately as ³²

$$I_1(T) \approx \frac{\alpha}{[\sum_j G_j \exp(\frac{-\Delta E_{0j}}{kT})][1 + \beta \exp(\frac{T}{T_c})]} \quad (4)$$

$$I_2(T) \approx \frac{\alpha' \exp(\frac{-\Delta E_{02}}{kT})}{[\sum_j G_j \exp(\frac{-\Delta E_{0j}}{kT})][1 + \beta \exp(\frac{T}{T_c})]} \quad (5)$$

where I_1, I_2 is the excitation intensity of the 325, 488 nm lights, $\alpha = I_s \sigma_0 n_0(0)$, $\alpha' = I_s' \sigma_2 G_2 n_0(0)$, I_s, I_s' is the excitation intensity of the 325, 488 nm light, respectively. σ_2 is the absorption cross section from 7F_2 to 5D_0 . $\beta = W_0/W_R$. The $\Delta E_{01} = 370 \text{ cm}^{-1}$, $\Delta E_{02} = 970 \text{ cm}^{-1}$ ⁴³. Using the equation (4) and (5), both of experimental data were well fitted as shown in Fig. 3.13 (a) and (b). The parameters $\sigma_0=1.5$, $\sigma_2=7.6$, $\beta=0.15$ and $T_c=149$ were obtained by fitting. Therefore, the variation of the TDPL intensity of the Eu doped Ga_2O_3 film mainly attributed to two reasons. One reason is the thermal activated distribution of electrons among 7F_j . From Fig. 3.13 (c), it is clear that the electron population of 7F_0 state decreases, while the populations of 7F_1 and 7F_2 increase with the increasing of temperature. Since the ground state 7F_0 state is close to the 7F_1 and 7F_2 states, some electrons on 7F_0 state will be thermally activated to the nearby states, causing the electron populations on 7F_0 decrease with the increase of temperature⁴³. To explain the behavior of TDPL, the scheme of the energy levels of Eu ion and the corresponding transition processes under the excitation of the 325 and 488 nm lights was drawn as Figure 3.13 (d). It has been demonstrated that the 488 nm photon is resonance with the 7F_2 to 5D_2 transition considering the Stark splitting effect³². The electron population on 7F_1 and 7F_2 increase with the increasing of the temperature, causing the electrons optically excited to 5D_2 to increase and thus the emission intensity of 5D_0 to 7F_2 to increase. Conversely, the emission intensity of 5D_0 to 7F_0 decreases with the increasing of temperature under the 325 nm light, the cause of the phenomenon is likely to be related to the 325 nm light can be in resonance with 7F_0 to 5D_0 transition. The other reason is thermal quenching effect of luminescence,

which includes the non-radiative transitions of 5D_0 to 7F_j and energy transfer from excited Eu^{3+} to impurity centers or defects nearby⁴³. From equation (3), it is clear that the thermal quenching rate increases dramatically with increasing of temperature. The thermal quenching effect causes the emission intensity of 5D_0 to 7F_2 to decrease. Considering these two factors, under the 325 nm light, the decreases of the emission intensity is likely to be related to the resonance excited emission of 7F_0 to 5D_0 as well as thermal quenching effect in all the temperature range. Under the 488 nm light, the resonance excited emission of 7F_2 to 5D_0 was dominant in the temperature range from 77 to 500 K, and then, the thermal quenching effect is comparable with the resonance excited when the temperature over 500 K. Thus, a maximum should appear in the temperature dependence of the Eu^{3+} emission. We can conclude that the behavior of Eu in Ga_2O_3 and in silicate glass is substantially the same in this respect. However, it has been demonstrated that the RE doped Ga_2O_3 films allow light emission from RE ions in the visible wavelength region for full-color display applications due to a high transparency^{1,36}. Ga_2O_3 is also attractive as a host material for phosphors in emissive display application such as thin film electroluminescence (TFEL) display^{45,46}.

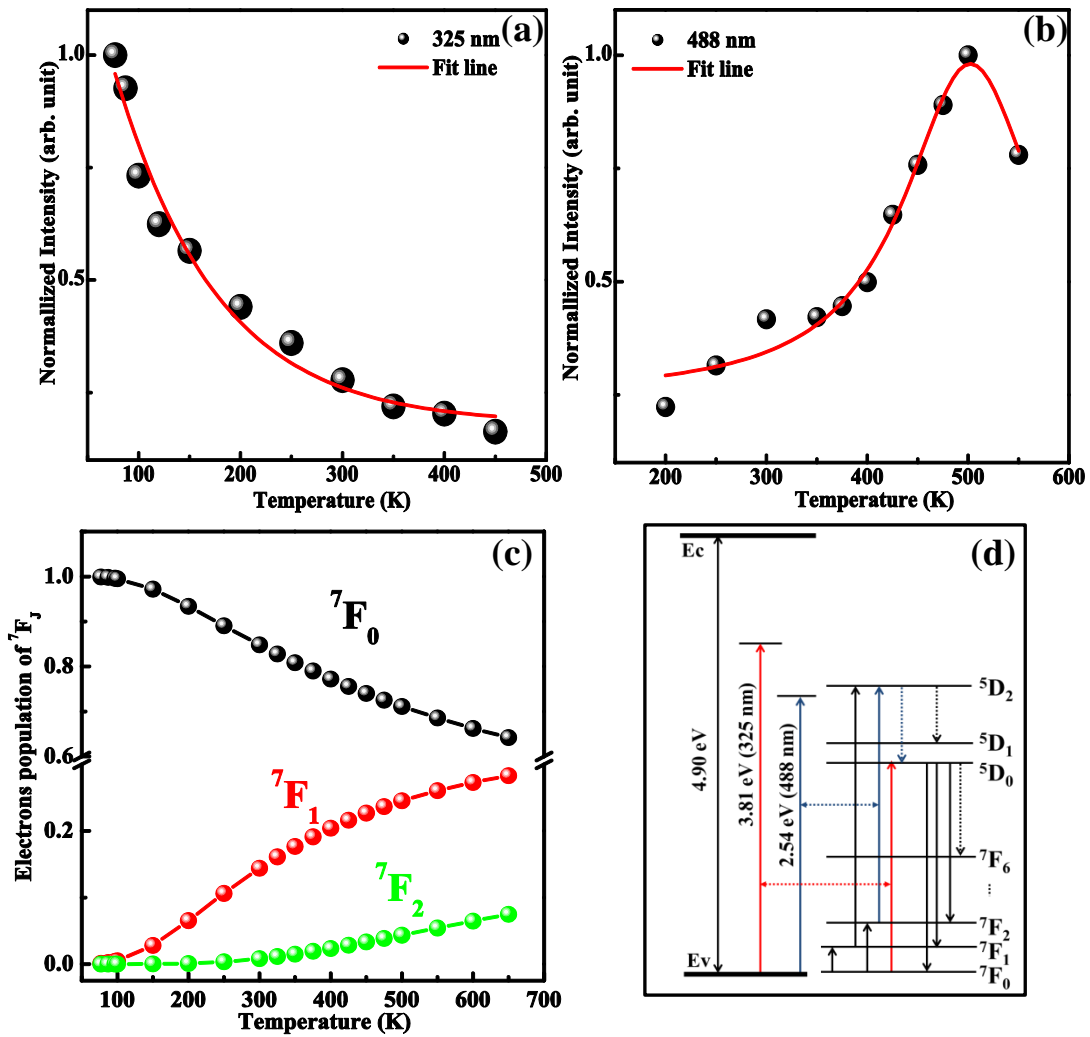


Figure 3.13 Temperature dependence emission intensity of Eu³⁺ under the excitation of different lights (a) 325 nm, (b) 488 nm. (c) Normalized population of ⁷F₀, ⁷F₁, and ⁷F₂ as a function of temperature calculated by the equation (2). (d) Energy diagrams of Ga₂O₃ and Eu and the proposed mechanisms for both laser excitations.

3.3 Conclusions

We have grown Eu doped Ga₂O₃ films on sapphire substrates by PLD with varying Eu contents at substrate temperature as low as 500 °C. EDS results revealed that films with different Eu contents can be obtained by changing the Eu composition in the targets. XRD and Raman spectra analyses indicated that all films have the monoclinic structure with a preferable (-201) orientation. The films exhibited high transmittance more than 90% in the visible region and 80% in the UV region. Intense red emissions at 613 nm due to the transitions from ⁵D₀ to ⁷F₂ levels in Eu were clearly observed for the Eu doped Ga₂O₃ films, suggesting PLD is a promising method for obtaining high quality Eu doped Ga₂O₃ films at low growth temperature. Furthermore, we have also fabricated the high quality single (-201) oriented Ga₂O₃ film at substrate temperature of 400 °C. The emission intensity of Eu³⁺ decreased solely with elevated temperature by using 325 nm light, while it had a maximum value at a certain temperature under 488 nm light. Both of the experimental data can be well fitted by the luminescence dynamic equation models, suggesting that the variation of the emission intensity may be attributed to the thermal activated distribution of electrons among ⁷F_j and thermal quenching effect. We believe that all of this work paves the way for developing future generations of flat panel displays devices and phosphors in wide temperature range.

References

- 1 A. Wakahara, H. Sekiguchi, H. Okada, Y. Takagi, J. Lumin. 132 (2012) 3113.
- 2 L.J. Ren, X.H. Lei, X.Q. Du, L. J, W.M. Chen, Y.A. Feng, J. Lumin. 142 (2013) 150.
- 3 M. Kanemoto, H. Sekiguchi, K. Yamane, H. Okada, A. Wakahara, J. Lumin. 166 (2015) 60.
- 4 T. Arai, D. Timmerman, R. Wakamatsu, D. Lee, A. Koizumi, Y. Fujiwara, J. Lumin. 158 (2015) 70.
- 5 J. Heikenfeld, M. Garter, D.S. Lee, R. Birkhahn, A.J. Steckl, Appl. Phys. Lett. 75 (1999) 1189.
- 6 S. Shirakata, R. Sasaki, T. Kataoka, Appl. Phys. Lett. 85 (2004) 2247.
- 7 A. Nishikawa, N. Furukawa, T. Kawasaki, Y. Terai, Y. Fujiwara, Appl. Phys. Lett. 97 (2010) 051113.
- 8 N. Woodward, J. Poplawsky, B. Mitchell, A. Nishikawa, Y. Fujiwara, V. Dierolf, Appl. Phys. Lett. 98 (2011) 011102.
- 9 M. Nakayama, S. Nakamura, H. Takeuchi, A. Koizumi, Appl. Phys. Lett. 106 (2015) 012102.
- 10 P.N. Favennec, H. L'Haridon, M. Salvi, D. Moutonnet, Y. L. Guillou, Electron. Lett. 25 (1989) 718.
- 11 Y.E. Romanyuk, L.D. Kranz, S.R. Leone, J. Appl. Phys. 103, (2008) 073104.
- 12 P. Gollakota, A. Dhawan, P. Wellenius, L.M. Lunardi, J.F. Muth, Appl. Phys. Lett. 88, (2006) 221906.

- 13 J.H. Hao, Z.D. Lou, L. Renaud, M. Cocivera, *Thin Solid Films*, 467, (2004) 182.
- 14 P. Gollakota, A. Dhawan, P. Wellenius, L.M. Lunardi, J.F. Muth, *Appl. Phys. Lett.* 88 (2006) 221906.
- 15 P. Wellenius, A. Suresh, J.F. Muth, *Appl. Phys. Lett.* 92 (2008) 021111.
- 16 P. Wellenius, E.R. Smith, S.M. LeBoeuf, H.O. Everitt, J.F. Muth, *J. Appl. Phys.* 107 (2010) 103111.
- 17 J.H. Hao, M. Cocivera, *J. Phys. D: Appl. Phys.* 35 (2002) 433.
- 18 Y. Tokida, S. Adachi, *Jpn. J. Appl. Phys.* 52 (2013) 101102.
- 19 H.M. Zhu, R.F. Li, W.Q. Luo, X.Y. Chen, *Phys. Chem. Chem. Phys.* 13 (2011) 4411.
- 20 Y. Tokida, S. Adachi, *J. Appl. Phys.* 112 (2012) 063522.
- 21 J. Vincent, O.G. Nođ, L. Binet, P. Aschehoug, Y.L. Du, *J. Appl. Phys.* 104 (2008) 133519.
- 22 Z.P. Wu, G.X. Bai, Q.R. Hu, D.Y. Guo, C.L. Sun, L.Y. Ji, M. Lei, L.H. Li, P.G. Li, J.H. Hao, W.H. Tang, *Appl. Phys. Lett.* 106 (2015) 171910.
- 23 F.B. Zhang, K. Saito, T. Tanaka, M. Nishio, Q.X. Guo, *Appl. Phys. Lett.* 105 (2014) 162107.
- 24 F.B. Zhang, K. Saito, T. Tanaka, M. Nishio, Q.X. Guo, *Solid State Commun.* 186 (2014) 28.
- 25 F.B. Zhang, K. Saito, T. Tanaka, M. Nishio, Q.X. Guo, *J. Cryst. Growth*, 387 (2014) 96.
- 26 X.H. Wang, F.B. Zhang, K. Saito, T. Tanaka, M. Nishio, Q.X. Guo, *J. Phys. Chem.*

- Solids, 75 (2014) 1201.
- 27 V. Gottschalch, K. Mergenthaler, G. Wagner, J. Bauer, H. Paetzelt, C. Sturm, U. Teschner, *Phys. Status Solidi A*, 206 (2009) 243.
- 28 Y. Kashiwagi, A. Koizumi, Y. Takemura, S. Furuta, M. Yamamoto, M. Saitoh, M. Takahashi, T. Ohno, Y. Fujiwara, K. Murahashi, K. Ohtsuka, M. Nakamoto, *Appl. Phys. Lett.* 105 (2014) 223509.
- 29 D. Dohy, G. Lucazeau, A. Revcolecchi, *J. Solid State Chem.* 45 (1982) 180.
- 30 C.W. Lee, H.O. Everitt, D.S. Lee, A.J. Steckl, J.M. Zavada, *J. Appl. Phys.* 95 (2004) 7717.
- 31 J.W. Wang, H.W. Song, X.G. Kong, W. Xu, H.P. Xia, *J. Appl. Phys.* 91 (2002) 9466.
- 32 H.S. Peng, H.W. Song, B.J. Chen, J.W. Wang, S.Z. Lu, X.G. Kong, J.H. Zhang, *J. Chem. Phys.* 118 (2003) 3277.
- 33 X. Wang, Z.W. Chen, F.B. Zhang, K. Saito, T. Tanaka, M. Nishio, Q.X. Guo, *Ceramics International* 42 (2016) 12783.
- 34 P. Sagan, G. Wisz, M. Bester, I.O. Rudyj, I.V. Kurilo, I.E. Lopatynskij, I.S. Virt, M. Kuzma, R. Ciach, *Thin Solid Films*, 480 (2005) 318.
- 35 X. Chen, W.P. Gao, S. Sivaramakrishnan, H.F. Hu, J.M. Zuo, *Appl. Surf. Sci.* 270 (2013) 661.
- 36 Z.W. Chen, K. Saito, T. Tanaka, M. Nishio, Q.X. Guo, *J. Cryst. Growth*, 430 (2015) 28.
- 37 H. Bang, S. Morishima, J. Sawahata, J. Seo, M. Takiguchi, M. Tsunemi, K.

- Akimoto, M. Nomura, *Appl. Phys. Lett.* 85 (2004) 227.
- 38 E. Nogales, B. Méndez, J. Piqueras, J.A. García, *Nanotechnol.* 20 (2009) 115201.
- 39 R. Lorenzi, A. Paleari, N.V. Golubev, E.S. Ignat'eva, V.N. Sigaev, M. Niederberger, A. Lauria, *J. Mater. Chem. C* 3 (2015) 41.
- 40 S. Kumar, C. Tessarek, S. Christiansen, R. Singh, *J. Alloys Compd.* 587 (2014) 812.
- 41 T.T. Zhang J. Lin, X.H. Zhang, Y. Huang, X.W. Xu, Y.M. Xue, J. Zou, C.C. Tang, *J. Lumin.* 140 (2013) 30.
- 42 M. Orita, H. Ohta, M. Hirano, H. Hosono, *Appl. Phys. Lett.* 77 (2000) 4166.
- 43 J.W. Wang, H.W. Song, X.G. Kong, W. Xu, H.P. Xia, *J. Appl. Phys.* 91 (2002) 9466.
- 44 Q.G. Zeng, Z.J. Ding, X. Ju, Y. Wang, Y.Q. Sheng, *Chin. Phys. Lett.* 24 (2007) 1368.
- 45 Z.W. Chen, X. Wang, S. Noda, K. Saito, T. Tanaka, M. Nishio, M. Airita, Q.X. Guo, *Superlattices Microstruct.* 90 (2016) 207.
- 46 T. Miyata, T. Nakatani, T. Minami, *J. Lumin.* 87 (2000) 1183.

Chapter 4

Growth and characterization of Er doped Ga₂O₃ films

4.1 Introduction

Efficient pure green light emission (~ 550 nm) is difficult to obtain because of the lack of semiconductors with direct bandgap in the range of 2.2~2.4 eV¹. Er doped semiconductors, which exhibit strong and sharp, green emission due to intra-4*f*-shell transitions in Er ion cores, have potential applications in color display and luminescence devices^{2,3}. Green luminescence from Er doped GaN films have been widely investigated due to its large bandgap (3.4 eV)⁴⁻⁷. It has been reported that the luminescence efficiency of dopant emissions could be highly improved with a wide bandgap host^{8,9}. Moreover, the wide bandgap semiconductors exhibit highly thermal and chemical stability, which make them ideal hosts for Er ions¹⁰. Recently, we have shown that Ga₂O₃ films with bandgap of 4.9 eV can be epitaxially grown by using PLD^{11,12}. It is expected that Er doped Ga₂O₃ films have more efficient and stability pure green light emission than GaN. However, up to now, there is no report available related to Er doped Ga₂O₃ pure green luminescence thin films although this research is of vital importance for the future application.

In this work, we demonstrate that pure green emissions at 550 nm are clearly observed from the Er doped Ga₂O₃ films. No peak shift at 550 nm is found with temperatures between 77 and 450 K. The intensity of the green emission decreases with increasing the temperature from 77 to 450 K. We find that the normalized

intensity of the Er doped Ga_2O_3 films has a smaller variation compared to Er doped GaN films. The correlation between the optical properties and lattice distortions are studies. All results indicate that Ga_2O_3 is a better host material for Er than GaN and potentially for other rare earth elements.

4.2 Experiment

Experiment details have been reported in Chapter 3. Herein, as show in Table 4.1, bulks with different Er contents are used as target.

Table 4.1 Growth conditions for Er content influence

Growth conditions	
Targets	0.0, 5.0, 7.0, 9.0, wt. % Er doped Ga ₂ O ₃
Substrate	α -Al ₂ O ₃ (0001)
Oxygen pressure (Pa)	1×10^{-1}
Growth temperature (°C)	500
Laser frequency (Hz)	2
Distance from target to substrate (mm)	40

After deposition, the thickness of all samples was determined by a surface step profile analyzer. XPS measurements were performed using Al $K\alpha$ X-ray source. The surface of the samples was Ar ion (3 keV) etched for 2 min before XPS analysis. The structural properties of the films were examined by conventional θ - 2θ scan XRD using $K\alpha$ emission line of copper. The optical transmission spectra were measured with a spectrophotometer. The surface morphology and roughness of the films were studied by AFM on $2 \times 2 \mu\text{m}$ areas under ambient conditions. PL measurements were performed using an Ar laser operating at a wavelength of 488 nm as the excitation source.

4.3 Results and discussion

Figure 4.1 shows the Er content influence on the growth rate of Ga_2O_3 films. It is clear that the growth rate of Ga_2O_3 films decreases monotonically with the increase of Er content due to the significant difference in ionic radii between Er and Ga. The incorporation of Er into the Ga_2O_3 film becomes difficult with increasing of Er content.

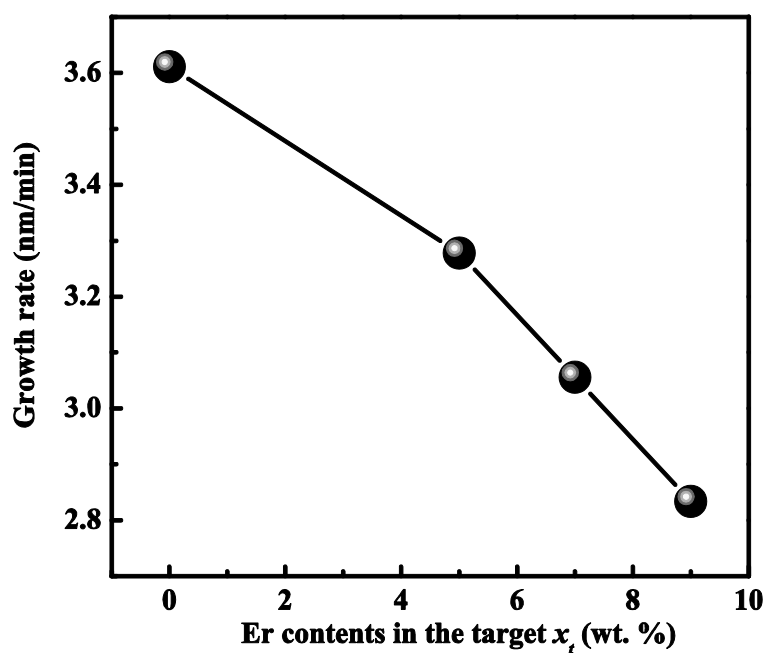


Figure 4.1 Influences of Er content on growth rate of Ga_2O_3 films.

Figure 4.2 (a) shows wide scan spectra of the Ga₂O₃ films grown with different Er contents in the targets (x_t). From the spectra, the peaks related with Ga, O, and Er are clearly observed. No other elements are detected from the wide scan spectra of the films. From Fig. 4.2 (b), it is clear that two symmetrical peaks of Ga $2p_{1/2}$ and Ga $2p_{3/2}$ are located at 1146.6 eV and 1119.9 eV, respectively, The separation energy between these two peaks is about 26.7 eV, which is in good agreement with the reported value for Ga₂O₃ bulk¹³. Fig. 4.2 (c) reveals the high resolution XPS spectra of Er $4p$ peak, centered at 321.6 eV. The intensity of the Er peak increases with the increase of Er contents (x_t). The Er content (x) in Ga₂O₃ films obtained from the XPS spectra after applying an atomic sensitivity factor is shown in Fig. 4.2 (d) as a function of Er content of the targets (x_t). We find that the Er contents (x) in the films increases almost linearly with the increase of Er contents of the targets (x_t). This suggests that the Er contents in Ga₂O₃ films (x) can be controlled by adjusting the Er contents in the targets (x_t).

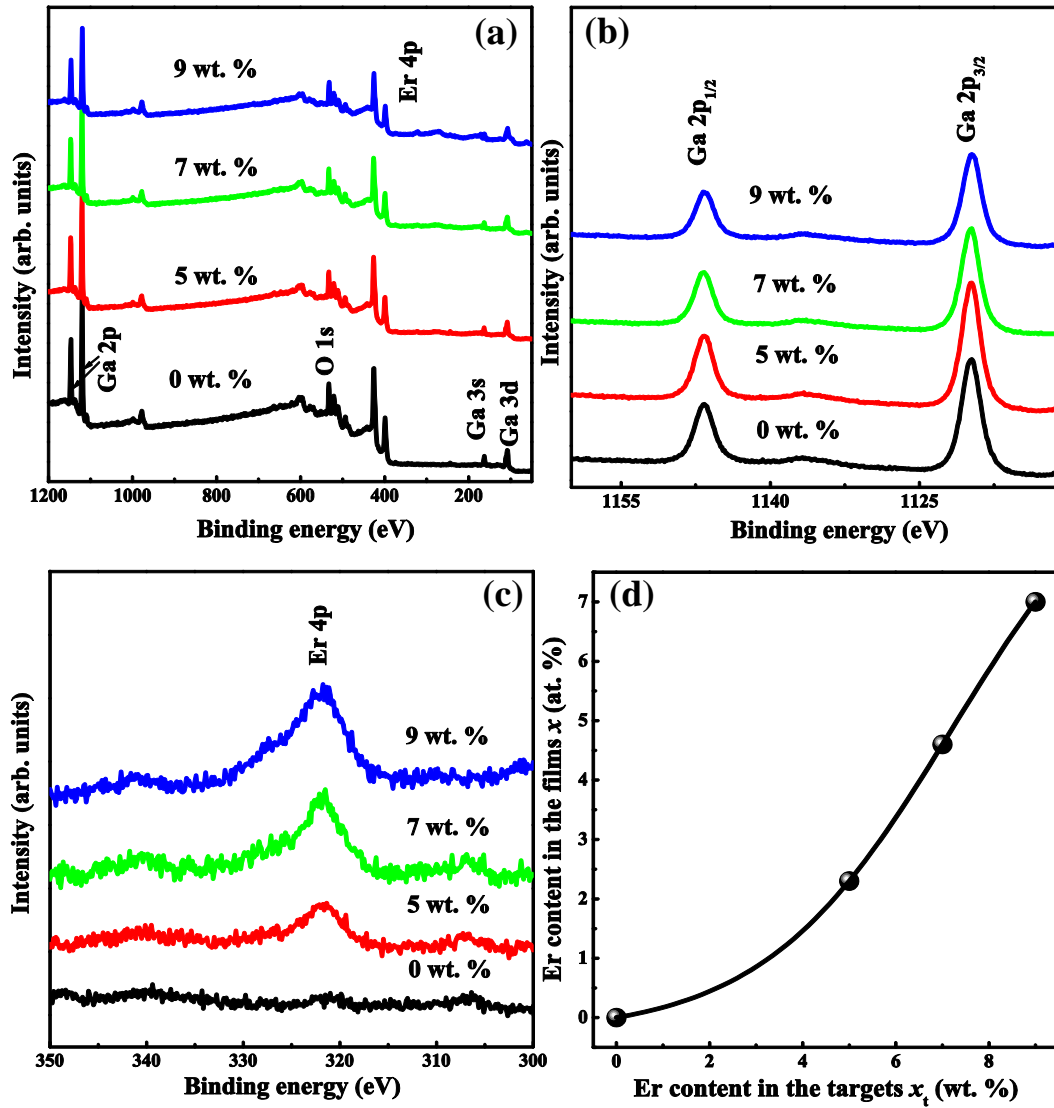


Figure 4.2 (a) XPS wide scan spectra, (b) Ga 2*p*, and (c) Er 4*p* core level spectra of Ga₂O₃ films with different contents in the targets x_t . (d) Er contents in the films (x) as a function of the Er contents of the targets (x_t).

Figure 4.3 shows the XRD patterns of Ga_2O_3 films with different Er contents (x). Three peaks are clearly observed at 18.89° , 38.05° , 58.93° which can be assigned as the (-201), (-402), and (-603) planes of monoclinic Ga_2O_3 ($\beta\text{-Ga}_2\text{O}_3$), respectively by comparing measured diffraction data with known diffraction peaks listed in the International Center for Diffraction Data catalog¹². These results identify an epitaxial relationship with (-201) of $\beta\text{-Ga}_2\text{O}_3 \parallel (0001)$ sapphire substrate. We find that with the increase of Er content (x) the peaks have slightly shifted to lower diffraction angle as shown by example of the (-402) peak in Fig. 4.3 (b), indicating an increase of the lattice constant which is due to the fact that the ion radius of Er^{3+} of 0.88 \AA is larger than that of Ga^{3+} of 0.62 \AA . The incorporation of Er into Ga_2O_3 in a form of Er^{3+} substituting for Ga^{3+} will increase lattice constants of Ga_2O_3 which results in the diffraction peaks shifts to the lower angle¹⁴.

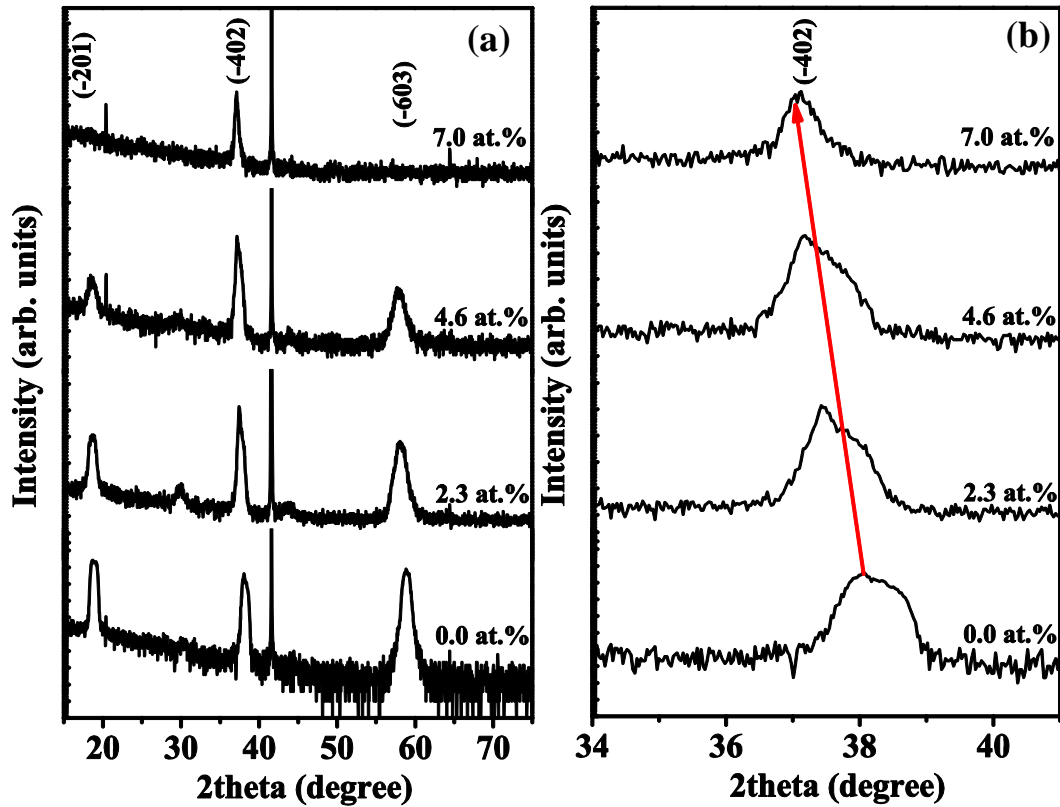


Figure 4.3 (a) XRD patterns of Ga₂O₃ thin films with different Er doping contents. (b) The corresponding XRD profiles of the near (-402) peaks.

Figure 4.4 shows the $2 \times 2 \mu\text{m}$ AFM images for Ga₂O₃ thin films with different Er doping contents (x). It is clear that the morphology changes with different Er doping contents. For pure Ga₂O₃ film, island like structure appears. As the Er contents increases, the resulting morphology transform from islands structure into splitting slim needle like structure. The root-mean-square (RMS) roughness gives an idea about quality of the surface under investigation. It is known that thicker films often result in rougher surface¹⁵. In this study, the thickness of all samples was determined to be about 500-550 nm. The surface RMS becomes higher with the increase of Er doping contents. That indicates the roughness difference in present experiments is

caused by Er doped into the Ga_2O_3 films. The maximum roughness of the films is below 9 nm, indicating the films have smooth surface.

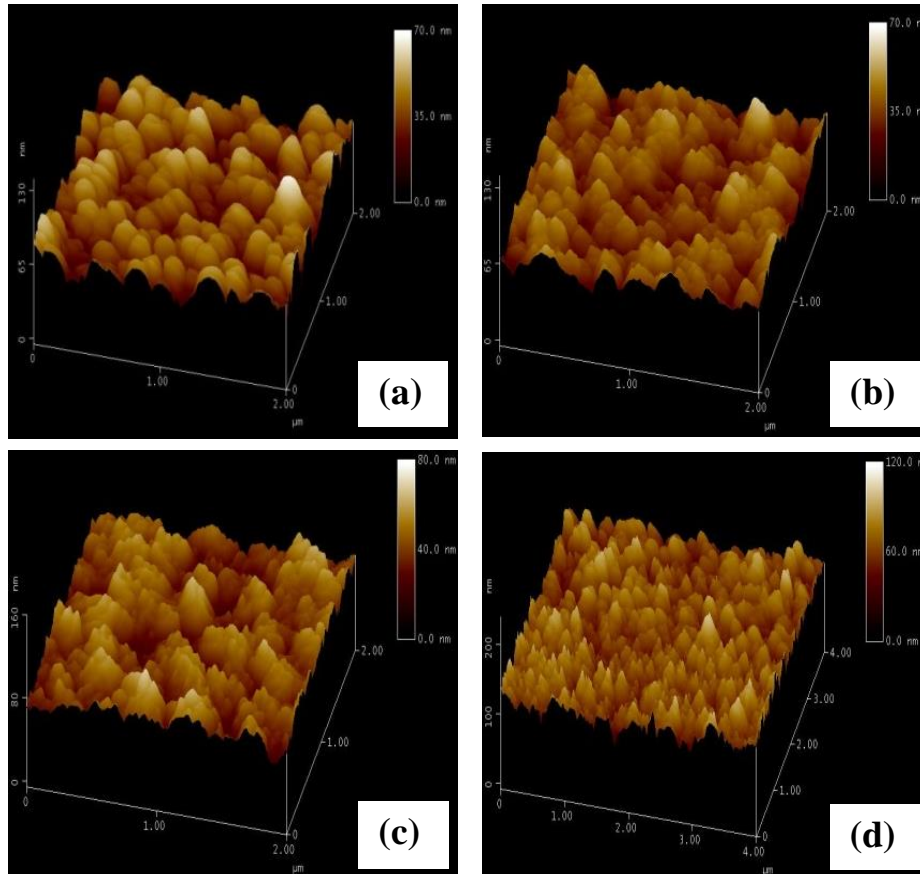


Figure 4.4 AFM images of Ga_2O_3 films with different Er doping contents (x), (a) 0.0, (b) 2.3, (c) 4.6, and (d) 7.0 at. %, respectively.

Figure 4.5 shows the room temperature optical transmission spectra of Ga_2O_3 films with different Er contents in the films (x). The transmittances of all samples in visible and infrared region are above 85%. The spectra of the pure Ga_2O_3 exhibit a sharp intrinsic absorption edge at wavelength of 250 nm, whilst those of Er doped films shift towards longer wavelength with increasing Er contents. Optical

transmission measurements were carried out to confirm the bandgap of the films ¹². By extrapolating the linear part of $(ah\nu)^2$ to the horizontal axis, one can obtain the bandgap of Er doped Ga₂O₃ films as shown in the insertion of Figure 4.5. From Table 4.1, we can see that the d spacing of (-402) increases and the bandgap decreases with increasing Er contents x . The decrease of the bandgap is ascribed to new unoccupied electron states in the gap below the conduction band edge due to the incorporation of Er ions on the substitutional sites of Ga₂O₃ ¹⁶.

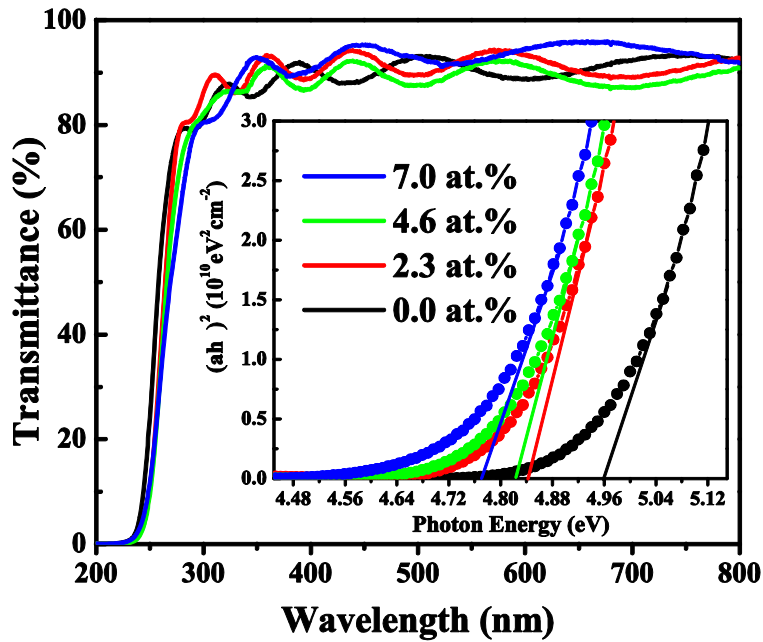


Figure 4.5 Transmittance spectra of Ga₂O₃ thin films with different Er doping contents (x), and the plot of $(ah\nu)^2$ versus $h\nu$ in the inset.

Table 4.1 Calculated values of lattice constants $d_{(-402)}$ and bandgap of Ga₂O₃ films with different Er contents in the films (x)

Er contents (at.%)	$d_{(-402)}$ (Å)	Bandgap (eV)
0.0	2.49	4.96
2.3	2.52	4.84
4.6	2.54	4.82
7.0	2.56	4.77

Figure 4.6 (a) shows the PL spectra of Ga₂O₃ thin films with different Er contents in the films (*x*) measured at room temperature. The PL spectra for the Er doped Ga₂O₃ films demonstrate characteristic Er ion emission with the strongest peak at 550 nm which is caused by the ⁴S_{3/2} to ⁴I_{15/2} transition⁴. The intensity of pure green emission line observed at 550 nm increases remarkably with increasing Er doping content in the Ga₂O₃ films. The 550 nm emission peak with a shoulder at longer wavelength is ascribed to Stark splitting because the spin-orbit splitting of the energy level¹⁷. Other PL peaks observed at 524, 655, 850, and 975 nm can be assigned to the transitions from ²H_{11/2}→⁴I_{15/2}, ⁴F_{9/2}→⁴I_{15/2}, ⁴I_{9/2}→⁴I_{15/2}, and ⁴I_{11/2}→⁴I_{15/2}, respectively⁴, as shown in Figure 4.6 (b). Since the excitation energy of incident light (2.54 eV) used for measurement in this work is lower than the bandgap of Ga₂O₃ (4.90 eV), the electrons are excited from the valence band to the donor band by the laser light source. The related energy due to the recombination of electrons in the defect state with the photogenerated holes can transfer to the excited states of Er ions, which results in the emissions observed in Figure 4.6 (a)^{2,16}.

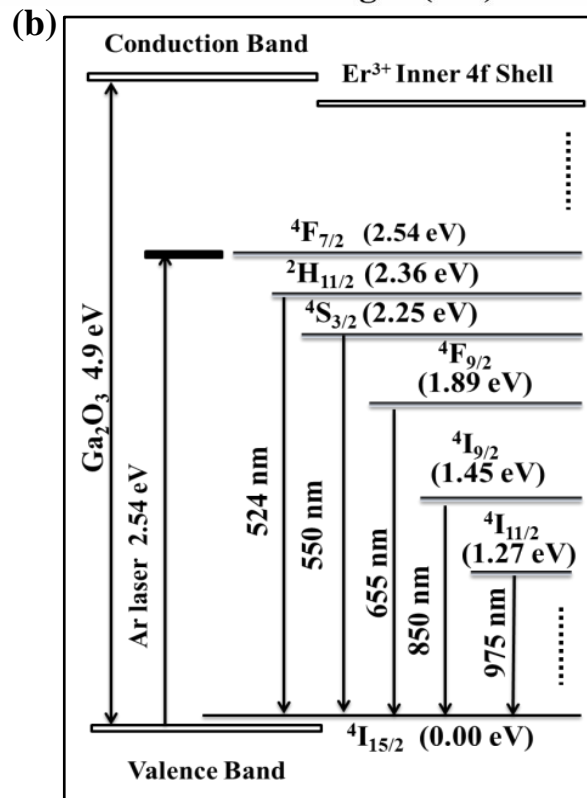
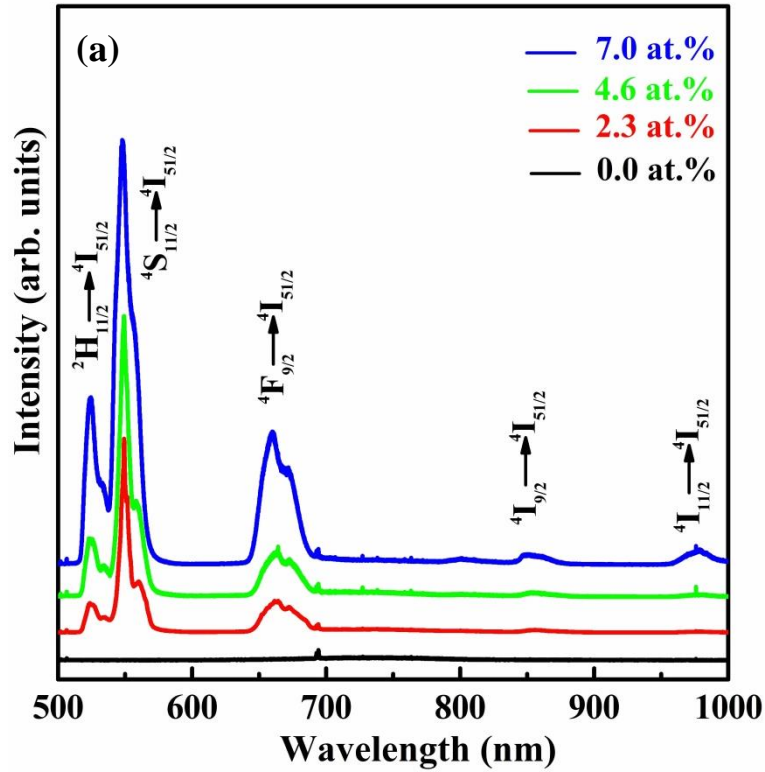


Figure 4.6 (a) PL spectra of Ga₂O₃ thin films with different Er doping contents in the film (x). (b) Energy diagram of Ga₂O₃ and Er and the proposed mechanisms for laser excitation less than 488 nm.

Figure 4.7 (a) - (c) shows the temperature dependent (TD) PL spectra of Ga₂O₃ films with different Er contents (*x*) recorded at the temperature ranging from 77 to 450 K. It is clear that no peak shifts at 550 nm in the PL spectrum for all samples but the intensity of these emission lines at 550 nm decreases monotonically with increasing temperature from 77 to 450 K, while intensity of the 524 nm emission line appears and increases with increasing temperature more than 150 K. The most likely explanation for the opposite temperature dependence between the two closely spaced electronic states is that electrons are thermally equilibrated between the two levels⁴. The ratio of luminescence intensity from the upper state and the lower state to a much lower state can be expressed by the following⁹

$$\frac{I_H}{I_S} = Ae^{-\frac{\Delta E}{K_B T}}$$

where I_H , and I_S are the luminescence intensities of 524 and 550 nm, A is a constant, K_B is the Boltzmann constant, T is the absolute temperature, and ΔE is the energy gap between $^4S_{3/2}$ and $^2H_{11/2}$ states¹⁸. The ΔE values calculated from these data are 106.2, 102.3, and 98.28 meV, which can be assigned as the 2.3, 4.6, and 7.0 at. % Er doped Ga₂O₃ films, respectively. These are comparable to the value of 112.0 meV obtained from the energy difference between the two PL peaks. It is interesting to also compare these results in this work to those obtained by Steckl *et al.*⁴ for Er doped GaN films. It is found that the behavior of Er in GaN and in Ga₂O₃ films is substantially the same. However, Fig. 4.7 (d) summaries of the normalized intensity as a function of the temperature ranging from 77 to 450 K, together with the reported data of the Er doped GaN for comparison. The normalized intensity of the green emission at 550 nm

decreases with the increase of temperature. Here it worth be noted that the normalized intensity of the Er doped Ga₂O₃ films have a smaller variation to Er doped GaN films. Favennec *et al.*⁸ and Neuhalfen *et al.*¹⁹ have demonstrated that the thermal quenching of the emission intensity is more severe for the smaller bandgap materials and the wide bandgap compounds exhibits the least temperature dependence, because the formation of defects and the shrinking of the distance between Er ions, or ion-defects cross relaxation could cause the photoluminescence quenching⁷. The thermal quenching of the intra-4*f* Er luminescence efficiency can be reduced by choosing wide bandgap materials, where the isoelectronic trap levels are deep²⁰. These results indicate that the Ga₂O₃ is a better host material for Er than GaN, opening the possibility of the applications in pure green luminescence devices based on Ga₂O₃ by using Er as dopant in the wide temperature range.

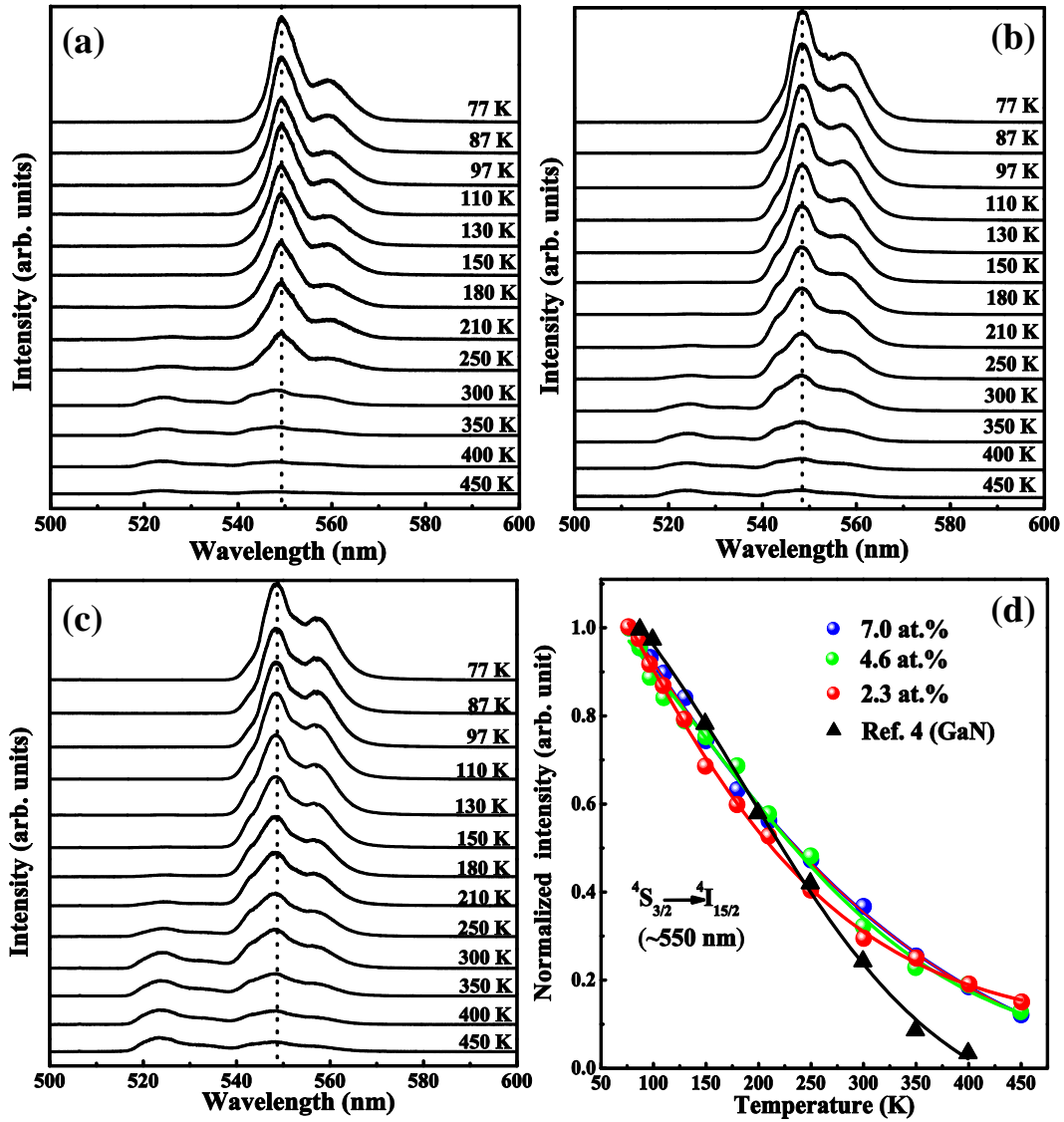


Figure 4.7 Temperature dependence PL spectra from 77 to 450 K of (a) 2.3, (b) 4.6 and (c) 7.0 at. % Er doped Ga_2O_3 films. (d) Dependence of the normalized intensity of the $^4S_{3/2}$ to $^4I_{15/2}$ (550 nm) emission on temperature.

4.3 Conclusion

In conclusion, we demonstrated that pure green emissions at 550 nm are clearly observed for the Er doped Ga₂O₃ films grown on (0001) sapphire substrates by PLD. No peak shift at 550 nm is found with temperatures ranging from 77 to 450 K. The intensity of the green emission decreases with the increase of temperature, and the normalized intensity of the Er doped Ga₂O₃ films has a smaller variation with temperature compared to Er doped GaN films. These results may provide a new insight for further optoelectronics applications based on Er doped Ga₂O₃ films.

References

- 1 M. Garter, J. Scofield, R. Birkhahn, A.J. Steckl, Appl. Phys. Lett. 74 (1999) 182-184.
- 2 J. Heikenfeld, M. Garter, D.S. Lee, R. Birkhahn, A.J. Steckl, Appl. Phys. Lett. 75 (1999) 1189.
- 3 Y. Takagi, T. Suwa, H. Sekiguchi, H. Okada, A. Wakahara, Appl. Phys. Lett. 99 (2011) 171905.
- 4 A.J. Steckl, R. Birkhahn, Appl. Phys. Lett. 73 (1998) 1700.
- 5 Y.Q. Wang, A.J. Steckl, Appl. Phys. Lett. 82 (2003) 502.
- 6 H.Q. Wu, C.B. Poitras, M. Lipson, M.G. Spencer, J. Hunting, F.J. DiSalvo, Appl. Phys. Lett. 86 (2005) 191918.
- 7 S.Q. Chen, B. Dierre, W. Lee, T. Sekiguchi, S. Tomita, et al. Appl. Phys. Lett. 96 (2010) 181901.
- 8 P.N. Favennec, H. L'Haridon, M. Salvi, D. Moutonnet, Y. L. Guillou, Electron. Lett. 25 (1989) 718.
- 9 Y.E. Romanyuk, L.D. Kranz, S.R. Leone, J. Appl. Phys. 103 (2008) 073104.
- 10 P. Gollakota, A. Dhawan, P. Wellenius, L.M. Lunardi, J.F. Muth, Appl. Phys. Lett. 88 (2006) 221906.
- 11 F.B. Zhang, K. Saito, T. Tanaka, M. Nishio, Q.X. Guo, J. Cryst. Growth, 387 (2014) 96.
- 12 Z.W. Chen, K. Saito, T. Tanaka, M. Nishio, Q.X. Guo, J. Cryst. Growth, 430 (2015) 28.
- 13 G. Schön, J. Electron. Spectrosc. Relat. Phenom. 2 (1973) 75.

- 14 X.H. Wang, F.B. Zhang, K. Saito, T. Tanaka, M. Nishio, Q.X. Guo, *J. Phys. Chem. Solids*, 75 (2014) 1201.
- 15 D.H.A. Blank, M.E. Bijlsma, R. Moerman, H. Rogalla, F.J.B. Stork, A. Roshko, *J. Alloy Compd.* 251 (1997) 31.
- 16 Z.P. Wu, G.X. Bai, Q.R. Hu, D.Y. Guo, C.L. Sun, L.Y. Ji, M. Lei, L.H. Li, P.G. Li, J.H. Hao, W.H. Tang, *Appl. Phys. Lett.* 106 (2015) 171910.
- 17 P. Wellenius, E.R. Smith, S.M. LeBoeuf, H.O. Everitt, J.F. Muth, *J. Appl. Phys.* 107 (2010) 103111.
- 18 J. Vincent, O. Guillot-Noël, L. Binet, P. Aschehoug, Y.L. Du, *J. Appl. Phys.* 104 (2008) 033519.
- 19 A.J. Neuhalfen, B.W. Wessels, *Appl. Phys. Lett.* 59 (1991) 2317.
- 20 X.Z. Wang, B.W. Wessels, *Appl. Phys. Lett.* 64 (1994) 1537.

Chapter 5

Light-emitting devices based on Ga₂O₃:Er/Si

5.1 Introduction

With a wide bandgap of ~ 4.9 eV and chemical and physical stabilities, Ga₂O₃ based heterojunctions, such as Ga₂O₃/GaN, Ga₂O₃/SiC and Ga₂O₃/Si, have been investigated for use as ultraviolet (UV) photodetectors,¹⁻⁵ and efficient host for rare earth light-emitting devices (LEDs).⁶⁻⁸ Among those heterojunctions, Ga₂O₃/Si is especially attractive due to the well-known advantage of Si substrate and its prominent application in Si-based optoelectronic integrated circuits.^{9,10} In section 4, we have fabricated Eu and Er doped Ga₂O₃ films on sapphire by using PLD and observed the red and green emissions around 613 nm, and 550 nm clearly, respectively.¹⁰ Therefore, the red and green EL could be enabled from the LEDs based on Eu and Er doped Ga₂O₃ film. In this chapter, we only selected Er as the research to try to fabricate green LEDs. Recently, Heikenfeld *et al.*⁴ reported that the green electroluminescence (EL) from GaN:Er/Si devices with a driven voltage of ~ 8.5 V. Zavada *et al.*⁵ have fabricated InGaN:Er/Si diodes, which exhibited green EL under forwards bias voltages ranging in 10~20 V. Harako *et al.*⁶ have demonstrated that the green EL from an ZnO:Er/Si diodes with a driven voltage of ~ 10 V. Miyata *et al.* have demonstrated that high luminescence in thin-film EL devices can be obtained with a rare-earth activated Ga₂O₃ (~ 4.8 eV) phosphor thin-film emitting layer.⁹ However, up to now, there is no report available related to it although this research is of vital

importance for the future application. On the other hand, we know that the crystallization of the host material has an influence on the luminescence intensity of devices. In this Chapter, firstly, we investigate the crystallization of Ga_2O_3 films at different Er content deposited on Si substrate. And then, we select the 5 wt. % Er as target to fabricate $\text{Ga}_2\text{O}_3:\text{Er}/\text{Si}$ LEDs. The green EL at 548 nm is clearly observed and the driven voltage of $\text{Ga}_2\text{O}_3:\text{Er}/\text{Si}$ LEDs is lower than that of $\text{ZnO}:\text{Er}/\text{Si}$ or $\text{GaN}:\text{Er}/\text{Si}$ devices, opening the door for developing Si compatible green LEDs based on the Er doped wide bandgap oxide semiconductors.

5.2 Experiment

As shown in Table 5.1, Er doped Ga₂O₃ thin films were grown on (111) Si substrates by PLD method using a KrF excimer laser source with a frequency of 2 Hz and energy of 225 mJ. Before growth, the Si substrate was ultrasonically cleaned in organic solvents, chemically etched in 2% HF solution, and then rinsed in deionized water, blow-dried with nitrogen gas before it was introduced into the growth chamber to etch the native SiO_x layer from Si substrate. Facing the substrate, bulks (diameter of 20 mm) with different Er contents in the target ($x_{tar.}$) were used as targets. The distance between target and substrate is about 40 mm. High purity oxygen gas (99.9999%) were introduced through mass flow controllers after the pressure of chamber was evacuated to below 10⁻⁶ Pa using a turbo molecular pump. The deposition time was 180 minutes for all samples.

Table 5.1 Growth conditions for Er content influence

Growth conditions	
Targets	0.0, 5.0, 7.0, 9.0, 11.0 wt. % Er
Substrate	Si (111)
Oxygen pressure (Pa)	1 × 10 ⁻¹
Growth temperature (°C)	500
Laser frequency (Hz)	2
Distance from target to substrate (mm)	40

After deposition, the structural properties of the films were examined by

conventional θ - 2θ scan XRD using $K\alpha$ emission line of copper. XPS measurements were performed using Al $K\alpha$ X-ray source. The surface of the sample was Ar ion (3 keV) etched for 2 min before XPS analysis. PL measurements were performed using an Ar laser operating at a wavelength of 488 nm as the excitation source. The surface morphology and roughness of the film were studied by AFM on $4 \times 4 \mu\text{m}^2$ areas under ambient conditions.

Herein, in order to fabricate the light-emitting devices, bulk with 2.6 at.% Er contents is used as target. The oxygen pressure was set at 1×10^{-1} Pa while deposition time was 180 minutes. The films were grown at substrate temperature of 500 °C. After deposition, the thickness of Er doped Ga_2O_3 film was determined to be about 600 nm measured by a surface step profile analyzer. XPS measurements were performed using Al $K\alpha$ X-ray source. The surface of the sample was Ar ion (3 keV) etched for 2 min before XPS analysis. PL measurements were performed using an Ar laser operating at a wavelength of 488 nm as the excitation source.

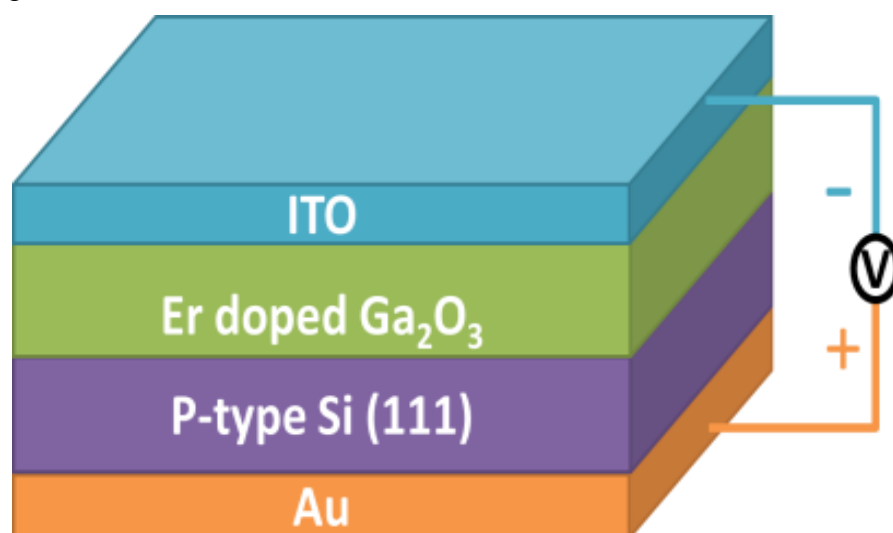


Figure 5.1 Schematic drawing of the $\text{Ga}_2\text{O}_3\text{:Er/Si}$ LEDs

From Fig 5.1, to form electrical contacts, ~ 200 nm thick indium tin oxide (ITO) layer onto the Er doped Ga₂O₃ film were deposited by using direct current sputtering. ~250 nm Au film on the backside of Si substrate by using electron beam evaporated technique. The current-voltage (*I-V*) characteristics, electroluminescence (EL) spectrum are measured by Advantest DC voltage current source (R6364), while the EL spectra in the visible recorded by using high sensitivity spectra multi-channel photo detector (MCPD-7000).

5.3 Results and discussion

Figure 5.2 (a) shows wide scan spectra of the Ga_2O_3 films grown with different Er contents in the targets (x_i). From the spectra, the peaks related with Ga, O, and Er are clearly observed. No other elements are detected from the wide scan spectra of the films. From Fig. 5.2 (b), it is clear that two symmetrical peaks of Ga $2p_{1/2}$ and Ga $2p_{3/2}$ are located at 1146.6 eV and 1119.9 eV, respectively, The separation energy between these two peaks is about 26.7 eV, which is in good agreement with the reported value for Ga_2O_3 bulk. Fig. 5.2 (c) reveals the high resolution XPS spectra of Er $4p$ peak, centered at 321.6 eV. The intensity of the Er peak increases with the increase of Er contents (x_i).

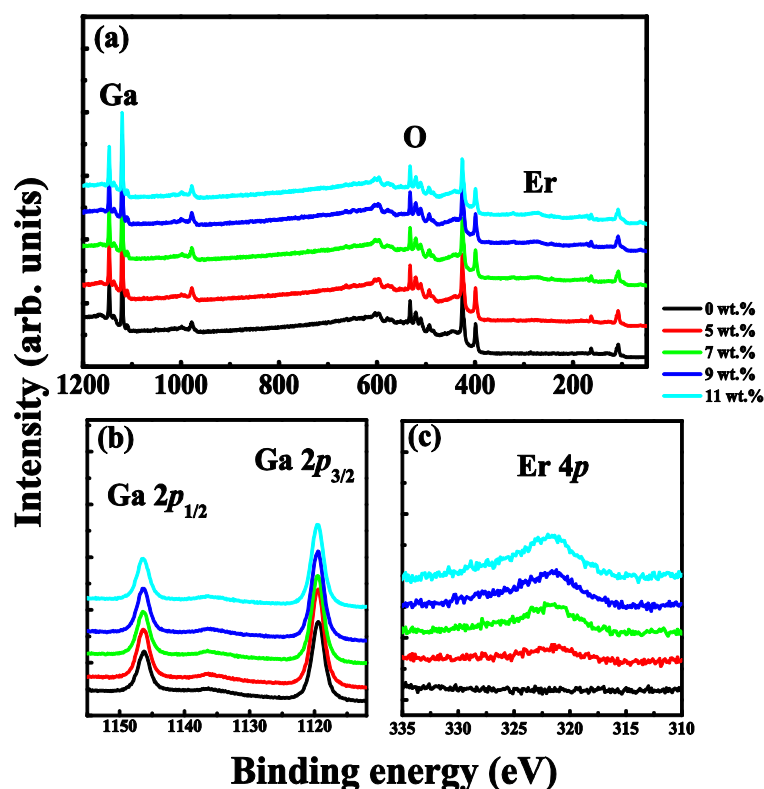


Figure 5.2 (a) XPS wide scan spectra, (b) Ga 2p, and (c) Er 4p core level spectra of Ga_2O_3 films with different contents in the targets x_i .

From Fig. 5.3, we find that the Er contents (x) in the films increases almost linearly with the increase of Er contents of the targets (x_t). This suggests that the Er contents in Ga_2O_3 films (x) can be controlled by adjusting the Er contents in the targets (x_t).

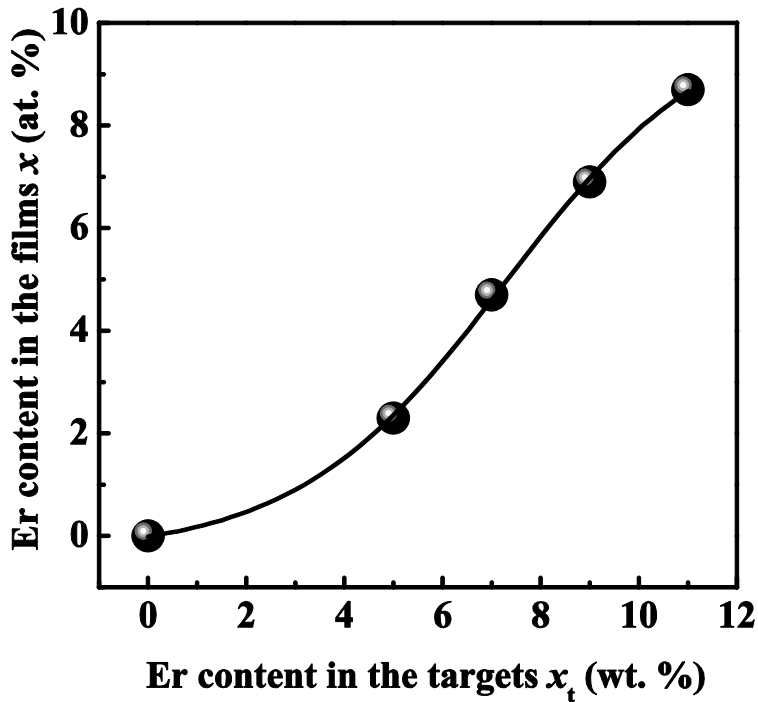


Figure 5.3 Er contents in the films (x) as a function of the Er contents of the targets (x_t).

Figure 5.4 shows the XRD patterns of Ga_2O_3 films with different Er contents on Si substrate. Two peaks are clearly observed at 30.5° and 44.5° which can be assigned as the (-401) and (-601) planes of monoclinic Ga_2O_3 ($\beta\text{-Ga}_2\text{O}_3$), respectively by comparing the PDF card (NO.:43-1012). No other peaks related to the Er_2O_3 are observed in the spectrum. It is clear that the incorporation of Er into Ga_2O_3 film leads to degradation of crystal quality. On the other hand, we can see that the RHEED pattern obvious diffused rings, indicating that the films are polycrystalline and

crystalline quality of the film was deteriorated with increasing of Er content.

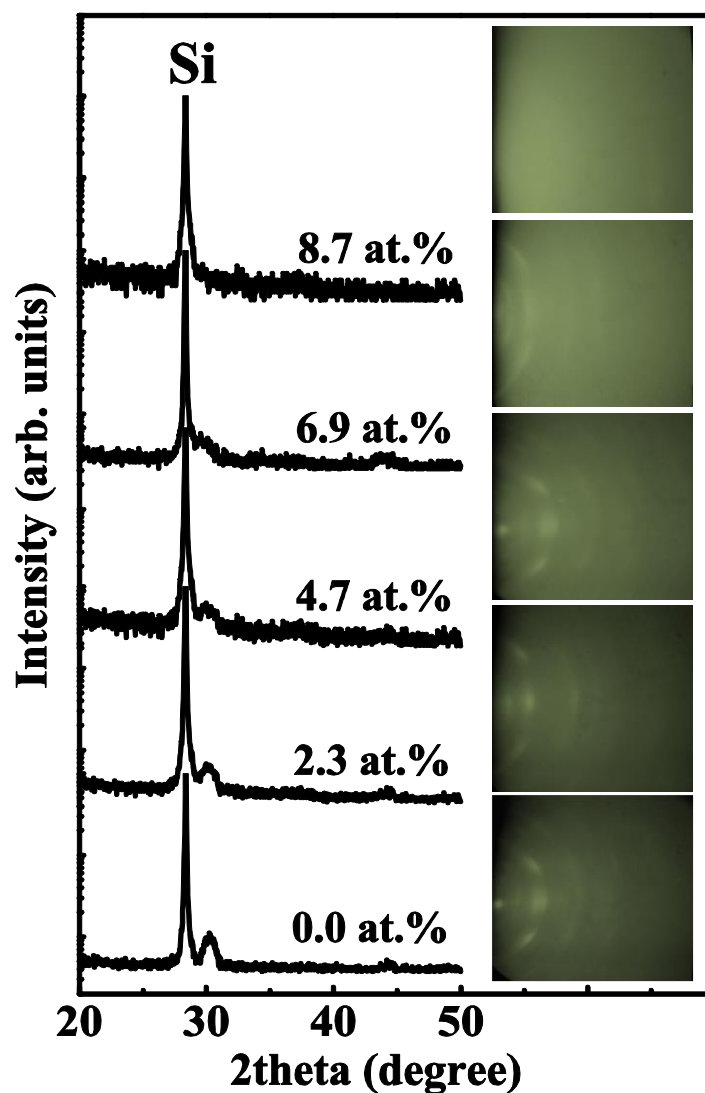


Figure 5.4 XRD patterns of Ga₂O₃ films deposited on Si substrates with various Er contents. Insert is the RHEED images for these films.

Figure 5.5 shows the AFM morphologies of the Ga₂O₃ films with different Er contents. It is clear that the grain like structure was seen on the surfaces of the films from 0.0 to 4.7 at. %. And then, with increasing Er content, obvious difference between the surface morphologies of the films can be observed. It also demonstrates

that the incorporation of Er into Ga_2O_3 film leads to degradation of crystal quality. Herein, the root-mean-square roughness of the 2.3 at. % film is 3.6 nm, indicating the film has a smooth surface.

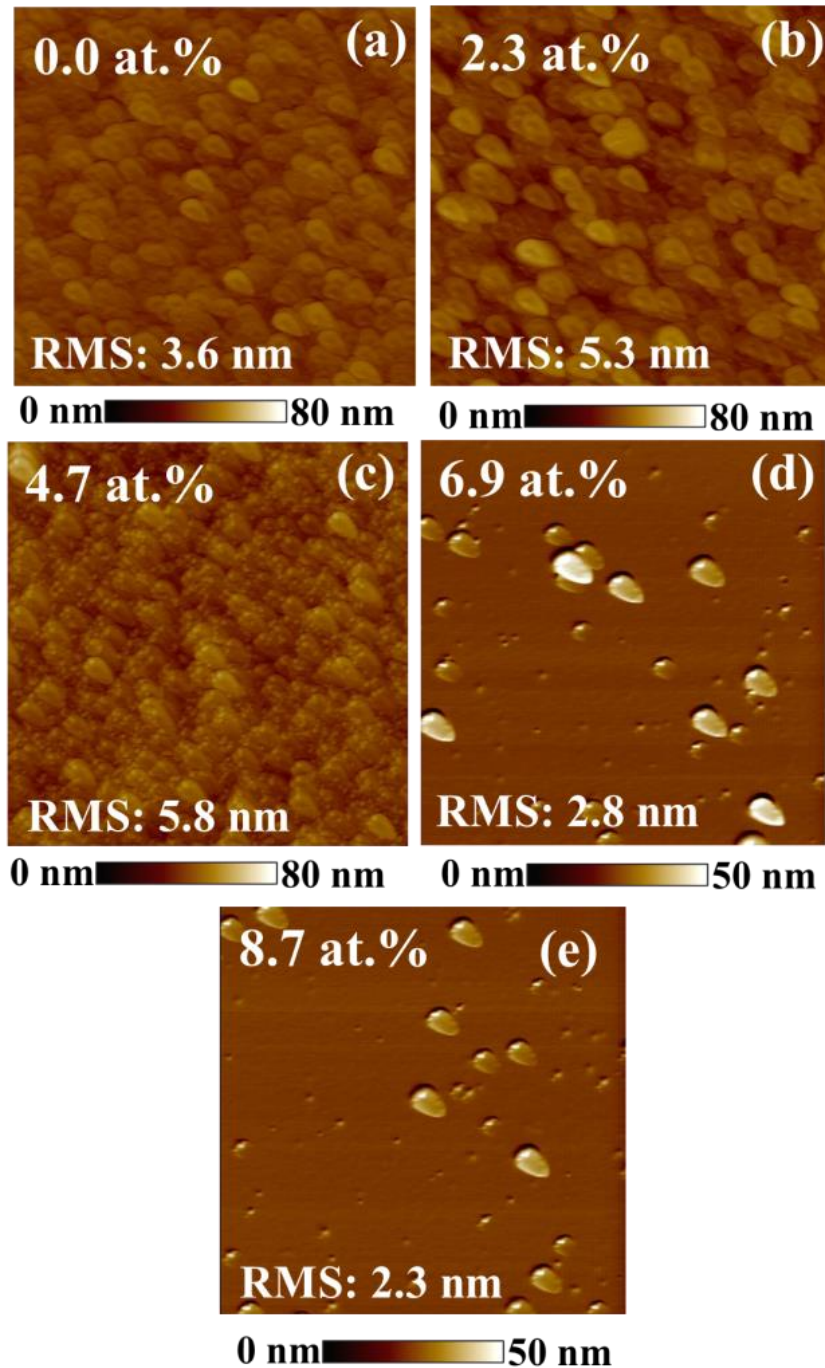


Figure 5.5 AFM images of Ga_2O_3 films with different Er doping contents (x), (a) 0.0, (b) 2.3, (c) 4.6, (d) 6.9 and 8.7 at. %, respectively.

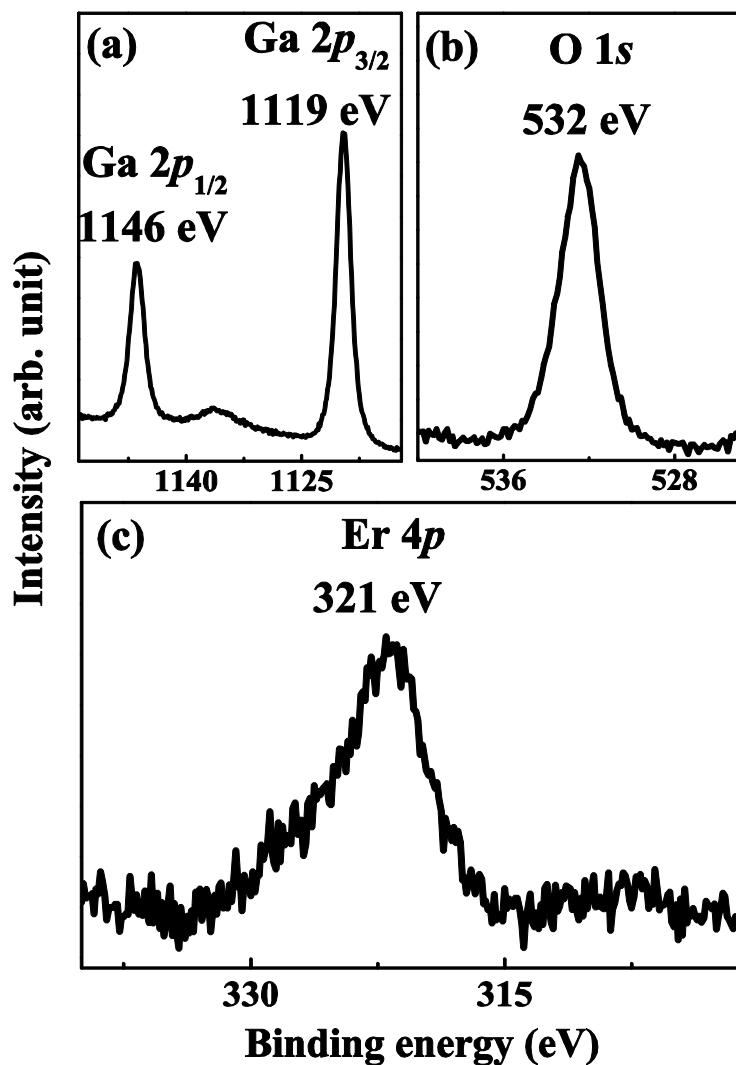


Figure 5.6 XPS spectra of (a) Ga 2p_{1/2}, Ga 2p_{3/2}, (b) O 1s, and (c) Er 4p core level for Er doped Ga₂O₃ film.

The deposited film was characterized using XPS to illustrate the chemical compositions and chemical state. From Fig. 5.6 (a), it is clear that two symmetrical peaks of Ga 2p_{1/2} and Ga 2p_{3/2} are located at 1146 eV and 1119 eV, respectively. The separation energy between these two peaks is about 27 eV, which is in good agreement with the reported value for Ga₂O₃ bulk.¹¹ Since the surface of the film was etched, the O 1s peak at 532 could be assigned to the oxygen in Ga₂O₃ lattice as

shown in Fig. 5.6 (b). Fig. 5.6 (c) reveals the high resolution XPS spectrum of Er 4*p* peak, centered at 321 eV. The Er content in Ga₂O₃ film is obtained to be 2.7 at.% from the XPS spectra after applying an atomic sensitivity factor, which is almost the same as that in the target. The results confirmed that Er atoms have been effectively incorporated into the oxide matrix.

Figure 5.7 shows the *I-V* characteristic of the Ga₂O₃:Er/Si LEDs. It is noted that an excellent rectification character is obtained, indicating that the device is a *p-n* heterojunction. Herein, the devices are electroluminescent only under the forward bias, demonstrating that the simultaneous injection of electrons and holes is necessary for the EL.¹² Strikingly, the current increases rapidly when the forward bias voltage is above 6.2 V, and it is strongly blocked under the reverse bias. It is validated that the green emission originated from Er ions incorporated into Ga₂O₃ can be activated with voltage as low as 6.2 V. From the insert of Fig. 5.7, a leakage current of 2.0 mA can be determined at -6.2 V, while the current reaches 60 mA at 6.2 V. Meanwhile, it should be mentioned that the brightly green emitted light can be observed by naked eye at forwards bias of 6.2 V.

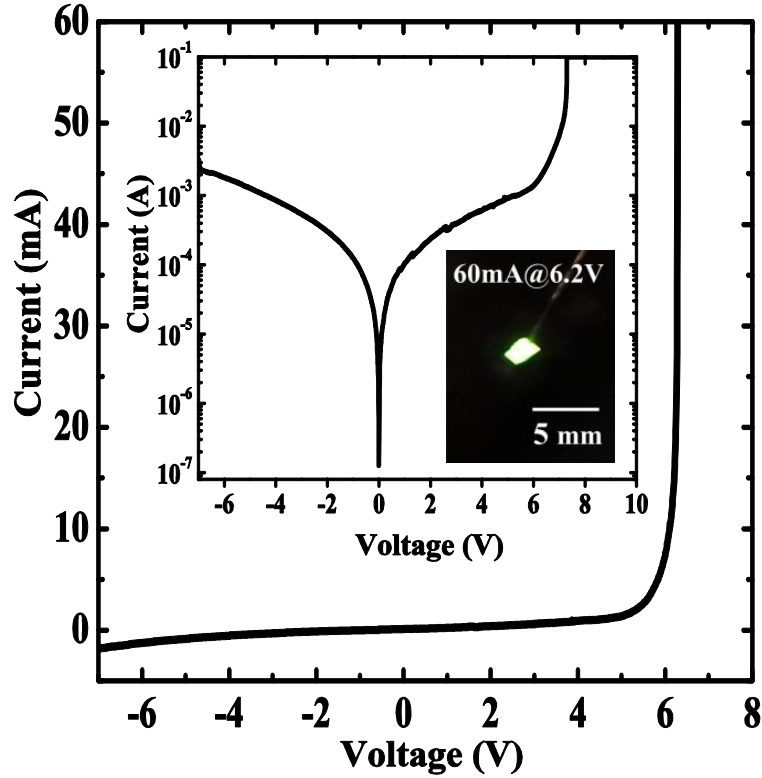


Figure 5.7 The I-V characteristic of the Ga₂O₃:Er/Si LEDs. Insert shows the same characteristic with log scale and the EL photo of this device in dark at 60 mA.

In order to investigate the origin of EL emission of Er ions, PL spectrum of Er doped Ga₂O₃ film excited by the 488 nm light is shown in Fig. 5.8 (a). The strongest green emission band centered at 548 nm can be observed from the PL spectrum, which is caused by the $^4S_{3/2} \rightarrow ^4I_{15/2}$ transition. Other PL peaks observed at 524, 660, 850 and 975 nm can be assigned to the transitions from $^2H_{11/2} \rightarrow ^4I_{15/2}$, $^4F_{9/2} \rightarrow ^4I_{15/2}$, $^4I_{9/2} \rightarrow ^4I_{15/2}$ and $^4I_{11/2} \rightarrow ^4I_{15/2}$, respectively.^{10,13} We have deconvoluted the green emission bands in this spectrum with four Gaussian curves at wavelengths positioned at 524, 533, 548 and 559 nm. Here, two weak peaks at 533 and 559 nm are ascribed to Stark splitting because the spin-orbit splitting of the energy level.¹⁰ In our study, the

excitation energy of incident light used for measurement is lower than the bandgap of Ga_2O_3 . However, the electrons can be excited from the valence band to the donor band (oxygen vacancy) by this light source. The related energy due to the recombination of electrons in the defect state with the photogenerated holes can transfer to a resonant excitation of Er^{3+} ions with 488 nm excitation wavelength, owing to $^4I_{15/2} \rightarrow ^4F_{7/2}$ transition.¹³⁻¹⁵ Similar observation has been reported in Er doped GaN films,¹³ and Er doped Ga_2O_3 bulk.¹⁴ Fig. 5.8 (b) shows EL spectra of the fabricated $\text{Ga}_2\text{O}_3:\text{Er}/\text{Si}$ LEDs under different forward bias voltages. It is clear that the EL intensity increases with the forward bias, and no peak shift in the EL spectrum is observed with injection current from 3 to 60 mA. Moreover, the EL spectra have two narrow, strong green emission bands centered at 524 and 548 nm, which are consistent with the PL results.

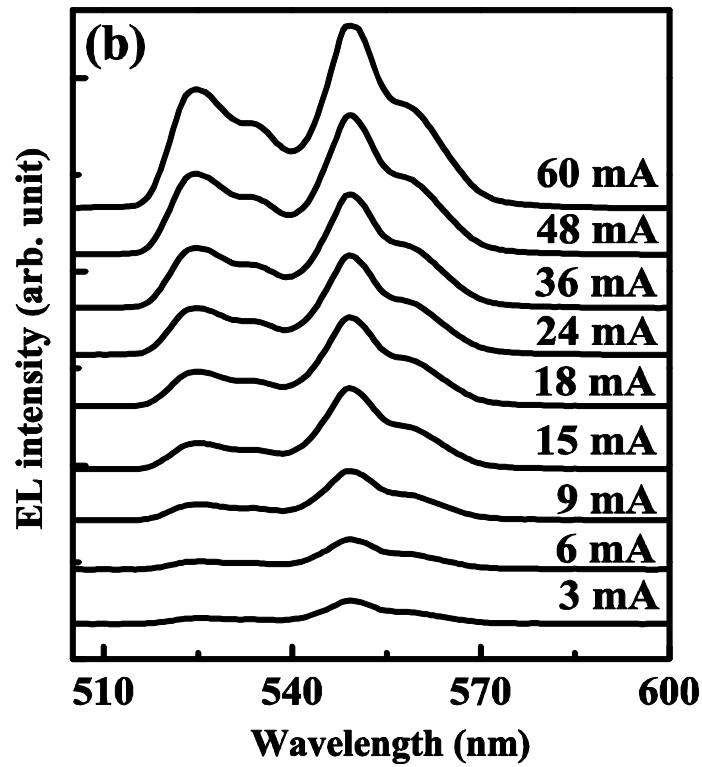
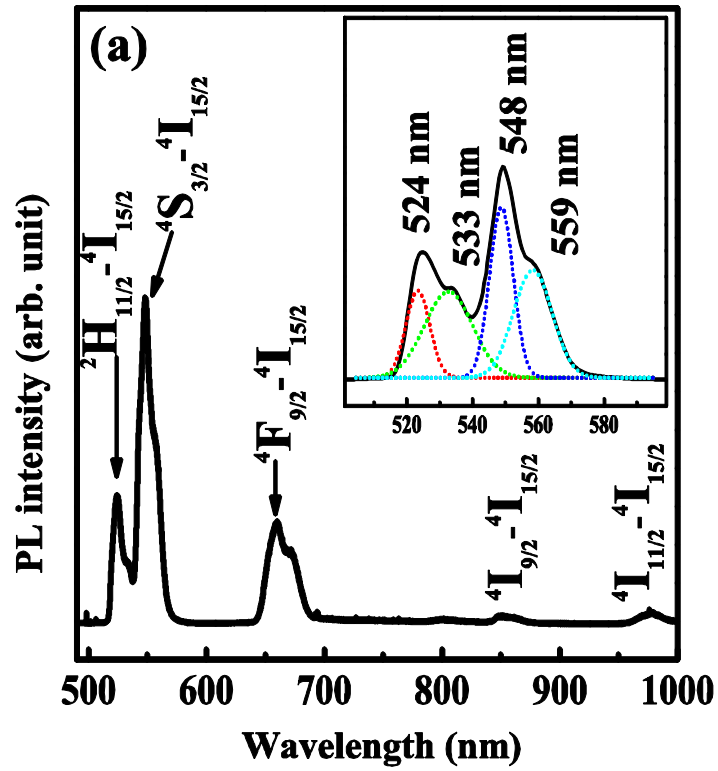


Figure 5.8 (a) Room temperature (RT) PL spectrum of Er doped Ga₂O₃ films.

(b) RT-EL spectra for the Ga₂O₃:Er/Si LEDs with different current injections.

Figure 5.9 (a) shows plots of the EL intensity of green emissions at 524 and 548 nm with the forward bias voltage. The EL intensity of 548 nm is consistently stronger than the 524 nm emission with increasing the injection current. The most likely explanation is that the intensity from the upper $^2H_{11/2}$ (524 nm) level is reduced as it increasingly feeds electrons to the lower $^4S_{3/2}$ (548 nm) level due to the two closely spaced electronic state.¹³ It should be noted the EL intensity increases rapidly when the forward bias voltage is above 6.2 V, which confirmed that the driven voltage for the onset green emission is ~ 6.2 V. In Fig. 5.9 (b), we present the light intensity of green emissions at 524 and 548 nm and the injection current ($L-I$) characteristic of this device. In agreement with the spectral evolution, the results can be fitted by the power law:¹⁶

$$L \propto I^m$$

where m accounts for the influence of the defects in the characteristics of the light emission. The two curves indicate the superlinear dependence at low current level with slopes of 1.7 and 1.3, respectively, and become almost linear ($m=0.9, 0.8$) at higher current level (>35 mA). The superlinear zone is directly related to the presence of non-radiative centers that provide a shunt path to the current.¹⁷ However, small deviation from linear relation at high current level is possibly related to the limitation of the electrical-to-optical conversion efficiency caused by Auger recombination or by heating effect and series resistances at high current level.¹⁷⁻¹⁹

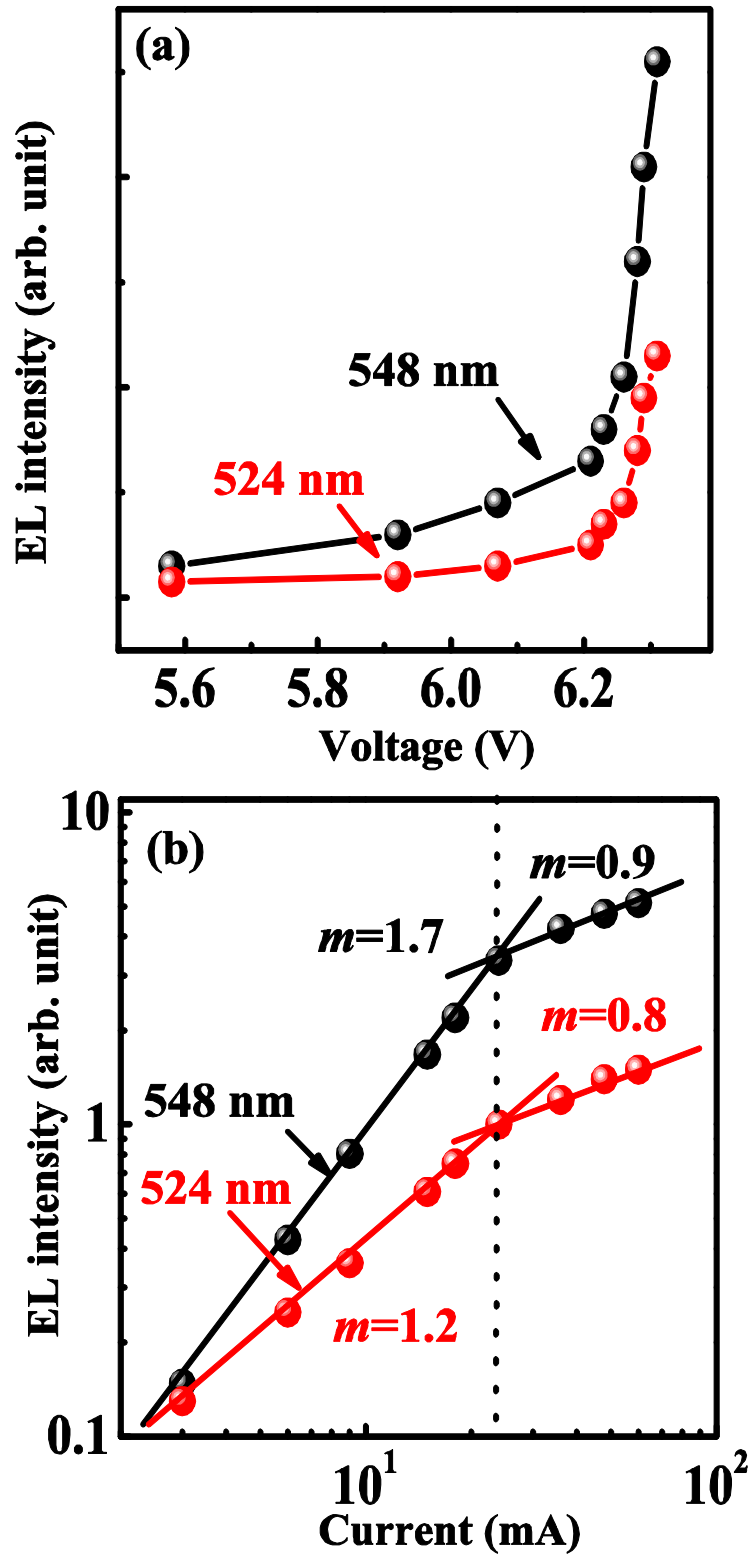


Figure 5.9 (a) Forward bias voltage dependence of the EL intensities of the Ga₂O₃:Er/Si LEDs. (b) EL intensity as a function of injection current for the green emission at 524 and 548 nm.

The values of band offset are estimated using the electron affinity 4.05, 4.00, 4.80 eV and bandgap 1.12, 4.90, 3.80 eV for *p*-Si (χ_{Si}), Ga₂O₃ ($\chi_{\text{Ga}_2\text{O}_3}$), and ITO (χ_{ITO}) respectively.^{20,21} From Fig. 5.10 (a), the bandgap discontinuity at conduction band and valence band are therefore equal to $\Delta E_c = \chi_{\text{Si}} - \chi_{\text{Ga}_2\text{O}_3} = 0.05$ eV and $\Delta E_v = E_{g, \text{Ga}_2\text{O}_3} - E_{g, \text{Si}} - \Delta E_c = 3.73$ eV by using Anderson model.²¹ Obviously, ΔE_v is much larger than ΔE_c . As shown in Fig. 5.10 (b), when forward bias is applied on the heterojunction, an amount of electrons in ITO electrode can be thermally activated to tunnel into the trap states nearby the interface.²⁰ The electrons flow from the conduction band of Ga₂O₃ to that of Si. The holes can be injected from the valence band of the Si substrate into that of Ga₂O₃ under a certain bias, in spite of the possibility that the device may be electron flow dominated.²² In this context, under the aforementioned forward bias voltage, a part of electrons in the conduction band of the Ga₂O₃ will directly recombine with holes in the valence band. However, since Ga₂O₃ is a direct bandgap semiconductor,^{10,23,24} transfer of the energy released from the direct electron-hole recombination to the Er ions is negligible due to the short lifetime.¹² On the other hand, other electrons will firstly transit to the defect-related energy levels (E_{Defect}) and then recombine with holes in the valence band of Ga₂O₃. The indirectly recombination of carriers in the Ga₂O₃ host could transfer energy to the incorporated Er³⁺ ions nearby the defects. Similar energy transfer mechanism has been demonstrated in ZnO:Er/Si devices.¹² Heikenfeld *et al.*⁴ have observed a driven voltage of ~8.5 V when the thickness of GaN:Er layer is 600 nm. Zavada *et al.*⁵ have reported on the Er doped InGaN diodes, which exhibited green luminescence under

the forward bias voltage ranging in 10~15 V. Harako *et al.*⁶ have demonstrated that the green EL from ZnO:Er/Si diode with a driven voltage of ~10 V. In this work, it is obvious from the above experimental results that the driven voltage of green emission from Ga₂O₃:Er/Si LEDs is lower than that of ZnO:Er/Si or GaN:Er/Si devices. It has been demonstrated that the wide bandgap of Ga₂O₃ contains more defect-related levels.^{23,25-27} Thus, we believe that the low driven voltage from Ga₂O₃:Er/Si LEDs is ascribed to the wide bandgap of Ga₂O₃ which will enhance the effects of radiative recombination between electrons in the defect-related level and hole in the valence band, resulting in improvement of the transfer energy.²⁶

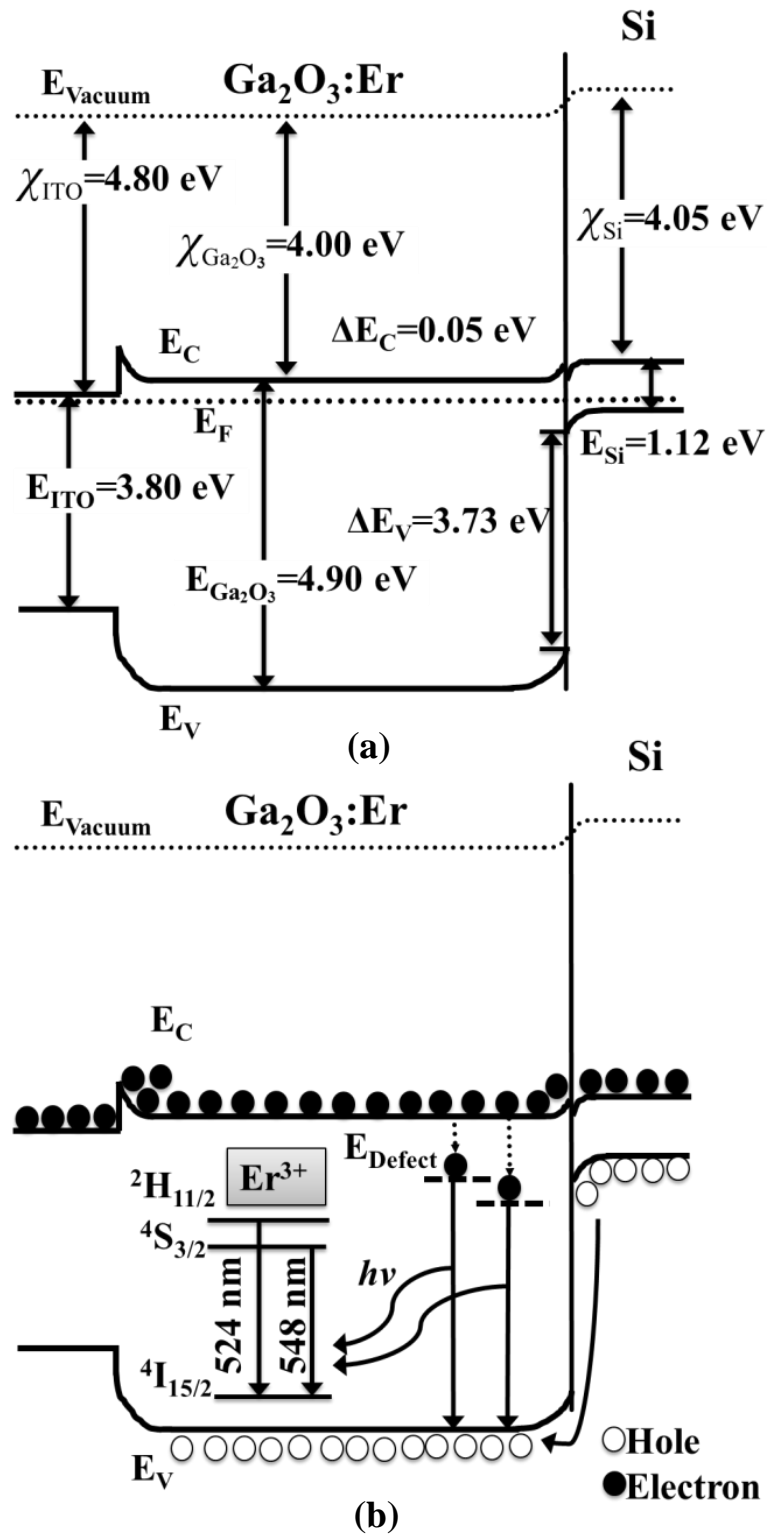


Figure 5.10 Schematic diagram for the energy band structure and transfer energy process of the Ga₂O₃:Er/Si LEDs (a) at thermal equilibrium and (b) under forward bias.

5.4 Conclusions

In conclusions, Er doped Ga₂O₃ thin films have been grown on Si substrate by PLD. The XPS results confirmed that Er atoms have been effectively incorporated into the Ga₂O₃. We have further fabricated the LEDs by using Ga₂O₃:Er/Si heterojunction. The brightly green emitted light could be observed by naked eye. The *I-V* characteristic measurement indicated that the driven voltage of the LEDs as low as 6.2 V. In order to investigate the origin of the green emission, PL spectrum of Er doped Ga₂O₃ film has been measured. The observed strongest green emission band at 548 nm was ascribed to the $^4S_{3/2} \rightarrow ^4I_{15/2}$ transition.

References

- 1 M. Garter, J. Scofield, R. Birkhahn, A.J. Steckl, Appl. Phys. Lett. 74 (1999) 182.
- 2 J. Heikenfeld, M. Garter, D.S. Lee, R. Birkhahn, A.J. Steckl, Appl. Phys. Lett. 75 (1999) 1189.
- 3 Y. Takagi, T. Suwa, H. Sekiguchi, H. Okada, A. Wakahara, Appl. Phys. Lett. 99 (2011) 171905.
- 4 J. Heikenfeld, D.S. Lee, M. Garter, R. Birkhahn, A.J. Steckl, Appl. Phys. Lett. 76 (2000) 1365.
- 5 J.M. Zavada, S.X. Lin, N. Nepal, J.Y. Lin, H.X. Jiang, P. Chow, B. Hertog, Appl. Phys. Lett. 84 (2004)1061.
- 6 S. Harako, S. Yokoyama, K. Ide, X. Zhao, S. Komoro, Phys. Stat. Sol. (a) 205 (2008) 19.
- 7 P.N. Favennec, H. L'Haridon, M. Salvi, D. Moutonnet, Y. L. Guillou, Electron. Lett. 25 (1989) 718.
- 8 Z.W. Chen, K. Saito, T. Tanaka, M. Nishio, M. Arita, Q.X. Guo, J. Cryst. Growth, 430 (2015) 28.
- 9 T. Miyata, T. Nakatani, T. Minami, J. Lumin. 87-89 (2000) 1183.
- 10 Z.W. Chen, X. Wang, S. Noda, K. Saito, T. Tanaka, M. Nishio, M. Arita, Q.X. Guo, Superlattices Microstruct. 90 (2016) 207.
- 11 G. Schön, J. Electron. Spectrosc. Relat. Phenom. 2 (1973) 75.
- 12 Y. Yang, Y.P. Li, L.L. Xiang, X.Y. Ma, D.R. Yang, Appl. Phys. Lett. 102 (2013) 181111.
- 13 A.J. Steckl, R. Birkhahn, Appl. Phys. Lett. 73 (1998) 1700.

- 14 E. Nogales, J.A. Garc ía, B. Méndez, J. Piqueras, K. Lorenz, E. Alves, J. Phys. D: Appl. Phys. 41 (2008) 065406.
- 15 Z.P. Wu, G.X. Bai, Q.R. Hu, D.Y. Guo, C.L. Sun, L.Y. Ji, M. Lei, L.H. Li, P.G. Li, J.H. Hao, W.H. Tang, Appl. Phys. Lett. 106 (2015) 171910.
- 16 I. M átil, E. Redondo, A. Ojeda, J. Appl. Phys. 81 (1997) 2442.
- 17 J.D. Ye, S.L. Gu, S.M. Zhu, W. Liu, S.M. Liu, R. Zhang, Y. Shi, Y.D. Zheng, Appl. Phys. Lett. 88 (2006) 182112.
- 18 Y.I. Alivov, J.E.V. Nostrand, D.C. Look, M.V. Chukichev, B.M. Ataev, Appl. Phys. Lett. 83 (2003) 2943.
- 19 M. Ishii, A. Koizumi, Y. Takeda, Y. Fujiwara, J. Appl. Phys. 115 (2014) 133510.
- 20 B. He, Z.Q. Ma, J. Xu, L. Zhao, N.S. Zhang, F. Li, C. Shen, L. Shen, X.J. Meng, C.Y. Zhou, Z.S. Yu, Y.T. Yin, Superlattices Microstruct. 46 (2009) 664.
- 21 D.Y. Guo, Z.P. Wu, Y.H. An, X.C. Guo, X.L. Chu, C.L. Sun, L.H. Li, P.G. Li, W.H. Tang, Appl. Phys. Lett. 105 (2014) 023507.
- 22 Z.Z. Yuan, D.S. Li, M.H. Wang, P.L. Chen, D.R. Gong, P.H. Cheng, D.R. Yang, Appl. Phys. Lett. 92 (2008) 121908.
- 23 J.B. Varley, J.R. Weber, A. Janotti, and C.G. Van de Walle, Appl. Phys. Lett. 97 (2010) 142106.
- 24 F.B. Zhang, K. Saito, T. Tanaka, M. Nishio, Q.X. Guo, Solid State Commun. 186 (2014) 28.
- 25 L. Binet, D. Gourier, Appl. Phys. Lett. 77 (2000) 1138.
- 26 K. Irscher, Z. Galazka, M. Pietsch, R. Uecker, R. Fornari, J. Appl. Phys. 110,

063720 (2011).

27 Z. Zhang, E. Farzana, A.R. Arehart, S.A. Ringel, *Appl. Phys. Lett.* 108, 052105

(2016).

6. Summary

In summary, we have investigated structural, morphological and optical properties of Eu and Er doped Ga₂O₃ films on sapphire substrate with different Eu and Er contents. All the films were deposited on sapphire substrates by PLD. We confirmed that Eu, Er atoms could be effectively incorporated into the Ga₂O₃. Temperature insensitive red (~ 613 nm) and pure green (~ 550 nm) luminescence have been demonstrated from Eu doped Ga₂O₃, and Er doped Ga₂O₃ films, respectively. Moreover, We have fabricated the LEDs by using Ga₂O₃:Er/Si heterojunction. The brightly green emitted light could be observed by naked eye. The *I-V* characteristic measurement indicated that the driven voltage of the LEDs was as low as 6.2 V.

In Chapter 1, we present the background of this study, including the properties of RE ions and the introductions of wide bandgap semiconductors. The purpose of this study was presented.

In Chapter 2, we introduce the film growth and characterization methods.

In Chapter 3, we have investigated the Eu contents and substrate temperature influence on the structure and properties of Ga₂O₃ films deposited on sapphire substrate by PLD. Herein, (1) Eu doped Ga₂O₃ films were obtained at substrate temperature as low as 500 °C. Moreover, the single crystal film can be obtained at 400 °C. (2) Eu doping amount in the films can be controlled by adjusting Eu contents in the target. (3) Intense red emissions at 613 nm are clearly observed for the Eu doped films and we demonstrated that intensity quenching is related to polycrystalline growth of Ga₂O₃. (4) Temperature dependence of luminescence spectra in Eu doped

Ga₂O₃ films were investigated by using different light source. And we demonstrated that the variation of the emission intensity may be attributed to the thermal activated distribution of electrons among ⁷F_j and thermal quenching effect.

In Chapter 4, we have investigated the Er contents influence on the structure and properties of Ga₂O₃ films deposited on sapphire substrate by PLD. In this chapter, (1) We have fabricated Er doped Ga₂O₃ films on sapphire substrates for the first time. (2) Intense pure green emissions at ~ 550 nm were clearly observed for the Er doped films. (3) Temperature dependence of luminescence spectra in Er doped Ga₂O₃ films were investigated by using 488 nm light source. No peak shift at 550 nm was found with temperatures ranging from 77 to 450 K. (4) The intensity of the Er doped Ga₂O₃ films has a smaller variation with temperature compared to GaN.

In Chapter 5, we have fabricated the Ga₂O₃:Er/Si light-emitting devices (LEDs). In this chapter, (1) Bright green emission (548 nm) can be observed by naked eye from Ga₂O₃:Er/Si LEDs. (2) The driven voltage of this LEDs is 6.2V which is lower than that of ZnO:Er/Si or GaN:Er/Si devices. (3) The mechanism has been demonstrated that Ga₂O₃ contain more defect-related level which will enhance the effects of recombination, resulting in the improvement of the energy transfer to Er ions.

Acknowledgments

I would like to express my gratitude to all those who helped me during the writing of this thesis.

First of all, I would like to express my sincerest gratitude to Professor Qixin Guo of Saga University for supervising this study and for main fruitful discussion. Without his consistent and illuminating instruction, this thesis could not have reached its present form.

Thanks also go to Professor Mitsuhiro Nishio, Professor Tooru Tanaka, and Doctor Katsuhiko Saito for their help on the daily experiment, instructions, and discussions. I also would like to express my thanks to my colleagues: Doctor Xu Wang, and Fabi Zhang, for their invaluable helps.

I also want to show my gratitude to Doctor Makoto Arita in Kyusyu University for his help on experiment and analysis.

I am also greatly obliged to Professor Tooru Tanaka, Professor Kazutoshi Takahashi for their useful advises and for revising the thesis carefully.

Finally, I am particularly grateful to my farther, Tianshun Chen, mother, Ruiying Zhou, Fiancee, Yuan Fang, and sister, Jiawei Chen, for their patience and encouragement.

List of Publications

A. Original Papers Related to This Dissertation:

- 1 **Zhengwei Chen**, Katsuhiko Saito, Tooru Tanaka, Mitsuhiro Nishio, Makoto Arita, Qixin Guo, Low temperature growth of europium doped Ga₂O₃ luminescent films, *Journal of Crystal Growth* 430 (2015) 28-33.
- 2 **Zhengwei Chen**, Xu Wang, Fabi Zhang, Shinji Noda, Katsuhiko Saito, Tooru Tanaka, Mitsuhiro Nishio, Qixin Guo, Temperature dependence of luminescence spectra in europium doped Ga₂O₃ film, *Journal of Luminescence* 177 (2016) 48-53.
- 3 **Zhengwei Chen**, Xu Wang, Shinji Noda, Katsuhiko Saito, Tooru Tanaka, Mitsuhiro Nishio, Makoto Arita, Qixin Guo, Effects of dopant contents on structural, morphological and optical properties of Er doped Ga₂O₃ films, *Superlattices and Microstructures* 90 (2016) 207-214.
- 4 **Zhengwei Chen**, Xu Wang, Fabi Zhang, Shinji Noda, Katsuhiko Saito, Tooru Tanaka, Mitsuhiro Nishio, Makoto Arita, Qixin Guo, Observation of low voltage driven green emission from erbium doped Ga₂O₃ light-emitting devices, *Applied Physics Letters* 109 (2016) 022107.

B. Original Papers on Other Subjects:

- 1 **Zhengwei Chen**, Xianghu Wang, Katsuhiko Saito, Tooru Tanaka, Mitsuhiro Nishio, Qixin Guo, The impact of growth temperature on the structural and optical properties of catalyst-free β -Ga₂O₃ nanostructures, *Materials Research Express*, 3, (2016) 025003.
- 2 **Zhengwei Chen**, Kazuo Nishihagi, Xu Wang, Katsuhiko Saito, Tooru Tanaka, Mitsuhiro Nishio, Makoto Arita, Qixin Guo, Band alignment of Ga₂O₃/Si heterojunction interface measured by X-ray photoelectron spectroscopy, *Applied Physics Letters* 109, (2016) 102106.
- 3 **Zhengwei Chen**, Katsuhiko Saito, Tooru Tanaka, Mitsuhiro Nishio, Qixin Guo, Highly transparent conductive Ga doped ZnO films in the near-infrared wavelength range, *Journal Materials Science: Materials Electronic* 27(9), (2016) 9291-9296.
- 4 Xu Wang, **Zhengwei Chen**, Fabi Zhang, Katsuhiko Saito, Tooru Tanaka, Mitsuhiro Nishio, Qixin Guo, Temperature dependence of Raman scattering in β -(AlGa)₂O₃ thin films, *AIP Advance*, 6, (2016) 015111.
- 5 Xu Wang, **Zhengwei Chen**, Fabi Zhang, Katsuhiko Saito, Tooru Tanaka, Mitsuhiro Nishio, Qixin Guo, Influence of substrate temperature on the properties

- of (AlGa)₂O₃ thin films prepared by pulsed laser deposition, *Ceramics international*, 42, (2016) 12783-12788.
- 6 Xu Wang, **Zhengwei Chen**, Fabi Zhang, Katsuhiko Saito, Tooru Tanaka, Mitsuhiro Nishio, Qixin Guo, Temperature-dependent Raman scattering in cubic (InGa)₂O₃ thin films, *Journal of Alloys and compound* 690, (2017) 287-292.
 - 7 Fabi Zhang, Makoto Arita, Xu Wang, **Zhengwei Chen**, Katsuhiko Saito, Tooru Tanaka, Mitsuhiro Nishio, Qixin Guo, Toward controlling the carrier density of Si doped Ga₂O₃ films by pulsed laser deposition, *Applied Physics Letters* 109, (2016) 102105.
 - 8 X.H. Wang, L.Q. Huang, L.J. Niu, R.B. Li, D.H. Fan, F.B. Zhang, **Z.W. Chen**, X. Wang, Q.X. Guo, The impacts of growth temperature on morphologies, compositions and optical properties of Mg-doped ZnO nanomaterials by chemical vapor deposition, *Journal of Alloys and Compounds* 622 (2015) 1201-1204.